



**ARISTOTLE UNIVERSITY OF  
THESSALONIKI**

**SCHOOL OF GEOLOGY**

***M.Sc. "HYDROCARBONS EXPLORATION AND EXPLOITATION"***

# **ACCELERATION OF GAS CONDENSATE RESERVOIRS SIMULATION USING MACHINE LEARNING**

**MASTER'S THESIS**

**ANASTASIADOU VASILIKI**

**SUPERVISOR: Dr. GAGANIS VASILEIOS, ASSISTANT PROFESSOR, NATIONAL  
TECHNICAL UNIVERSITY OF ATHENS (NTUA)**

**THESSALONIKI, 2021**





# ACCELERATION OF GAS CONDENSATE RESERVOIRS SIMULATION USING MACHINE LEARNING

A

Thesis

by

ANASTASIADOU VASILIKI

Supervisor: Dr. Gaganis Vasileios, Assistant Professor (NTUA)

## **Three-member Examining Board:**

Professor Andreas Georgakopoulos (AUTH)

Assist. Professor Vasilis Gaganis (NTUA)

Professor Sofia Stamataki (NTUA)







## ACKNOWLEDGEMENTS

First and foremost, I cannot fully express my deep sense of gratitude to my mentor, Dr. Vasilis Gaganis for his support and guidance through all the stages of this beautiful and challenging journey of research and writing of this thesis. It was his continuous motivation and advice that made this work possible.

I would also like to give special thanks to Professor Andreas Georgakopoulos who introduced me to the world of hydrocarbons and was always eager to offer scientific insight, as well as Professor Sofia Stamataki whose exceptional career over the years serves as a bright example for all women in science.

I am also indebted to Mrs. Evangelia Koffa for her generous assistance during my first encounters with fluid behaviour software. With her valuable help my work was made a lot easier.

Finally, I owe a big thank you to my parents for their unfailing encouragement, support and patience throughout the years. Without them I would not be the person that I am today.



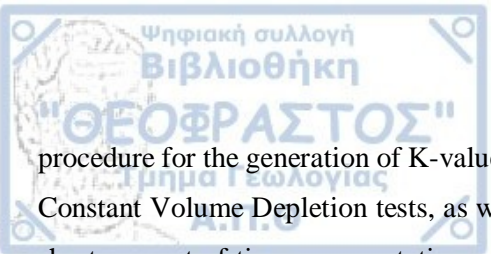


## ABSTRACT

During the production life of a gas condensate reservoir, the dew point is reached at a specific pressure which marks the beginning of liquid condensation in the reservoir rock. This liquid phase is characterised by zero relative permeability due to insufficient saturation and is therefore unable to move. This results in its entrapment in the reservoir pores and in the formation of condensate banks around production wells, since these regions exhibit the greatest pressure decline. As a result, well productivity is ultimately weakened, first, by obstruction of the gas flow caused by the trapped condensate, and second and most important, by loss of the economically valuable heavier condensate fractions retained in the reservoir. A technique referred to as Gas Recycling is often used to handle condensate blockage effects taking place in retrograde gas condensate reservoirs, during which the produced gas is stripped from its intermediate and heavy components at the surface and is subsequently reinjected in the reservoir as dry gas, causing revaporisation of the trapped condensate, by modifying the overall reservoir fluid composition and enabling its production.

Planning and optimisation of the gas recycling procedure are significant steps in the reservoir management process. They are accomplished with the assistance of sophisticated compositional reservoir simulation techniques, which employ intricate systems of non-linear differential equations that operate based on the principles of mass and momentum conservation, as well as the establishment of thermodynamic equilibrium between the existing phases. The latter is achieved through the determination, via complex iterative numerical methods, of specific equilibrium coefficient values,  $K_i$ , that correspond to the existing gas and liquid phase compositions. The iterative numerical methods which provide the equilibrium coefficients that ensure thermodynamic equilibrium, along with the differential equations that provide pressure and saturation solutions for the gas, liquid and water phases present, must be applied in every grid block of the reservoir model, at each time step, throughout the whole simulation process. In addition, since it is a compositional model, each component present in the multicomponent hydrocarbon mixture is individually inspected.

Considering the complexity and diversity of an actual retrograde gas reservoir undergoing the process of dry gas recycling, as well as the long production period that usually lasts decades, it is evident that the simulation process involves an enormous number of computations that undeniably require an equivalent amount of computational time (CPU time) for their completion. As a result, some means of acceleration of the simulation process is needed. Various approaches are examined, including a new experimental



procedure for the generation of K-values based on the classic Constant Composition Expansion (CCE) and Constant Volume Depletion tests, as well as a technique based on Machine Learning that can provide in a short amount of time representative sets of equilibrium coefficients that characterise the entire system at various reservoir pressures. The derived sets of equilibrium coefficients can then be introduced directly into the simulator, thereby omitting their calculation during the simulation process, leading to a reduction of 50% or more of the required CPU time.



## ΠΕΡΙΛΗΨΗ

Κατά την αξιοποίηση κοιτασμάτων φυσικού αερίου που συνοδεύονται από παραγωγή συμπυκνώματος (gas condensate reservoirs), όταν η πίεση του ταμιευτήρα λάβει τιμές χαμηλότερες του σημείου δρόσου, παρατηρείται το φαινόμενο δημιουργίας υγρού συμπυκνώματος, ιδιαίτερα στην περιοχή πέριξ των παραγωγικών γεωτρήσεων, το οποίο καταλαμβάνει μέρος του πορώδους και παγιδεύεται σε αυτό. Αποτέλεσμα της παραπάνω διαδικασίας είναι η μείωση της παραγωγής, αλλά και η απώλεια σημαντικής ποσότητας υγρού συμπυκνώματος το οποίο αποτελεί προϊόν με σημαντική οικονομική αξία. Συνήθης πρακτική για την διαχείριση ταμιευτήρων αυτού του τύπου, αποτελεί η εκ νέου αεριοποίηση του παραχθέντος υγρού συμπυκνώματος μέσω αλλαγής της σύστασης του ρευστού του ταμιευτήρα. Η αλλαγή της σύστασης επιτυγχάνεται με την επανεισπίεση (ανακύκλωση) ξηρού αερίου μέσα στον ταμιευτήρα, το οποίο συνήθως προέρχεται από τον ίδιο τον ταμιευτήρα κατά το διαχωρισμό του παραγόμενου ρευστού στους διαχωριστήρες της επιφάνειας. Η πρακτική αυτή αναφέρεται στη διεθνή βιβλιογραφία με τον όρο Gas Recycling.

Η διαδικασία του gas recycling όντας πολύπλοκη και εξαιρετικά σύνθετη όσον αφορά τις μεταβολές συστάσεων που πραγματοποιούνται μέσα στον ταμιευτήρα, δεν είναι δυνατό να μοντελοποιηθεί με χρήση απλών τεχνικών προσομοίωσης ταμιευτήρων τύπου black oil. Στην περίπτωση αυτή, για το σχεδιασμό και την βελτιστοποίηση της διαδικασίας είναι αναγκαία η χρήση των λεγόμενων μοντέλων πλήρους σύστασης (compositional models). Κατά την προσομοίωση με μοντέλα πλήρους σύστασης, γίνεται χρήση πολύπλοκων συστημάτων μη γραμμικών διαφορικών εξισώσεων για τον υπολογισμό των πιέσεων και κορεσμών των φάσεων που βρίσκονται μέσα στον ταμιευτήρα, οι οποίες διέπονται από τις αρχές διατήρησης μάζας και ορμής, αλλά και πολύπλοκων επαναληπτικών αριθμητικών μεθόδων οι οποίες παρέχουν τις τιμές των συντελεστών θερμοδυναμικής ισορροπίας,  $K_i$ , που εξασφαλίζουν την απαιτούμενη θερμοδυναμική ισορροπία μεταξύ των υπαρχουσών φάσεων. Οι παραπάνω υπολογισμοί εκτελούνται για το σύνολο των κελιών του μοντέλου του ταμιευτήρα και για όλες τις χρονικές στιγμές, καθ' όλη τη διάρκεια της προσομοίωσης, ενώ κάθε συστατικό του πολυσυστατικού μείγματος παρακολουθείται ξεχωριστά.

Συνεπώς, η προσομοίωση ενός πραγματικού ταμιευτήρα αέριων συμπυκνωμάτων ο οποίος υφίσταται την διαδικασία ανακύκλωσης αερίου, αποτελεί μια εξαιρετικά πολύπλοκη διαδικασία αφού εμπεριέχει ένα τεράστιο υπολογιστικό μέρος το οποίο αναπόφευκτα οδηγεί σε σημαντικά αυξημένο χρόνο προσομοίωσης της τάξης των ημερών. Επομένως, γίνεται φανερό η ανάγκη εύρεσης ενός τρόπου επιτάχυνσης της διαδικασίας προσομοίωσης. Στην εργασία αυτή, ερευνώνται τεχνικές που μπορούν να οδηγήσουν στη

ταχεία συλλογή αντιπροσωπευτικών τιμών των συντελεστών ισορροπίας, όπως η ανάπτυξη μιας καινούργιας πειραματικής διαδικασίας βασιζόμενης στο κλασικά πειράματα Εκτόνωσης υπό Σταθερή Σύσταση (Constant Composition Expansion – CCE) και υπό Σταθερό Όγκο (Constant Volume Depletion – CVD) αλλά και μιας μεθόδου βασιζόμενης σε τεχνικές Μηχανικής Εκμάθησης. Η εκ των προτέρων γνώση των συντελεστών ισορροπίας που χαρακτηρίζουν το σύστημα σε διάφορες πιέσεις ταμειυτήρα, και η εισαγωγή τους μέσα στο μοντέλο της προσομοίωσης, παρακάμπτει την χρονοβόρα διαδικασία υπολογισμού τους από το ίδιο το μοντέλο και μπορεί να οδηγήσει σε μείωση του απαιτούμενου υπολογιστικού χρόνου κατά ποσοστό 50% ή και περισσότερο.



# TABLE OF CONTENTS

<b>ACKNOWLEDGEMENTS</b> .....	v
<b>ABSTRACT</b> .....	vii
<b>ΠΕΡΙΛΗΨΗ</b> .....	ix
<b>TABLE OF CONTENTS</b> .....	xi
<b>LIST OF FIGURES</b> .....	xv
<b>LIST OF TABLES</b> .....	xxii
<b>1 INTRODUCTION</b> .....	1
1.1 Basic principles for fluid flow in porous media.....	1
1.1.1 Fluid Saturation .....	1
1.1.2 Permeability .....	2
1.1.3 Relative Permeability Curves.....	3
1.2 Phase Envelopes.....	5
1.2.1 Introduction.....	5
1.2.2 Single-Component Systems .....	5
1.2.3 Binary Systems.....	7
1.2.4 Multi-Component Systems .....	9
1.3 Reservoir Types Defined With Reference To Phase Diagrams .....	10
1.4 Retrograde Behaviour of Gas Condensate Systems .....	13
1.5 Condensate Blockage and the need for Gas Recycling .....	15
1.6 Need for computational acceleration during compositional simulation processes .....	17
1.7 Purpose and Objectives .....	18
<b>2 EQUATIONS OF STATE</b> .....	20
2.1 Definition of equilibrium ratio, $K_i$ .....	20
2.2 Fugacity and fugacity coefficient.....	21

2.3	Cubic Equations of State .....	23
2.3.1	van der Waals EoS (vdW EoS) .....	23
2.3.2	Redlich-Kwong EoS (RK EoS).....	25
2.3.3	Soave-Redlich-Kwong EoS (SRK EoS) .....	26
2.3.4	Peng-Robinson EoS (PR EoS) .....	27
2.4	Mixing rules.....	31
2.4.1	Roots selection .....	33
2.5	Volume translation (volume shift) .....	34
2.6	C <sub>7+</sub> characterisation .....	37
<b>3</b>	<b>BASIC PRINCIPLES GOVERNING RESERVOIR SIMULATION PROCESSES .....</b>	<b>40</b>
3.1	Black-oil modelling and Compositional modelling .....	41
3.2	Basic principles of compositional modelling.....	42
3.2.1	Introduction.....	42
3.2.2	Compositional modelling equations .....	42
3.2.3	Discretisation and solution techniques of partial differential equations .....	45
3.3	Phase-stability analysis.....	48
3.3.1	Graphical interpretation of phase stability .....	48
3.3.2	Michelsen's stability test algorithm.....	52
3.4	Phase split.....	57
3.4.1	Two-phase flash algorithm .....	60
3.5	CPU time requirements and importance of the in advance knowledge of K-values .....	64
<b>4</b>	<b>SOURCES OF K-VALUES .....</b>	<b>66</b>
4.1	Determination of equilibrium ratios using empirical correlations .....	66
4.1.1	A simplified method for the determination of K-values .....	67
4.1.2	Wilson's method (1968) .....	68
4.1.3	Hoffman et al. correlation (1953).....	69
4.1.4	Standing's method (1979).....	70



4.1.5	The Convergence Pressure method .....	70
4.1.6	Whitson & Torp's correlation (1981) .....	74
4.2	Equilibrium coefficients of the Plus Fraction .....	75
4.2.1	Katz & Hachmuth's correlation (1937) .....	75
4.2.2	Standing's method (1979).....	75
4.2.3	Winn's correlation (1954).....	76
4.2.4	Campbell's method (1976) .....	76
4.3	Correlations for non-hydrocarbon components .....	76
4.3.1	Lohrenze et al.'s correlations (1963).....	76
4.4	Equilibrium coefficients based on an EoS .....	77
4.5	Introduction to routine laboratory PVT tests .....	78
4.5.1	Constant Composition (Constant Mass) Expansion test .....	79
4.5.2	Constant Volume Depletion (CVD) test .....	82
4.6	The extended Constant Volume Depletion (eCVD) experimental method .....	85
4.6.1	Gathering of K-value data from the extended CVD test.....	88
<b>5</b>	<b>METHODOLOGY – RESULTS .....</b>	<b>97</b>
5.1	Depletion scenarios .....	99
5.1.1	Natural depletion .....	99
5.1.2	Water flooding .....	102
5.2	Gas recycling scenarios .....	105
5.2.1	Gas recycling 80% (direct flash at stc) .....	106
5.2.2	Gas recycling 60% (direct flash at stc) .....	111
5.2.3	Gas recycling 40% (direct flash at stc) .....	115
5.2.4	Gas Recycling 20% (direct flash at stc).....	118
5.2.5	Gas Recycling 80% (separators train) .....	122
5.2.6	Gas Recycling 40% (separators train) .....	133
5.3	Conclusions .....	138



**REFERENCES**



## LIST OF FIGURES

<b>Figure 1.1:</b> Relative permeability curves of a particular rock for a gas-oil system (Ezekwe, 2010). ....	4
<b>Figure 1.2:</b> Relative permeability curves for a gas condensate system (Ezekwe, 2010). ....	4
<b>Figure 1.3:</b> Pressure-volume phase diagram for a single-component system (Standing, 1977). ....	6
<b>Figure 1.4:</b> Pressure-temperature phase diagram for a single-component system (Danesh, 1998). ....	7
<b>Figure 1.5:</b> Typical pressure-volume diagram for binary mixtures (Danesh, 1998). ....	7
<b>Figure 1.6:</b> Pressure-temperature diagram (phase envelope) for a binary system (Ezekwe, 2010). ....	8
<b>Figure 1.7:</b> Pressure-temperature phase diagram for the C <sub>2</sub> /nC <sub>7</sub> mixture at various concentrations of C <sub>2</sub> (Kay, 1938). ....	9
<b>Figure 1.8:</b> Typical pressure-temperature diagram of a multicomponent system (Ahmed, 2010). ....	9
<b>Figure 1.9:</b> Typical phase envelope of an ordinary black oil (Ahmed, 2010). ....	10
<b>Figure 1.10:</b> Typical phase envelope of a volatile oil. Numerous quality lines are crossed rapidly during the isothermal pressure depletion (E-F), resulting in the vaporisation of even 50% of the liquid volume for a small reduction in pressure, hence the term volatile. ....	11
<b>Figure 1.11:</b> Phase envelope of a wet gas reservoir. The pressure and temperature conditions of the surface facilities (Sep.) fall within the two-phase region. ....	11
<b>Figure 1.12:</b> Phase envelope of a dry gas reservoir. Due to lighter composition, the phase envelope is shifted counter-clockwise hence, the pressure and temperature conditions of the surface facilities (Sep.) are outside the two-phase region. ....	12
<b>Figure 1.13:</b> Typical phase envelope of a retrograde gas condensate reservoir (Ahmed, 2010). ....	12
<b>Figure 1.14:</b> Typical phase envelope of a near-critical gas condensate reservoir. During the isothermal pressure depletion (1-2) numerous quality lines are crossed for a slight pressure reduction (Ahmed, 2010). ....	13
<b>Figure 1.15:</b> Typical phase envelope of a gas condensate system illustrating retrograde condensation along the ABDE line (Ezekwe, 2010). ....	14
<b>Figure 1.16:</b> Schematic illustration of the entrapment of liquid condensate in the pores of the reservoir rock. ....	15
<b>Figure 1.17:</b> Condensate yield (STB/MMscf) as a function of pressure (b), for a gas retrograde reservoir undergoing isothermal pressure depletion along line BI (a) (Dake, 2001). ....	16
<b>Figure 1.18:</b> Schematic illustration of the dry gas recycling process. ....	17
<b>Figure 2.1:</b> Binary Interaction Coefficients ( $k_{ij}$ ) for the SRK and PR EoS (Whitson, 2000). ....	33

<b>Figure 2.2:</b> Characterisation of the plus fraction (Pedersen et al. 2014). ....	39
<b>Figure 3.1:</b> A gridblock showing fluid flow in three directions (Ezekwe, 2010). ....	43
<b>Figure 3.2:</b> Principle of stability analysis for a binary mixture (Pedersen et al. 2014). ....	49
<b>Figure 3.3:</b> Gibbs energy surface for a binary system (Whitson, 2000). ....	50
<b>Figure 3.4:</b> The feed composition F is separated into the two equilibrated phases B and D characterised with equal chemical potential values, resulting in reduced Gibbs energy (Danesh, 1998). ....	51
<b>Figure 3.5:</b> Gibbs energy plots illustrating two false two-phase solutions yielding only a local minimum in the mixture Gibbs energy and the correct three-phase solution (Baker et al., 1982; Whitson, 2000). ...	52
<b>Figure 3.6:</b> Michelsen's parallel tangent plane criterion for phase stability. The figure illustrates the case of an unstable mixture with the parallel tangent plane of the second phase composition located below the tangent plane of the original mixture composition (Whitson, 2000). ....	53
<b>Figure 3.7:</b> Flow chart of the flash calculation algorithm using an EoS. ....	63
<b>Figure 4.1:</b> Equilibrium ratios for a hydrocarbon system on a K-value/Pressure log-log diagram converging to unity at the convergence pressure, $p_k$ (Ahmed, 2010). ....	71
<b>Figure 4.2:</b> Convergence pressures for binary systems. (Gas Processors Suppliers Association, Engineering Data Book, 10th Ed., 1978). ....	72
<b>Figure 4.3:</b> Rzasa et al.'s convergence pressure correlation (American Institute of Chemical Engineers). ....	74
<b>Figure 4.4:</b> CCE laboratory test for a) a crude oil sample and b) a gas condensate sample. ....	81
<b>Figure 4.5:</b> Pressure/Relative volume diagram for a black oil sample showing an apparent discontinuity and a change in slope at the bubble point pressure, representing the transition from the single-phase to the two-phase system ("Core Laboratories Good Oil Company Oil Well No. 4 PVT Study," Core Laboratories, Houston). ....	82
<b>Figure 4.6:</b> Pressure/Relative volume diagram for a gas condensate sample showing no apparent change in slope at the dew point pressure (Danesh, 1998). ....	82
<b>Figure 4.7:</b> CVD laboratory test procedure for a gas condensate sample. ....	84
<b>Figure 4.8:</b> Schematic illustration of the new suggested extended CVD experimental procedure for a gas condensate sample with direct flash of the released gas at standard conditions. ....	86
<b>Figure 4.9:</b> Schematic illustration of the new suggested extended CVD experimental procedure for a gas condensate sample with the introduction of a series of separators before flashing of the released gas at standard conditions. ....	87
<b>Figure 4.10:</b> Schematic illustration of the counter-clockwise shift of a phase envelope for a gas condensate system as a result of lighter fluid composition. Along the isothermal production path at the same	

pressure  $P_1$ , the phase envelope belonging to the leaner composition shows a reduced liquid percentage due to revaporisation. .... 88

**Figure 4.11:** Schematic illustration of the extended CVD experimental process for the simulation of dry gas recycling in a gas condensate reservoir. .... 94

**Figure 5.1:** Phase envelope of the reservoir fluid typical of a retrograde gas condensate system. .... 98

**Figure 5.2:** Natural depletion scenario by pressure reduction. The variation in oil saturation throughout the years is evident. .... 99

**Figure 5.3:** Average reservoir pressure (psia) for the ten year production period of the natural depletion scenario. .... 100

**Figure 5.4:** Average liquid condensate saturation (fraction) for the ten year production period of the natural depletion scenario. .... 100

**Figure 5.5:** Pressure/K-values plots for the natural depletion scenario showing an exact match between the simulation derived and CCE derived data. .... 101

**Figure 5.6:** The water flooding scenario was designed to check whether water injection and well positioning have an impact on the equilibrium coefficient values. .... 102

**Figure 5.7:** Average reservoir pressure (psia) for the ten year production period of the water flooding scenario. The amount of the injected water is not sufficient to provide pressure maintenance. .... 103

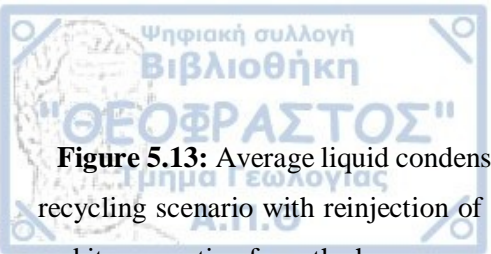
**Figure 5.8:** Average liquid condensate saturation (fraction) for the ten year production period of the water flooding scenario. The retrograde condensation is more pronounced compared to the natural depletion scenario because of the much more reduced reservoir pressure at the last years of the production period. .... 103

**Figure 5.9:** Pressure/K-values plots for the water flooding scenario showing an exact match between the simulation and CCE data demonstrating that water injection in the reservoir and well positioning do not affect the derived K-values. .... 104

**Figure 5.10:** Cell (3,2) in the 10x10 block of the simplistic gas condensate reservoir whose composition was regarded as representative of the average overall reservoir composition at the times of recalculation of the injection gas composition. .... 105

**Figure 5.11:** Gas recycling scenario where 80% of the produced gas is reinjected in the reservoir as dry gas after its direct flash at surface conditions and its separation from the heavy components. .... 107

**Figure 5.12:** Average reservoir pressure (psia) for the ten year production period of the gas recycling scenario with reinjection of 80% of the produced gas after its direct flash at surface conditions and its separation from the heavy components. A change in slope at five years of production indicates a partial pressure maintenance, owing to the increased amount of reinjection gas during the last five years of production. .... 108



**Figure 5.13:** Average liquid condensate saturation (fraction) for the ten year production period of the gas recycling scenario with reinjection of 80% of the produced gas after its direct flash at surface conditions and its separation from the heavy components. The observed revaporisation happens due to a change in the reservoir fluid's composition as a result of the gas recycling process and not because of a reduced reservoir pressure. .... 108

**Figure 5.14:** Pressure/K-values plots for the gas recycling scenario with reinjection of 80% of the produced gas after its direct flash at surface conditions and its separation from the heavy components compared with the results of the CCE experiment. The diagrams show a good match between the simulation and the CCE derived data although some scattering is observed at lower pressures where the CCE underestimates the K-values. .... 109

**Figure 5.15:** Pressure/K-values plots for the gas recycling scenario with reinjection of 80% of the produced gas after its direct flash at surface conditions and its separation from the heavy components compared with the results of the eCVD experiment. The simulation data exhibit a perfect match when compared with the results of the extended CVD for components up to C<sub>11</sub>C<sub>11</sub>, excluding CO<sub>2</sub>. .... 110

**Figure 5.16:** Gas recycling scenario where 60% of the produced gas is reinjected in the reservoir as dry gas after its direct flash at surface conditions and its separation from the heavy components. .... 111

**Figure 5.17:** Average reservoir pressure (psia) for the ten year production period of the gas recycling scenario with reinjection of 60% of the produced gas after its direct flash at surface conditions and its separation from the heavy components. The amount of the re reinjected gas is not sufficient to provide pressure maintenance and there is a steady decline in reservoir pressure. .... 112

**Figure 5.18:** Average liquid condensate saturation (fraction) for the ten year production period of the gas recycling scenario with reinjection of 60% of the produced gas after its direct flash at surface conditions and its separation from the heavy components. The observed revaporisation happens due to a change in the reservoir fluid's composition, as a result of the gas recycling process, in combination with the reduced reservoir pressure. .... 112

**Figure 5.19:** Pressure/K-values plots for the gas recycling scenario with reinjection of 60% of the produced gas after its direct flash at surface conditions and its separation from the heavy components, compared with the results of the CCE experiment. The diagrams show a good match between the simulation and the CCE derived data even though the CCE experiment seems to slightly underestimate the K-values for the heavy components. Some scattering is observed at lower pressures but less pronounced than in the previous 80% scenario. .... 113

**Figure 5.20:** Pressure/K-values plots for the gas recycling scenario with reinjection of 60% of the produced gas after its direct flash at surface conditions and its separation from the heavy components

compared with the results of the eCVD experiment. The simulation data exhibit a perfect match when compared with the results of the extended CVD for components up to C<sub>11</sub>C<sub>11</sub>, excluding CO<sub>2</sub>. ..... 114

**Figure 5.21:** Gas recycling scenario where 40% of the produced gas is reinjected in the reservoir as dry gas after its direct flash at surface conditions and its separation from the heavy components. .... 115

**Figure 5.22:** Average reservoir pressure (psia) for the ten year production period of the gas recycling scenario with reinjection of 40% of the produced gas after its direct flash at surface conditions and its separation from the heavy components. The amount of the injected gas was not sufficient to provide pressure maintenance and there was a steady decline in reservoir pressure. .... 116

**Figure 5.23:** Average liquid condensate saturation (fraction) for the ten year production period of the gas recycling scenario with reinjection of 40% of the produced gas after its direct flash at surface conditions and its separation from the heavy components. Revaporisation happens due the reduced reservoir pressure, since the amount of the injected gas is not sufficient to provide reservoir-scale compositional changes. .... 116

**Figure 5.24:** Pressure/K-values plots for the gas recycling scenario with reinjection of 40% of the produced gas after its direct flash at surface conditions and its separation from the heavy components compared with the results of the CCE experiment. The diagrams show a good match between the simulation and the CCE derived data even though the CCE experiment seems to slightly underestimate the K-values for the heavy components. .... 117

**Figure 5.25:** Gas recycling scenario where 20% of the produced gas is reinjected in the reservoir as dry gas after its direct flash at surface conditions and its separation from the heavy components. .... 119

**Figure 5.26:** Average reservoir pressure (psia) for the ten year production period of the gas recycling scenario with reinjection of 20% of the produced gas after its direct flash at surface conditions and its separation from the heavy components. In this scenario the reservoir pressure was reduced in such a degree that caused the production wells to switch from producing with a fixed rate to producing with a fixed bottomhole pressure and that explains the change in slope at the end of the diagram. .... 120

**Figure 5.27:** Average liquid condensate saturation (fraction) for the ten year production period of the gas recycling scenario with reinjection of 20% of the produced gas after its direct flash at surface conditions and its separation from the heavy components. The liquid saturation curve of this scenario is similar to the liquid saturation curves of the depletion scenarios. .... 120

**Figure 5.28:** Pressure/K-values plots for the gas recycling scenario with reinjection of 20% of the produced gas after its direct flash at surface conditions and its separation from the heavy components compared with the results of the CCE experiment. The diagrams indicate a very good match between the simulation and the CCE derived data. This scenario presents less scattering of the K-values since the amount of the reinjection gas is small. .... 121



**Figure 5.29:** Gas recycling scenario where 80% of the produced gas is reinjected in the reservoir after passing through a system of two separators before arriving at the tank at surface conditions. Separation of liquid and dry gas is performed at each stage and the total amount of separated dry gas is recombined before being reinjected back in the reservoir. .... 123

**Figure 5.30:** The produced gas passes through a train of separators before its recombination and reinjection in the reservoir. .... 125

**Figure 5.31:** At each separation stage the generated dry gas is collected and the remaining liquid condensate is forwarded to the next separation stage. .... 125

**Figure 5.32:** Average reservoir pressure (psia) for the twenty year production period of the gas recycling scenario with reinjection of 80% of the produced gas, after passing through a system of two separators before reaching the tank surface conditions. Separation of liquid and dry gas is performed at each stage and the total amount of separated dry gas is recombined before being reinjected back in the reservoir. The amount of reinjection gas provides partial pressure maintenance so that the production period can be prolonged to twenty years without major decline in reservoir pressure. .... 130

**Figure 5.33:** Average liquid condensate saturation (fraction) for the twenty year production period of the gas recycling scenario with reinjection of 80% of the produced gas after passing through a system of two separators before reaching the tank surface conditions. Condensate revaporisation is happening as a response to the reservoir's overall composition being modified by the gas recycling process rather than reservoir pressure decline. .... 130

**Figure 5.34:** Pressure/K-values plots for the gas recycling scenario with reinjection of 80% of the produced gas after passing through a system of two separators before reaching the tank surface conditions. The CCE experiment underestimates the K-values of the light components and overestimates the K-values of the heavy components, therefore it is not suitable to describe the process of production and gas injection of this scenario in terms of the K-values. .... 131

**Figure 5.35:** Pressure/K-values plots for the gas recycling scenario with reinjection of 80% of the produced gas after passing through a system of two separators before reaching the tank surface conditions compared with the results of the eCVD experiment. The extended CVD derived K-values can present a good match with the simulation derived values for components up to C11C11 and excluding the CO<sub>2</sub>, better than the classic CCE experiment. .... 132

**Figure 5.36:** Gas recycling scenario where 40% of the produced gas is reinjected in the reservoir after passing through a system of two separators before reaching the tank at surface conditions. Separation of liquid and dry gas is performed at each stage and the total amount of separated dry gas is recombined before being reinjected back in the reservoir. .... 133



**Figure 5.37:** Average reservoir pressure (psia) for the ten year production period of the gas recycling scenario with reinjection of 40% of the produced gas, after passing through a system of two separators before reaching the tank surface conditions. The amount of reinjection gas does not provide much pressure maintenance and the reservoir pressure reaches almost 700 psia at the end of the production period. .... 136

**Figure 5.38:** Average liquid condensate saturation (fraction) for the ten year production period of the gas recycling scenario with reinjection of 40% of the produced gas after passing through a system of two separators before reaching the tank surface conditions. Condensate revaporisation is happening as a response to the reservoir's decline in pressure and not the reservoir overall composition being modified by the gas recycling process. .... 136

**Figure 5.39:** Pressure/K-values plots for the gas recycling scenario with reinjection of 40% of the produced gas after passing through a system of two separators before reaching the tank surface conditions. The CCE experiment underestimates the K-values of the light components and overestimates the K-values of the heavy components, although the scattering of the simulation derived K-values is not as intense as in the previous 80% reinjection scenario. .... 137

**Figure 5.40:** Pressure/Liquid saturation plot demonstrating the change in average liquid saturation in the reservoir for the scenarios of natural depletion, water flooding and gas injection. The reduced amount of liquid condensate in the reservoir throughout the production is evident for the scenario of gas injection. .... 139

**Figure 5.41:** Pressure/Liquid saturation plot for the comparison of the depletion scenarios and the gas injection scenarios where the gas recycling process benefits the production. .... 139

**Figure 5.42:** Pressure/Liquid saturation plot for the comparison of the depletion scenarios with the gas injection scenarios with an insufficient amount of injection gas. The liquid saturation curves of the 20% and 40% reinjection scenarios are very similar to the saturation curves of the depletion scenarios. .... 140



## LIST OF TABLES

<b>Table 2.1:</b> Comparison of the mathematical expressions of the vdW, RK, SRK and PR equations of state, along with the expressions for the calculation of their parameters. ....	29
<b>Table 2.2:</b> Comparison of the cubic forms of the vdW, RK, SRK and PR equations of state. ....	30
<b>Table 2.3:</b> Comparison of the expressions for the calculation of the parameter $a$ between the SRK and PR equations of state. ....	30
<b>Table 2.4:</b> Values for the dimensionless shift parameters, $s_i$ , for pure hydrocarbon components (Jhaveri & Youngren, 1988). ....	37
<b>Table 2.5:</b> Positive correlation coefficients values for the estimation of dimensionless shift parameters for hydrocarbons heavier than C6 (Jhaveri & Youngren, 1988). ....	37
<b>Table 3.1:</b> Number of equations that control hydrocarbon fluid flow through a porous medium in compositional reservoir modelling. ....	45
<b>Table 3.2:</b> Total number of selected unknown variables for equations (3.1)-(3.10). ....	45
<b>Table 3.3:</b> Stability test result selection. ....	56
<b>Table 4.1:</b> Values for the coefficients $a_i$ and $b_i$ for the C <sub>2</sub> – C <sub>7</sub> fractions (Ahmed, 2010). ....	68
<b>Table 4.2:</b> Optimised values of $b_i$ and $T_{bi}$ from Eqs. (4.7) and (4.8) for use in Standing's low pressure K-value correlation (Ahmed, 2010). ....	70
<b>Table 4.3:</b> Outline of the extended CVD experimental process with a summary of the related parameters at each step. ....	95
<b>Table 5.1:</b> Initial reservoir fluid composition. ....	97
<b>Table 5.2:</b> Reinjection dry gas composition at the start of the production period based on the initial overall reservoir fluid composition for the gas recycling scenarios with a direct flash at stc. ....	106
<b>Table 5.3:</b> Composition of the injected gas after five years of production calculated based on the composition of cell (3,2) that was considered as representative of the average reservoir fluid composition after five years of production and the process of dry gas recycling. ....	107
<b>Table 5.4:</b> Composition of the injected gas after five years of production calculated based on the composition of cell (3,2) that was regarded as representative of the average reservoir fluid composition after five years of production and the process of dry gas recycling. ....	112
<b>Table 5.5:</b> Composition of the injected gas after five years of production calculated based on the composition of cell (3,2) that was regarded as representative of the average reservoir fluid composition after five years of production and the process of dry gas recycling. ....	116

**Table 5.6:** Composition of the injected gas after five years of production calculated based on the composition of cell (3,2) that was regarded as representative of the average reservoir fluid composition after five years of production and the process of dry gas recycling. .... 119

**Table 5.7:** Calculation of the initial reinjection composition by passing the initial overall reservoir fluid composition through a train of separators..... 124

**Table 5.8:** Calculation of the reinjection dry gas composition after five years of production by treating the composition of cell (3,2) through a train of separators for the 80% reinjection scenario. .... 126

**Table 5.9:** Calculation of the reinjection dry gas composition after ten years of production by treating the composition of cell (3,2) through a train of separators for the 80% reinjection scenario. .... 127

**Table 5.10:** Calculation of the reinjection dry gas composition after fifteen years of production by treating the composition of cell (3,2) through a train of separators for the 80% reinjection scenario. .... 128

**Table 5.11:** Calculation of the reinjection dry gas composition after 5 years of production by treating the composition of cell (3,2) through a train of separators for the 40% reinjection scenario. .... 134





# 1 INTRODUCTION

Hydrocarbon reservoirs display a variety of properties and characteristics which are mainly dependent upon the geologic framework, the hydrocarbon fluid that they contain and their prevailing initial pressure and temperature conditions. Based on these properties, reservoirs are classified into different categories which considerably define the production techniques and reservoir management strategies, as well as the drilling units, facilities and installations required for the safe, economically viable and environmentally responsible exploitation of hydrocarbons.

In this introductory chapter, the various reservoir hydrocarbon types are discussed in relation to their Pressure-Volume-Temperature (PVT) phase diagrams. Emphasis is placed on retrograde gas condensate reservoirs, their characteristics and associated problems, i.e. condensate blockage effects that occur during their production. The method of gas recycling is presented for the mitigation of condensate blockage effects responsible for production decline.

## 1.1 Basic principles for fluid flow in porous media

In this section, a number of definitions are briefly presented for the sake of accuracy and better comprehension of rock and fluid properties mentioned in the following chapters.

### 1.1.1 Fluid Saturation

The term fluid saturation refers to the volume occupied by a certain fluid in the pores of a reservoir rock, divided by the total pore volume. Consequently, three kinds of saturation may be encountered in a hydrocarbon reservoir, namely, oil saturation ( $S_o$ ), gas saturation ( $S_g$ ) and water saturation ( $S_w$ ). Saturation is expressed as a fraction or percentage and ranges from zero to 100%. The sum of water and hydrocarbon saturations in a reservoir is always equal to unity:



$$S_o + S_g + S_w = 1 \quad (1.1)$$

From Eq. (1.1) it is evident that if water saturation in the reservoir is low, then hydrocarbon saturations are high and vice versa.

### 1.1.2 Permeability

Another essential property for the description of fluid flow through a porous medium is permeability, as it acts as a controlling factor in the directional movement and the rate at which reservoir fluids flow through the formation. Permeability is a measure of the ability of the porous medium, to transmit fluids through its system of interconnected pore spaces. If the porous medium is completely (100%) saturated with a single fluid, the permeability measured is the absolute permeability (Ezekwe, 2010). Absolute permeability is entirely a property of the rock and not of the fluids flowing through it. It is an anisotropic property, meaning that it does not present the same values for different directions in the same rock formation. In addition, vertical permeability is generally less than horizontal permeability, owing to the nature of the sedimentation process, while at the same time, horizontal permeabilities in the principal directions are also diverse.

When more than one fluids are present in the porous medium, the permeability measured is called the effective permeability to each one of the existing fluids. For instance, effective permeability to oil ( $k_o$ ) is the permeability to oil when water and gas are also present.

Relative permeability ( $k_r$ ) is the ratio of effective permeability to absolute permeability. It ranges from zero to unity and is expressed as follows

$$k_{ro} = \frac{k_o}{k} \quad (1.2)$$

$$k_{rg} = \frac{k_g}{k} \quad (1.3)$$

$$k_{rw} = \frac{k_w}{k} \quad (1.4)$$

In Eqs. (1.2) – (1.4),  $k_{ro}$  = relative permeability to oil,  $k_{rg}$  = relative permeability to gas,  $k_{rw}$  = relative permeability to water,  $k$  = absolute permeability.

### 1.1.3 Relative Permeability Curves

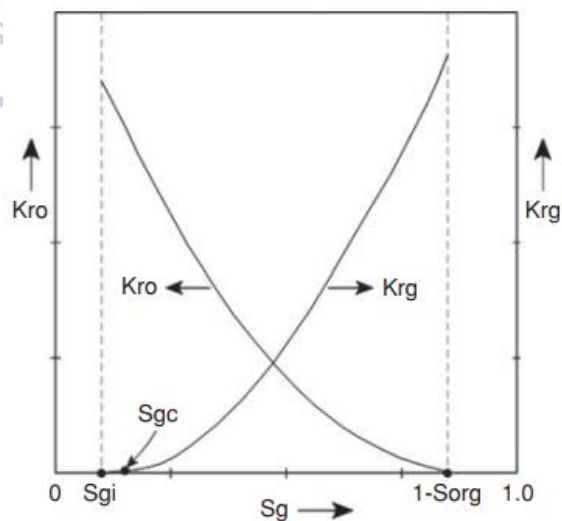
Relative permeability data can be presented graphically in plots called relative permeability curves. In Figure (1.1) a typical plot of the relative permeability curves of a particular rock for a gas-oil system as a function of gas saturation is presented. Relative permeability is plotted as a function of gas saturation ( $S_g$ ) only, as oil saturation ( $S_o$ ) is related to the former by the following simple relationship

$$S_o = 1 - S_g \quad (1.5)$$

According to Fig. 1.1, gas reaches its maximum saturation at point 1- $S_{org}$ . At this point, relative permeability to gas is also at its highest. As gas saturation declines, so does relative permeability to gas and it becomes zero at the minimum gas saturation at point  $S_{gc}$ . As far as the oil phase is concerned, taking into account Eqs. 1.1 and 1.5 and the fact that this is a two-phase gas-oil system, it is evident that oil saturation will be maximum at point  $S_{gc}$  where gas saturation is at its minimum. Equivalently, relative permeability to oil is greatest at this point and declines with reducing oil saturation. Taking into consideration all the above observations, it becomes clear that the introduction of a second phase in the system, results in the reduction of the relative permeability to the first phase.

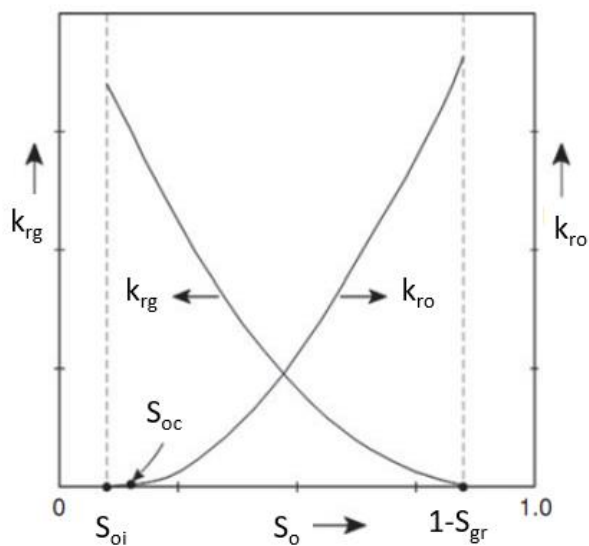
The two marginal saturation values,  $S_{gc}$  and 1- $S_{org}$ , are called critical gas saturation and residual oil saturation, respectively. Critical gas saturation ( $S_{gc}$ ) is the minimum saturation required for gas to become mobile in the reservoir, while residual oil saturation ( $S_{org}$ ) is the lowest possible saturation that oil can obtain and is irreducible below this point.

In the context of a gas condensate reservoir that initially exists as a single-phase vapour, when reservoir pressure falls below the dew point, liquid condensate (oil) begins to form (Section 1.4). At this moment, oil is characterised by its initial saturation ( $S_{oi}$ ) (Fig. 1.2). As pressure further declines, oil saturation increases until it reaches its critical saturation value at point ( $S_{oc}$ ) that marks the beginning of oil mobility in the reservoir. Further increase in oil saturation results in the rise of relative permeability to oil and a simultaneous decrease of relative permeability to gas. However, it should be pointed out that liquid volume in a gas condensate reservoir, seldom exceeds more than 15% to 19% of the pore volume (Ahmed, 2010), an amount generally not adequate to cause mobility of the condensate, yet enough to restrain production by occupying part of the reservoir's pore space.



**Figure 1.1:** Relative permeability curves of a particular rock for a gas-oil system (Ezekwe, 2010).

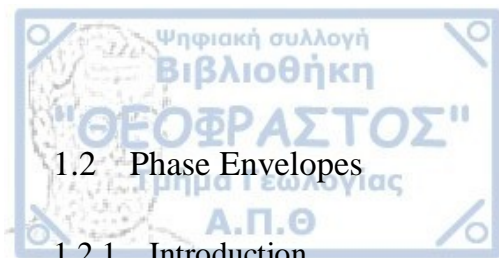
The above description of relative permeability plots can also be adjusted to oil-water and gas-water systems, where the same general principles apply.



**Figure 1.2:** Relative permeability curves for a gas condensate system (Ezekwe, 2010).

It should be pointed out that there are numerous properties that are used to characterise reservoir rocks and fluids, like wettability, isothermal compressibility etc., although, in this section only a brief presentation of the most fundamental properties mentioned throughout this dissertation was made.





## 1.2 Phase Envelopes

### 1.2.1 Introduction

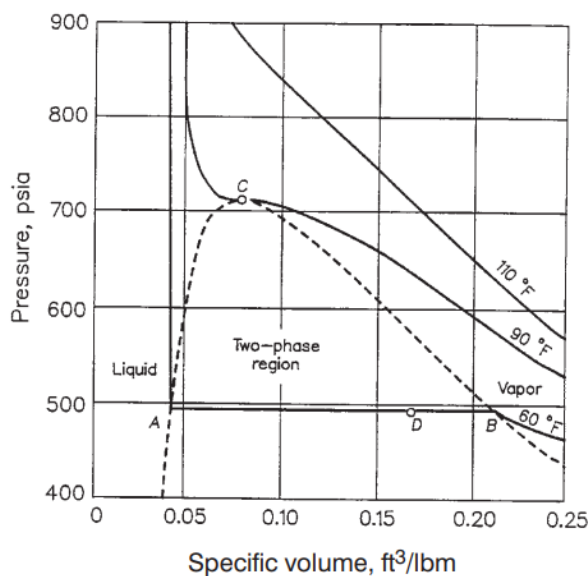
The prediction of volumetric and phase behaviour of hydrocarbon fluids is of primary interest in petroleum engineering, as it is necessary for reservoir type determination, establishment of a development plan and estimation of recoverable reserves. The term phase describes a homogeneous part of a system that is physically separated by distinct boundaries from other parts of the system. Hydrocarbons usually exist as liquid phase, (oil or liquid condensate), as well as vapour or gas phase (natural gas), while the solid state is not excluded, as is often indicated by the presence of waxes, asphaltenes or hydrates in the reservoir. The state at which fluids exist in the reservoir, depends on the prevailing pressure and temperature conditions. As these conditions vary during the production life of a reservoir, the phases of fluids change as well. This shift in phases that a fluid undergoes as pressure and temperature conditions change, is referred to as phase behaviour.

Commonly, the phase behaviour of fluid systems is presented on pressure-volume or pressure-temperature diagrams, called phase diagrams or phase envelopes. In literature, the description of phase diagrams generally starts with the introduction of phase diagrams for single-component systems, then proceeds to two-component (or binary systems), and concludes with phase diagrams for multi-component systems, i.e., hydrocarbon systems which contain hundreds of components and therefore, constitute multi-component mixtures. The same pattern is adopted in this thesis as well.

### 1.2.2 Single-Component Systems

A single-component system is one that only contains one kind of atoms or molecules, for example, a system that is entirely composed of ethane. For the construction of the pressure-volume diagram of a single-component system, the following experiment is assumed. A quantity of ethane is inserted into a cylinder that carries a frictionless piston to assist in the reduction of the cylinder's volume. The temperature inside the cylinder is kept constant throughout the experiment and the fluid is initially kept in low pressure in order to occur as a single-phase vapour. As the volume of the cylinder is reduced, the pressure increases until a point is reached (point B, Fig. 1.3) where the first liquid drop is observed. This point is termed the dew point,  $p_d$ , where the single-phase vapour is in equilibrium with an infinitesimal amount of liquid. As the cylinder volume is further reduced, the amount of generated liquid increases, although the pressure inside the cylinder during this interval, remains constant (line AB, Figure 1.3). As the process continues, point A (Fig. 1.3) is reached where the last gas bubble is observed. This point is termed the bubble point,  $p_b$ , where the single-phase liquid in this case, is in equilibrium with an infinitesimal amount of gas. After

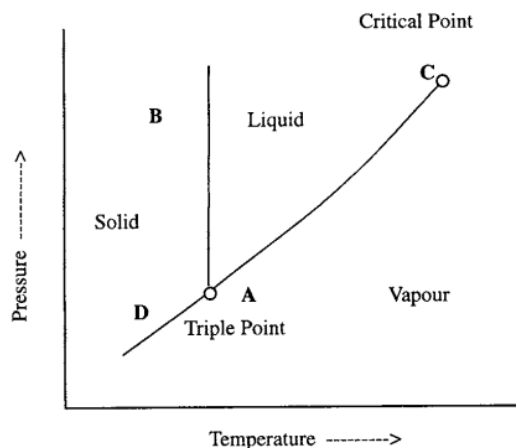
this certain point, as the volume of the cell keeps decreasing, an abrupt rise in pressure is observed, owing to the low compressibility of the liquid phase.



**Figure 1.3:** Pressure-volume phase diagram for a single-component system (Standing, 1977).

This procedure repeated at various temperatures gives the diagram of Fig. 1.3. All the bubble points across line AC form the bubble point curve, while all the dew points across line BC form the dew point curve. The bubble point and dew point curves join at point C which is the critical point. At the critical point, the fluid is characterised by its critical pressure,  $p_c$ , critical temperature,  $T_c$  and critical volume,  $V_c$ . At the critical point all the intensive properties (pressure, temperature, density, composition etc.) are equal for both the vapour and liquid phases and the two phases cannot be distinguished from each other. For a single-component system, the critical point is the maximum temperature and pressure at which two phases, vapour and liquid, can coexist.

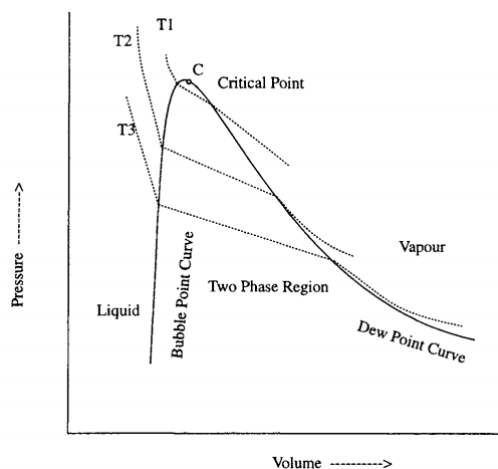
Figure 1.4 is the phase diagram of a single-component system, this time with pressure and temperature being the independent parameters. In this figure, line AC concludes at the critical point and acts as a separation boundary between the two phases. This line is termed the vapour-pressure curve, along which vapour and liquid exist in equilibrium. It is evident that for a specific temperature, a unique pressure exists along line AC where liquid and vapour phases can exist in equilibrium. This is characteristic for single-component systems but it is not the case for binary and multi-component systems as is discussed later.



**Figure 1.4:** Pressure-temperature phase diagram for a single-component system (Danesh, 1998).

### 1.2.3 Binary Systems

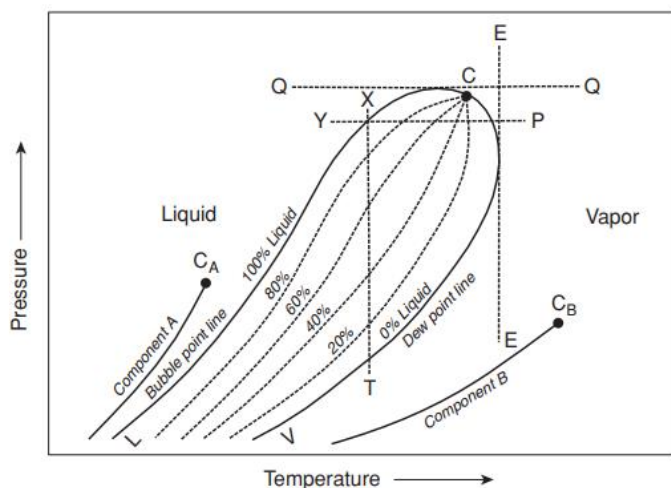
For binary mixtures, the same experiment can be performed, this time by inserting into the cylinder a two-component mixture. The pressure-volume diagram for the binary mixture is given in Figure 1.5. In this diagram, during the isothermal expansion in the two-phase region, the pressure is not constant but decreases as the dew point curve is reached. This is due to compositional changes that take place during this process. It is also important to note that at the dew point, the composition of the vapour phase is that of the entire mixture, since only a negligible amount of liquid is present at the time. Accordingly, at the bubble point the composition of the liquid phase is the same as that of the whole system, since at this point only an infinitesimal volume of gas is present.



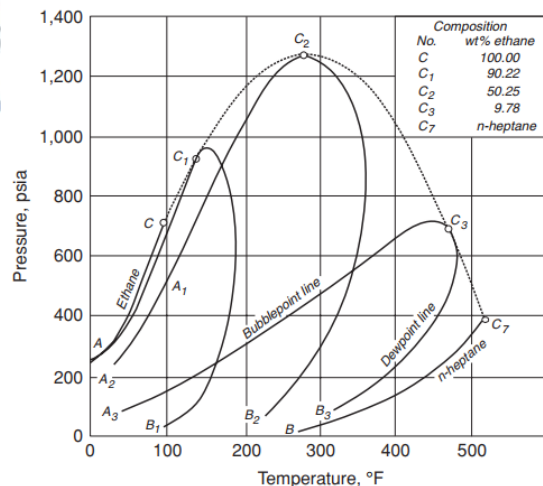
**Figure 1.5:** Typical pressure-volume diagram for binary mixtures (Danesh, 1998).

The p-T diagrams of binary and multi-component systems, are different from p-T diagrams of single-component systems, since the vapour-pressure curve cannot describe the relationship between pressure and temperature if more than one components are present. As a result, the two-phase region is not a line but an area where for a specific temperature, liquid and vapour can exist in equilibrium at various pressures. This area is enclosed by the bubble point curve and the dew point curve and is called a phase envelope. A characteristic p-T diagram for a binary mixture is given in Figure 1.6. Outside of the phase envelope only one phase can exist, i.e., liquid in the region left of the bubble point curve (line LC) and gas in the region right of the dew point curve (line VC). The critical point, C, is no longer the maximum pressure and temperature of the two-phase region, but vapour and liquid can exist in equilibrium in conditions above the critical point. Therefore, the maximum temperature at which two phases can exist regardless of pressure is called the cricondentherm (line EE), while the maximum pressure at which two phases can exist regardless of temperature is called the cricondenbar (line QQ). The dashed lines in the phase envelope that converge at the critical point, are called quality lines and describe the pressure and temperature conditions for equal volumes of liquid. At the bubble point curve there is 100% liquid, while at the dew point curve there is 100% gas.

An important characteristic of binary and multi-component systems is the variation of their thermodynamic and physical properties with composition (Ahmed, 2016). For instance, Figure 1.7 shows the phase envelopes of a  $C_2/nC_7$  mixture for various concentrations of  $C_2$ . Line AC is the vapour pressure curve of pure ethane, while line  $BC_7$  is the vapour pressure curve of pure n-heptane. If the concentration of ethane in the mixture is 90.22% wt., then phase envelope  $A_1C_1B_1$  is formed. Accordingly, if ethane concentration is 50.25% wt., the corresponding phase envelope is  $A_2C_2B_2$  and last, for a mixture containing only 9.78% wt. ethane, phase envelope  $A_3C_3B_3$  is generated.



**Figure 1.6:** Pressure-temperature diagram (phase envelope) for a binary system (Ezekwe, 2010).

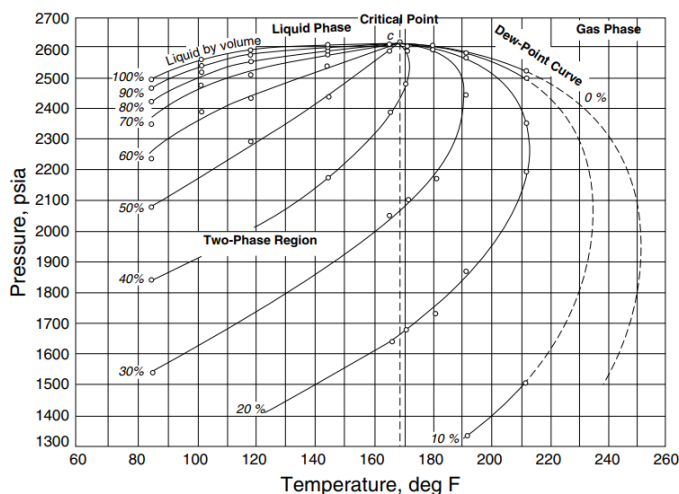


**Figure 1.7:** Pressure-temperature phase diagram for the C<sub>2</sub>/nC<sub>7</sub> mixture at various concentrations of C<sub>2</sub> (Kay, 1938).

Therefore, it is evident that system composition affects the size, as well as the shape of the phase diagram. Another observation is that when one of the constituents becomes predominant, the binary mixture tends to exhibit a relatively narrow phase envelope and displays critical properties close to the predominant component. The size of the phase envelope enlarges noticeably as the composition of the mixture becomes evenly distributed between the two components (Ahmed, 2016).

### 1.2.4 Multi-Component Systems

For multicomponent systems, the phase behaviour in the two-phase region and the shape and nature of their phase diagrams, are essentially similar to binary systems, although more complex, as the number of components increases. A typical phase diagram for a multicomponent system is presented in Figure 1.8. Phase envelopes are used for the classification of reservoir types as is discussed next.



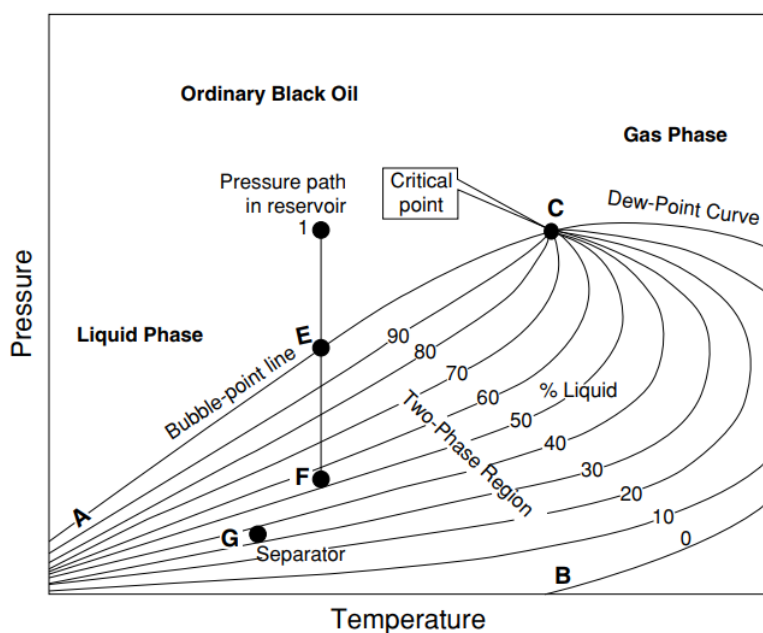
**Figure 1.8:** Typical pressure-temperature diagram of a multicomponent system (Ahmed, 2010).

### 1.3 Reservoir Types Defined With Reference To Phase Diagrams

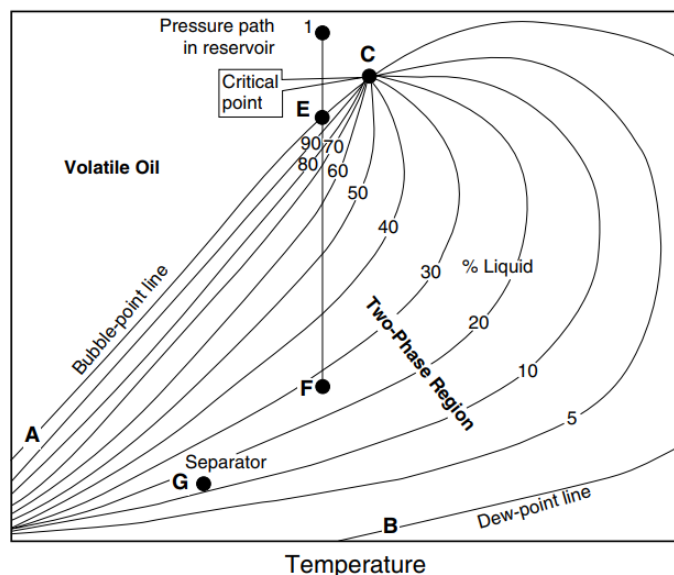
Petroleum reservoirs are generally classified as i) black oil, ii) volatile oil, iii) near critical gas condensate, iv) retrograde gas condensate, v) wet gas and vi) dry gas reservoirs. This classification is dependent on (Ahmed, 2007, 2016):

1. The composition of the reservoir hydrocarbon mixture, which defines the shape and size of the phase envelope,
2. Initial reservoir pressure and temperature conditions,
3. Pressure and temperature conditions of the surface production,
4. Location of the reservoir temperature with respect to the critical temperature and the cricondentherm.

Based on the above parameters, if the initial reservoir temperature,  $T_i$ , is less than the critical temperature, the reservoir is described as a black oil reservoir (Fig. 1.9). Accordingly, if reservoir temperature is close to the critical temperature as shown in Figure 1.10, the reservoir is characterised as a volatile oil reservoir.

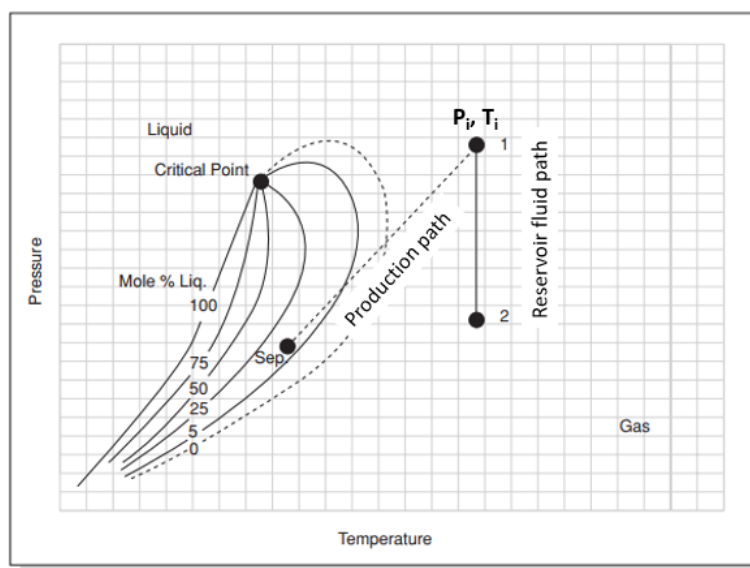


**Figure 1.9:** Typical phase envelope of an ordinary black oil (Ahmed, 2010).



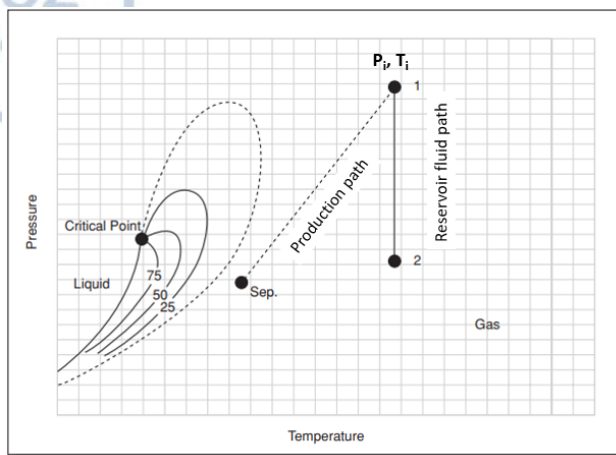
**Figure 1.10:** Typical phase envelope of a volatile oil. Numerous quality lines are crossed rapidly during the isothermal pressure depletion (E-F), resulting in the vaporisation of even 50% of the liquid volume for a small reduction in pressure, hence the term volatile.

Regarding gas reservoirs, if the initial reservoir temperature, is greater than the cricondentherm, the fluid is a single-phase gas and the reservoir is classified as either a wet gas or a dry gas reservoir. In the case of a wet gas, as the fluid is produced, the prevailing pressure and temperature conditions of the surface facilities may fall within the two-phase region. Hence, the gas production at the surface is accompanied by liquid condensation and the reservoir is classified as a wet gas reservoir (Fig. 1.11).

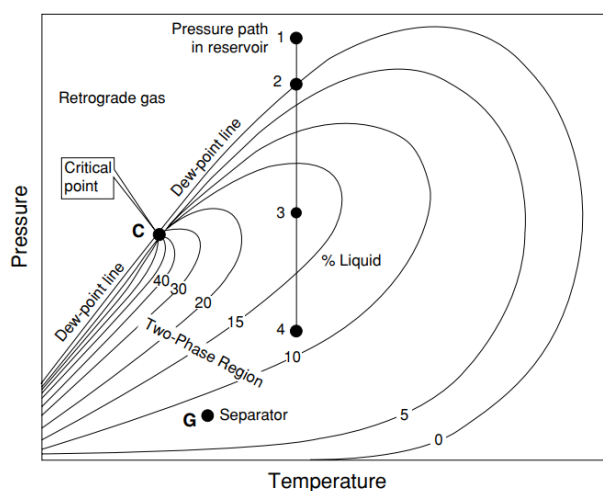


**Figure 1.11:** Phase envelope of a wet gas reservoir. The pressure and temperature conditions of the surface facilities (Sep.) fall within the two-phase region.





**Figure 1.12:** Phase envelope of a dry gas reservoir. Due to lighter composition, the phase envelope is shifted counter-clockwise hence, the pressure and temperature conditions of the surface facilities (Sep.) are outside the two-phase region.



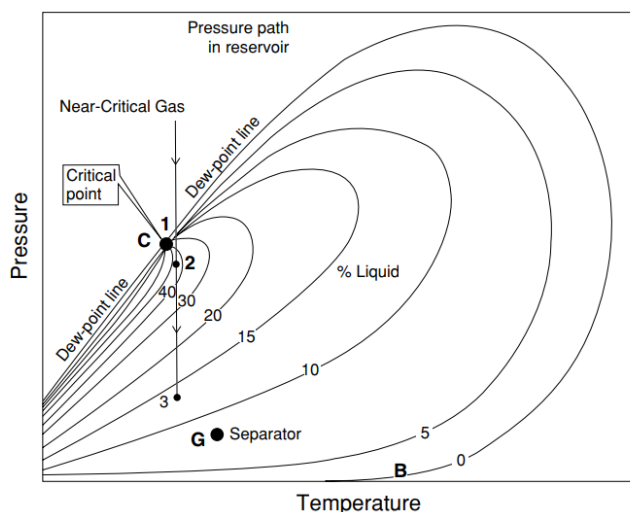
**Figure 1.13:** Typical phase envelope of a retrograde gas condensate reservoir (Ahmed, 2010).

Obviously, liquid condensation only takes place at the surface facilities and not in the reservoir. On the other hand, in a dry gas reservoir, the reservoir fluid mostly consists of methane and non-hydrocarbons such as nitrogen and carbon dioxide. Therefore, this lighter composition leads to a counter-clockwise shift of the phase envelope, so that the pressure and temperature conditions of the surface facilities in this case, fall outside the two-phase region (Fig 1.12). This indicates that the reservoir fluid exists as a single-phase gas both in the reservoir and at the surface facilities, and the only liquid that might be present during dry gas production is water.

If the reservoir temperature lies between the critical temperature and the cricondentherm, the reservoir is classified as a retrograde gas condensate reservoir (Fig. 1.13), while if the reservoir temperature is very



close to the critical temperature, then it is a near-critical gas condensate reservoir (Fig. 1.14). In this latter type of reservoir, after the dew point curve is reached during the isothermal pressure depletion (1-2), a large volume of liquid is rapidly condensed as many quality lines are crossed for a slight reduction in pressure. The retrograde behaviour of gas condensate systems is discussed in detail next (Section 1.4).



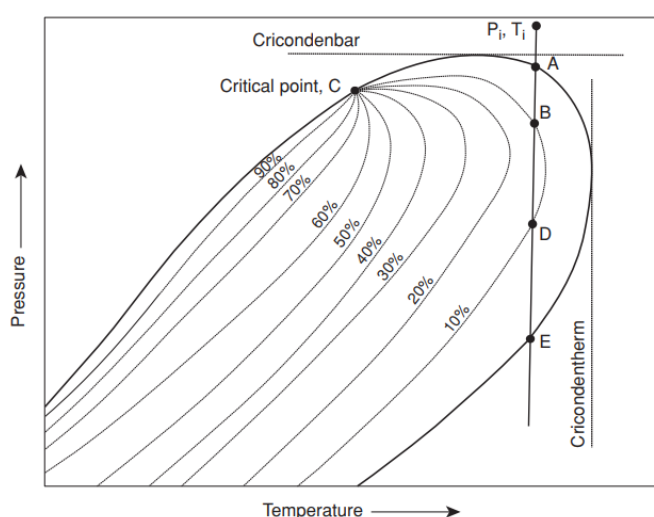
**Figure 1.14:** Typical phase envelope of a near-critical gas condensate reservoir. During the isothermal pressure depletion (1-2) numerous quality lines are crossed for a slight pressure reduction (Ahmed, 2010).

## 1.4 Retrograde Behaviour of Gas Condensate Systems

Reservoirs containing only free gas are termed gas reservoirs. Such a reservoir contains a mixture of hydrocarbons, which exists wholly in the gaseous state. The mixture may be a dry, wet, or condensate gas, depending on the composition of the gas, along with the pressure and temperature at which the accumulation exists (Ahmed, 2010). The occurrence of a gas condensate system is only possible if the reservoir temperature lies between the critical temperature and the cricondentherm on the p-T diagram of the gas condensate system. Figure (1.15) illustrates the phase envelope of a gas condensate reservoir, with  $P_i$  and  $T_i$ , the initial pressure and temperature conditions respectively, that occur in the reservoir. The dashed lines represent regions of constant liquid volume that range from 100% liquid at the bubble point line, to 0% liquid at the dew point line. As the initial conditions are above the upper dew point curve, the system exists as single-phase vapour.

If a production path is considered along the line ABDE, that is, an isothermal natural depletion production of the reservoir, pressure is initially reduced to point A on the dew point curve, where liquid begins to condense in the reservoir. At this point, the light and heavy hydrocarbon components move further apart

due to the decline in pressure, resulting in stronger attraction among the heavy components and thus, liquid condensation. As reservoir pressure further declines, point B is reached along the 10% constant liquid volume line, indicating the presence of 10% liquid and 90% gas in the reservoir at these pressure and temperature conditions. As pressure decline advances from point B to point D, liquid volume obtains a maximum value of approximately 12%, before the beginning of revaporisation at point D where liquid volume drops again to 10%. This is the process during which the amount of molecules that leave the liquid phase is greater than the amount of molecules that enter the liquid phase, prompting the revaporisation of the condensate. Provided that the process continues to reach point E on the lower part of the dew point curve, all the liquid that has condensed is currently revaporised leaving the reservoir with 0% liquid volume.



**Figure 1.15:** Typical phase envelope of a gas condensate system illustrating retrograde condensation along the ABDE line (Ezekwe, 2010).

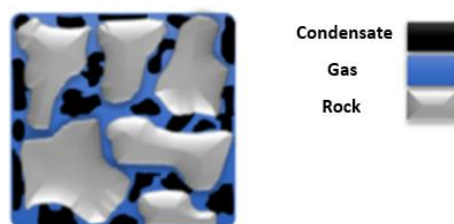
This condensation behaviour, which begins with increasing liquid volume followed by a reversal of liquid volume with pressure reduction at constant temperature in the reservoir, is described as **retrograde condensation** (Ezekwe, 2010). It is made clear that gas condensate reservoirs are quite exceptional in the sense that the thermodynamic behaviour of the reservoir fluid is the regulating parameter for the establishment of the optimum development plan.

Most known gas condensate reservoirs usually occur at pressures of 3,000 – 6,000 psia and temperatures of 200 – 400 °F. These ranges, along with wide variations in composition, provide a great variety of conditions for the physical behaviour of condensate deposits (Ikoku, 1984,1992). Gas condensate reservoirs generally produce light-coloured or colourless stock-tank liquids with gravities above 45 °API and gas-oil ratios in the range of 5,000 – 100,000 scf/STB. Although the initial phase is gas, typically the fluid of commercial interest is the gas condensate (Craft et al., 2015).

It is worth mentioning that during the isothermal pressure depletion along line ABDE, the overall reservoir composition was considered constant throughout the depletion process. This is not accurate for an actual reservoir considering that during condensate generation, the heavier components are gathered in the liquid phase which, as is explained in the following chapters, remains immobile and so none of the heavier components are produced. Consequently, as production progresses, reservoir composition changes resulting in a modified phase envelope and therefore, a different production path than the one previously demonstrated.

## 1.5 Condensate Blockage and the need for Gas Recycling

As mentioned in the previous sections, in a gas condensate reservoir liquid condensation takes place as a response to pressure reduction below the dew point. More specifically, when a gas condensate reservoir is depleted by a reduction in pressure, at a certain time during production, the dew point is reached and this marks the beginning of liquification of the reservoir fluid's heavy ends. The generated liquid, characterised by a saturation less than its critical flow saturation, is trapped in the pores of the reservoir rock unable to move due to surface tension forces (Fig. 1.16). As a result, two problems arise. First, the condensate accumulation blocks the gas flow, reduces the gas relative permeability, and ultimately weakens the well's productivity (Jianyi et al., 2001; Sheng et al., 2013; Wang et al., 2018; Yong et al., 2007), and second, the richer and more valuable hydrocarbon components are retained in the reservoir unable to be produced. This phenomenon is more intense in the near wellbore region where the decline in pressure is more pronounced, resulting in the formation of a condensate bank around the well. This is known as condensate blockage and was first addressed by Muskat (Muskat, 1945; Wang et al., 2018).

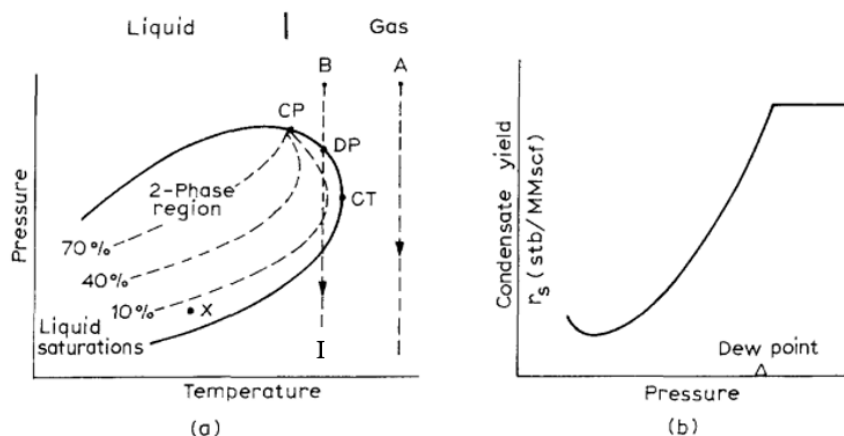


**Figure 1.16:** Schematic illustration of the entrapment of liquid condensate in the pores of the reservoir rock.

The region of condensate blockage may extend in size from tens of feet for lean gas condensate reservoirs to hundreds of feet for rich condensate reservoirs (Hinchman & Barree, 1985; Hameed, 2015). Typically, condensate blockage is significant for low to moderate permeability reservoirs and wells (<50 md). High permeability-thickness (kh) reservoirs experience little effect because most of the pressure drop occurs in the tubing (Noor et al., 2005).

There are several examples of gas condensate fields throughout the world that have displayed a decline in production as a result of condensate blockage. One of them is the Arun field of Indonesia, one of the world's giant retrograde gas reservoirs whose operation started in 1977 by ExxonMobil. In the Arun field, approximately 10 years after production began, a significant loss in well productivity (even more than 50%) occurred in some of the wells (Afidick et al., 1994; Barnum et al., 1995; Rahimzadeh et al., 2016; Silpnarmrmlers et al., 2005).

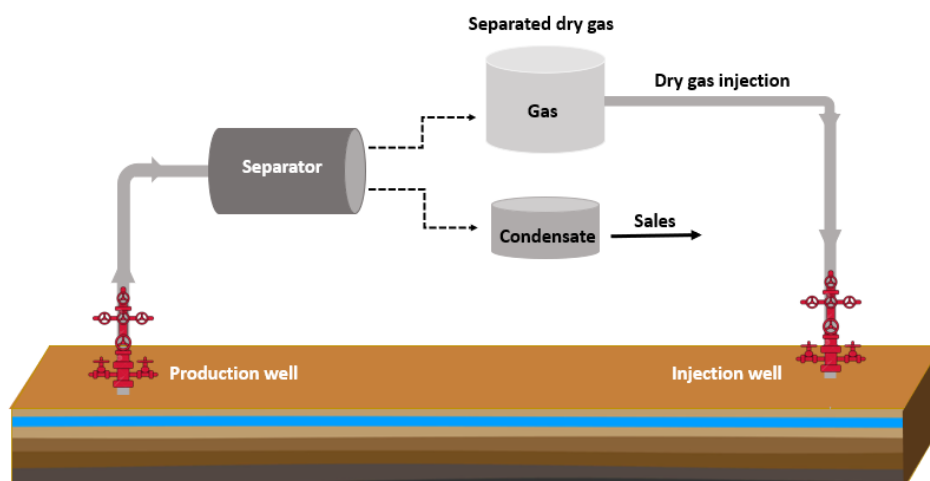
An important PVT parameter that is used to quantify the loss of condensate trapped in the reservoir is the condensate yield,  $r_s$ , (STB/MMscf). Above the dew point, all the liquid hydrocarbons contained in each MMscf of gas are recovered but below the dew point, since liquid is deposited in the reservoir, there is a growing deficiency in the volume of condensate recovered at the surface as the reservoir pressure continues to decline (Fig. 1.17) (Dake, 2001). If the lower dew point curve is reached, then some revaporisation occurs and  $r_s$  begins to increase again although, this situation almost never takes place in an actual reservoir as abandonment occurs at a higher pressure.



**Figure 1.17:** Condensate yield (STB/MMscf) as a function of pressure (b), for a gas retrograde reservoir undergoing isothermal pressure depletion along line BI (a) (Dake, 2001).

Numerous techniques are available for the management of gas condensate reservoirs and the mitigation of condensate blockage effects, including injecting solvents and wettability-alteration chemicals, injecting nitrogen and carbon dioxide, drilling horizontal wells, hydraulic fracturing and acidizing and gas recycling (Wang et al., 2018). Gas recycling is a method used to achieve pressure maintenance above or close to the dew point and minimisation of the liquid condensation phenomena that occur in a retrograde gas condensate reservoir. During this process, the heavy, liquifiable components of the produced gas are separated at the surface facilities and the lean, mostly composed of methane, “dry” gas is re-injected into the reservoir (Fig. 1.18). For most gas recycling projects below the dew point, the injection gas is fairly lean and recovery

efficiency of the reservoir retrograde condensate depends mostly on vaporisation (Coats, 1985; Whitson et al., 1999). Therefore, with gas recycling, the overall reservoir gas composition becomes leaner and can revaporise the condensed liquids, while at the same time a partial pressure maintenance is achieved that prevents further liquid condensation.



**Figure 1.18:** Schematic illustration of the dry gas recycling process.

Although the liquid condensate in the reservoir is regarded as immobile, it should be pointed out that around the production wells where pressure declines the most, a substantial volume of liquid may be generated that exceeds the critical flow saturation and therefore it is indeed produced at the surface.

Gas recycling is often used as a remedy procedure for condensate blockage effects taking place in retrograde gas condensate reservoirs, although there is a number of practical considerations concerning the application of this method. The reduction of income from the sales of gas that could be postponed for even 10 or 20 years, the availability and cost of the required facilities (injection wells, gas compressors, etc.), or even an early dry gas breakthrough, are issues that should be carefully considered before the initiation of a gas recycling project.

## 1.6 Need for computational acceleration during compositional simulation processes

During the planning and development of a gas recycling project, a number of sophisticated simulation techniques are used, commonly known as compositional reservoir modelling. The complexity of gas condensate systems undergoing gas recycling, make the use of compositional simulators indispensable for designing the parameters and studying the effectiveness of gas recycling, as well as optimising and enhancing production. Compositional simulators offer greater accuracy compared to the more traditional black oil simulators, although at the same time, their operation is remarkably time-consuming, as the

simulation process requires the solution of intricate systems of non-linear differential equations, in consistency with the principles of mass and momentum conservation, as well as thermodynamic equilibrium. The establishment of thermodynamic equilibrium between the gas and liquid condensate phases is achieved by determination of equilibrium ratios,  $K_i$ , defined as the ratio of the mole fraction of a component in the gas phase, to the mole fraction of the same component in the liquid phase (Section 2.1). The estimation of equilibrium coefficients however, relies upon complex iterative numerical methods that require numerous steps before approaching an appropriate value, while at the same time, the calculation must be carried out for the complete number of cells of the reservoir simulation model, at each timestep, throughout the whole simulation process. These iterative techniques therefore, along with the differential equations necessary for the conservation of mass and momentum, constitute the heart of the problem, as they usually require days of computational time (CPU time), in order to simply complete one simulation attempt, rendering production optimisation by means of reservoir simulation rather challenging.

## 1.7 Purpose and Objectives

The purpose of this master's dissertation is to examine the influence of gas recycling on the compositional variation of a gas condensate reservoir with respect to equilibrium coefficient values ( $K_i$ ) which are required as a part of the simulation process. A number of different production scenarios are constructed and the dependency of equilibrium coefficients on pressure and composition is studied. Particularly, it is examined whether the equilibrium coefficients possess a more substantial dependence on composition during gas recycling, rather than exclusively on pressure, as is the case for production with natural depletion. Several approaches are suggested, including a new experimental procedure, for the prediction of the composition throughout the reservoir at each timestep during the gas recycling simulation process. The prediction or at least, the approximation of the overall composition of a gas recycling project, enables the application of numerical techniques, based on Machine Learning, that considerably accelerate the computational process.

This thesis is developed as follows:

Chapter 2 is an introduction to equations of state and all the associated terminology and parameters for the proper understanding of the most known cubic equations of state used in reservoir engineering applications. The equilibrium coefficients ( $K$ -values) used throughout this dissertation for phase behaviour characterisations are defined.

In Chapter 3 the most fundamental principles of reservoir simulation are presented. A comparison between conventional black oil modelling and compositional modelling is made and the respective equations of compositional modelling along with techniques for their solution are provided. An elaborate

description of the phase stability and phase split algorithms, both necessary during reservoir simulation processes is also made.

Chapter 4 focuses on various sources for the collection of K-values. A new experimental procedure, based on the classic Constant Volume Depletion (CVD) experiment developed for the purposes of this thesis, is introduced.

In Chapter 5, the gas condensate reservoir simulation scenarios that were constructed in this thesis are extensively presented and the chapter closes with the results and conclusions that were derived from the above study.





## 2 EQUATIONS OF STATE

An Equation of State (EoS) is an analytical expression that relates pressure (P), volume (V) and temperature (T). When considering real hydrocarbon fluids it is necessary to accurately describe this PVT relationship in order to estimate their volumetric and phase behaviour properties, as well as to effectively manage the surface facilities operation. These calculations are carried out for hydrocarbon mixtures, with the assistance of a cubic equation of state (cubic EoS). Cubic EoS have a long history dating back to 1873 when the famous van der Waals (vdW) EoS was first introduced, however, it was almost a century later that the Redlich-Kwong (RK) EoS (1949) gained widespread acceptance as the first cubic EoS widely used. Since then, various modifications to the RK EoS have been proposed such as the Soave-Redlich-Kwong (SKR) EoS (1972) and the Peng-Robinson (PR) EoS (1976 and 1978), which along with the 1982 Peneloux et al. volume translation concept for the improvement of liquid density predictions, are all presented in this chapter as most publications, research work and software in the petroleum industry are based on these two latter cubic EoS.

In this second chapter, the equilibrium coefficients (K-values) are defined, along with the concept of fugacity, both of which constitute a major part in phase equilibria calculations of hydrocarbon reservoir fluids. Next, a detailed description of the previously mentioned equations of state is made, with attached tables for their comparison. The concept of volume translation is presented and the chapter closes with a brief section for the characterisation of the hydrocarbon plus fraction.

### 2.1 Definition of equilibrium ratio, $K_i$

The equilibrium ratio or equilibrium coefficient,  $K_i$ , of a certain component  $i$  that is part of a hydrocarbon mixture, is the ratio of the mole fraction of the component in the gas phase, over the mole fraction of the component in the liquid phase

$$K_i = \frac{y_i}{x_i} \quad (2.1)$$

In Eq. (2.1),  $K_i$  = equilibrium ratio,  $y_i$  = mole fraction of component  $i$  in the gas phase,  $x_i$  = mole fraction of component  $i$  in the liquid phase. The equilibrium ratio is a measure of the tendency of a component to remain or escape to the gas phase and is essentially a property that measures the volatility of the component at a specific pressure and temperature (Ahmed, 2016).



Equation (2.1) can also be expressed as a function of total system pressure,  $p$ , and vapour pressure of the component,  $p_{vi}$ , based on Raoult's and Dalton's laws of ideal solutions as follows,

Raoult's law:

$$p_i = x_i p_{vi} \quad (2.2)$$

where  $p_i$  = partial pressure of component  $i$  in the liquid phase.

Dalton's law:

$$p_i = y_i p \quad (2.3)$$

Merging of equations (2.2) and (2.3) results in the following relation,

$$K_i = \frac{y_i}{x_i} = \frac{p_{vi}}{p} \quad (2.4)$$

This relationship therefore, indicates that equilibrium coefficients are only a function of pressure and temperature and not composition when ideal solutions are concerned. However, even though equilibrium ratio predictions with Eq. (2.4) are accurate for pressures close to the atmospheric pressure, in higher pressures the resulting values tend to be unrealistic. When real solutions are concerned, composition,  $z_i$ , should also be taken into account as the following expression indicates

$$K_i = K(p, T, z_i) \quad (2.5)$$

Equilibrium ratios being tightly connected to other thermodynamic equilibrium parameters such as fugacity coefficients discussed next, constitute a substantial part of the compositional simulation process hence, accurate as well as fast determination of their values is crucial.

## 2.2 Fugacity and fugacity coefficient

In a multicomponent hydrocarbon mixture the concept of fugacity, as a thermodynamic quantity, can serve as a criterion for thermodynamic equilibrium among the different phases present in the mixture. The term fugacity denotes an isothermal change in the chemical potential of a substance in a system:



$$\mu_2 - \mu_1 = \mu(p_2, T) - \mu(p_1, T) = RT \ln \left( \frac{f_2}{f_1} \right) \quad (2.6)$$

where  $\mu_1, \mu_2$ : chemical potential of the substance in pressure  $p_1$  and  $p_2$  respectively,  $f_1, f_2$ : fugacity of the substance in pressure  $p_1$  and  $p_2$  respectively,  $T$ : temperature,  $R$ : universal gas constant.

Specifically, in a two-phase vapour/liquid mixture, the component tends to escape from the phase of the higher component fugacity to the phase characterised by the lower component fugacity. In the special case where the component fugacity is equal between the two phases, there is zero net transfer, and the two phases exist in thermodynamic equilibrium as is indicated by the following relation,

$$f_i^v = f_i^L \quad (2.6)$$

In Eq. (2.6),  $f_i^v$  = fugacity of component  $i$  in the vapour phase,  $f_i^L$  = fugacity of component  $i$  in the liquid phase.

A relationship between fugacity,  $f_i$ , and the equilibrium ratio,  $K_i$ , for a specific compound of a hydrocarbon mixture can be found by introducing the fugacity coefficient  $\varphi_i$ . The fugacity coefficient for compound  $i$  of a hydrocarbon mixture is defined by the following equations,

$$\varphi_i^v = \frac{f_i^v}{y_i p} \quad (2.7)$$

$$\varphi_i^L = \frac{f_i^L}{x_i p} \quad (2.8)$$

In Eqs. (2.7) and (2.8),  $\varphi_i^v$  = fugacity coefficient of component  $i$  in the vapour phase,  $y_i$  = mole fraction of component  $i$  in the vapour phase,  $\varphi_i^L$  = fugacity coefficient of component  $i$  in the liquid phase,  $x_i$  = mole fraction of component  $i$  in the liquid phase,  $p$  = system pressure. Equations (2.7) and (2.8) can be written accordingly as

$$\varphi_i^v y_i p = f_i^v \quad (2.9)$$

$$\varphi_i^L x_i p = f_i^L \quad (2.10)$$

Therefore, Equations (2.1), (2.6), (2.9) and (2.10) may be combined to produce the following expression where the fugacity coefficient is given as a function of the equilibrium ratio of component  $i$ ,



$$\frac{y_i}{x_i} = \frac{\varphi_i^L}{\varphi_i^v} = K_i \quad (2.11)$$

The fugacity coefficient for each component is related to pressure, temperature and volume by,

$$\ln \varphi_i = \frac{1}{RT} \int_V^\infty \left[ \left( \frac{\partial p}{\partial n_i} \right)_{T,V,n_{j \neq i}} - \frac{RT}{V} \right] dV - \ln Z \quad i = 1, 2, \dots, N \quad (2.12)$$

In Eq. (2.12),  $R$  = universal gas constant,  $T$  = system temperature,  $n_i$  = number of moles of component  $i$ ,  $V$  = total volume, and  $Z$  = mixture compressibility factor. As a result, it is made clear that the fugacity coefficient,  $\varphi_i$ , can be calculated through Eq. (2.12) with the assistance of an appropriate expression that relates pressure, temperature, volume and composition, thus, an equation of state (EoS).

## 2.3 Cubic Equations of State

### 2.3.1 van der Waals EoS (vdW EoS)

The simplest and most famous form of an equation of state is the ideal gas equation that can accurately describe the volumetric behaviour of ideal gases and is given by the following expression,

$$PV = nRT \quad (2.13)$$

In Eq. (2.13),  $P$  = pressure,  $V$  = total volume,  $n$  = number of moles,  $R$  = universal gas constant,  $T$  = temperature.

An ideal gas can be described as a hypothetical mixture of molecules that is generally characterised by the following conditions. The gas molecules of the mixture occupy an infinitesimal volume compared to the total gas volume, and there is no development of attractive or repulsive forces between the molecules. The ideal gas equation can also be used on real gases in low temperatures, provided that the pressure is kept close to the atmospheric pressure.

In an attempt to eliminate the assumptions made for the generation of the ideal gas equation, van der Waals (1873) proposed a new equation of state that could perform volumetric and phase equilibrium calculations on real gases and in a greater range of pressures and temperatures. For this reason, he introduced two parameters, parameter  $a$ , to account for the attraction between molecules, and parameter  $b$ , to correct for the volume occupied by the molecules. This last parameter,  $b$ , is usually referred to as the

covolume (effective molecular volume). Due to the presence of these two parameters, the van der Waals EoS, as well as all the subsequent equations that have derived from it, are characterized as two-parameter equations of state. The van der Waals EoS is mathematically presented as:

$$p + \frac{a}{V^2} = \frac{RT}{V - b} \quad (2.14)$$

The cubic forms of the van der Waals EoS are presented as:

$$V^3 - \left(b + \frac{RT}{p}\right)V^2 + \frac{a}{p}V - \frac{ab}{p} = 0 \quad (2.15)$$

$$Z^3 - (B + 1)Z^2 + AZ - AB = 0 \quad (2.16)$$

Constants  $a$  and  $b$  can be calculated from the following expressions:

$$a = \Omega_a \frac{R^2 T_c^2}{p_c} \quad (2.17)$$

$$b = \Omega_b \frac{RT_c}{p_c} \quad (2.18)$$

where

$$\Omega_a = 0.421875 \quad (2.19)$$

$$\Omega_b = 0.125 \quad (2.20)$$

In Eqs. (2.17) and (2.18),  $T_c$  = critical temperature,  $p_c$  = critical pressure.

Accordingly, the parameters  $A$  and  $B$  for Eq. (2.16) can be calculated from the following expressions:

$$A = \Omega_a \frac{p_r}{T_r^2} \quad (2.21)$$



$$B = \Omega_b \frac{p_r}{T_r} \quad (2.22)$$

In Eqs. (2.21) and (2.22),  $T_r$  = reduced temperature ( $T_r = T/T_c$ ),  $p_r$  = reduced pressure ( $p_r = p/p_c$ ).

For the van der Waals EoS, a universal critical compressibility factor of  $Z_c = 0.375$  arises, regardless of the type of substance considered. However, experimental studies have shown that for most substances, the values of  $Z_c$  range from 0.23 to 0.31 with an average value of 0.27. Therefore, the fact that the van der Waals EoS produces a larger value of  $Z_c$  compared to the experimental values, is indicative of a certain degree of inaccuracy concerning its associated parameters.

### 2.3.2 Redlich-Kwong EoS (RK EoS)

A modification of the original vdW EoS was proposed in 1949 by Redlich and Kwong in an effort to add a temperature correction to the attraction parameter  $a$ . The related expressions of the RK EoS are similar to the ones previously presented for the vdW EoS, with the analogous modifications for the temperature corrected parameter  $a$ ,

$$p + \frac{a}{\sqrt{T}V(V+b)} = \frac{RT}{V-b} \quad (2.23)$$

The cubic forms of the RK EoS are presented as:

$$V^3 - \frac{RT}{p}V^2 + \left(\frac{a}{\sqrt{T}} - bRT - pb^2\right)\frac{V}{p} - \frac{ab}{p\sqrt{T}} = 0 \quad (2.24)$$

$$Z^3 - Z^2 + (A - B - B^2)Z - AB = 0 \quad (2.25)$$

The expressions for the calculation of parameters  $a$  and  $b$  are:

$$a = \Omega_a \frac{R^2 T_c^{2.5}}{p_c} \quad (2.26)$$



$$b = \Omega_b \frac{RT_c}{p_c} \quad (2.27)$$

where

$$\Omega_a = 0.42748 \quad (2.28)$$

$$\Omega_b = 0.08664 \quad (2.29)$$

The parameters  $A$  and  $B$  for Eq. (2.25) are calculated from the following expressions:

$$A = \Omega_a \frac{p_r}{T_r^{2.5}} \quad (2.30)$$

$$B = \Omega_b \frac{p_r}{T_r} \quad (2.31)$$

RK EoS is characterized by an improved universal gas compressibility factor of  $Z_c = 0.333$ .

### 2.3.3 Soave-Redlich-Kwong EoS (SRK EoS)

In 1972, Soave further improved the RK EoS by defining the attraction parameter,  $a$ , in relation to both temperature,  $T$  and acentric factor,  $\omega$ . The inclusion of acentric factor, accounts for the better representation of the individual characteristics of each component participating in the mixture, especially concerning the components' shape. The SRK EoS, one of the most widely used equations of state in reservoir engineering applications, is mathematically expressed as follows,

$$p + \frac{a(T, \omega)}{V(V+b)} = \frac{RT}{V-b} \quad (2.32)$$

while in a cubic form it can be expressed by the following equations:

$$V^3 - \frac{RT}{p}V^2 + (a\alpha - bRT - pb^2)\frac{V}{p} - \frac{a\alpha b}{p} = 0 \quad (2.33)$$



$$Z^3 - Z^2 + (A - B - B^2)Z - AB = 0 \quad (2.34)$$

Parameters  $a$  and  $b$  are calculated from the following relations:

$$a(T, \omega) = a\alpha = \Omega_a \frac{R^2 T_c^2}{p_c} \alpha \quad (2.35)$$

$$\alpha = [1 + m(1 - \sqrt{T_r})]^2 \quad (2.36)$$

$$m = 0.480 + 1.574\omega - 0.176\omega^2 \quad (2.37)$$

$$b = \Omega_b \frac{RT_c}{p_c} \quad (2.38)$$

In Eqs. (2.35) and (2.38), the constants  $\Omega_a$  and  $\Omega_b$  are given from Eqs. (2.28) and (2.29) respectively.

The parameters  $A$  and  $B$  for Eq. (2.34) are calculated from the following expressions:

$$A = \Omega_a \frac{p_r}{T_r^2} \alpha \quad (2.39)$$

$$B = \Omega_b \frac{p_r}{T_r} \quad (2.40)$$

The SRK EoS is characterised by the same universal critical gas compressibility factor of  $Z_c = 0.333$  as the RK EoS.

#### 2.3.4 Peng-Robinson EoS (PR EoS)

Another cubic equation of state, which is also universally accepted for reservoir engineering applications along with the SRK EoS, was developed by Peng and Robinson in 1976. PR EoS offers greater accuracy in the calculation of liquid densities, especially around the critical region, compared to the SRK EoS that

greatly overestimates liquid volumes, thus underestimating liquid densities of petroleum mixtures. It is noteworthy that even though the PR EoS can produce more accurate results concerning the estimated liquid densities, both equations of state must be followed by volume translation for the proper acquisition of the required liquid densities (Section 2.6). PR EoS is given by,

$$p + \frac{a(T, \omega)}{V(V+b) + b(V-b)} = \frac{RT}{V-b} \quad (2.41)$$

The cubic form of PR EoS is as follows:

$$Z^3 - (1-B)Z^2 + (A-3B^2-2B)Z - (AB-B^2-B^3) = 0 \quad (2.42)$$

The parameters  $a$  and  $b$  of Eq. (2.41) are calculated by the following expressions:

$$a(T, \omega) = a\alpha = \Omega_a \frac{R^2 T_c^2}{p_c} \alpha \quad (2.43)$$

$$\alpha = [1 + m(1 - \sqrt{T_r})]^2 \quad (2.44)$$

$$m = 0.37464 + 1.54226\omega - 0.26992\omega^2 \quad (2.45)$$

If  $\omega > 0.49$  then:

$$m = 0.3796 + 1.485\omega - 0.1644\omega^2 + 0.01667\omega^3 \quad (2.46)$$

$$b = \Omega_b \frac{RT_c}{p_c} \quad (2.47)$$

In Eqs. (2.43) and (2.47),



$$\Omega_a = 0.45724 \quad (2.48)$$

$$\Omega_b = 0.07780 \quad (2.49)$$

Parameters  $A$  and  $B$  of the cubic form (Eq. 2.42) are calculated as follows:

$$A = \Omega_a \frac{p_r}{T_r^2} \alpha \quad (2.50)$$

$$B = \Omega_b \frac{p_r}{T_r} \quad (2.51)$$

The largest improvement of the PR EoS is the universal critical compressibility factor of  $Z_c = 0.3074$ , which is lower than the SRK value of 0.333 and closer to the experimental values for heavier hydrocarbons. Volumetric predictions from the PR EoS and the SRK EoS can be substantially different, however as is mentioned before, both equations must be accompanied by volume translation for reliable liquid density predictions.

The following tables are provided for an easier comparison of the expressions representing all four equations of state presented in this section.

**Table 2.1:** Comparison of the mathematical expressions of the vdW, RK, SRK and PR equations of state, along with the expressions for the calculation of their parameters.

vdW	RK	SRK	PR
$p + \frac{a}{V^2} = \frac{RT}{V - b}$	$p + \frac{a}{\sqrt{T}V(V + b)} = \frac{RT}{V - b}$	$p + \frac{a(T, \omega)}{V(V + b)} = \frac{RT}{V - b}$	$p + \frac{a(T, \omega)}{V(V + b) + b(V - b)} = \frac{RT}{V - b}$
$a = \Omega_a \frac{R^2 T_c^2}{p_c}$	$a = \Omega_a \frac{R^2 T_c^{2.5}}{p_c}$	$a(T, \omega) = \Omega_a \frac{R^2 T_c^2}{p_c} \alpha$	$a(T, \omega) = \Omega_a \frac{R^2 T_c^2}{p_c} \alpha$
$b = \Omega_b \frac{RT_c}{p_c}$	$b = \Omega_b \frac{RT_c}{p_c}$	$b = \Omega_b \frac{RT_c}{p_c}$	$b = \Omega_b \frac{RT_c}{p_c}$
$\Omega_a = 0.421875$	$\Omega_a = 0.42748$	$\Omega_a = 0.42748$	$\Omega_a = 0.45724$

$\Omega_b = 0.125$	$\Omega_b = 0.08664$	$\Omega_b = 0.08664$	$\Omega_b = 0.07780$
$A = \Omega_a \frac{p_r}{T_r^2}$	$A = \Omega_a \frac{p_r}{T_r^{2.5}}$	$A = \Omega_a \frac{p_r}{T_r^2} \alpha$	$A = \Omega_a \frac{p_r}{T_r^2} \alpha$
$B = \Omega_b \frac{p_r}{T_r}$	$B = \Omega_b \frac{p_r}{T_r}$	$B = \Omega_b \frac{p_r}{T_r}$	$B = \Omega_b \frac{p_r}{T_r}$
$Z_c = 0.375$	$Z_c = 0.333$	$Z_c = 0.333$	$Z_c = 0.3074$

**Table 2.2:** Comparison of the cubic forms of the vdW, RK, SRK and PR equations of state.

<b>vdW</b>	$Z^3 - (B + 1)Z^2 + AZ - AB = 0$
<b>RK</b>	$Z^3 - Z^2 + (A - B - B^2)Z - AB = 0$
<b>SRK</b>	$Z^3 - Z^2 + (A - B - B^2)Z - AB = 0$
<b>PR</b>	$Z^3 - (1 - B)Z^2 + (A - 3B^2 - 2B)Z - (AB - B^2 - B^3) = 0$

**Table 2.3:** Comparison of the expressions for the calculation of the parameter  $a$  between the SRK and PR equations of state.

<b>SRK</b>	<b>PR</b>
$a(T, \omega) = \Omega_a \frac{R^2 T_c^2}{p_c} \alpha$	$a(T, \omega) = \Omega_a \frac{R^2 T_c^2}{p_c} \alpha$
$\alpha = [1 + m(1 - \sqrt{T_r})]^2$	$\alpha = [1 + m(1 - \sqrt{T_r})]^2$
$m = 0.480 + 1.574\omega - 0.176\omega^2$	$m = 0.37464 + 1.54226\omega - 0.26992\omega^2$
	If $\omega > 0.49$ :
	$m = 0.3796 + 1.485\omega - 0.1644\omega^2 + 0.01667\omega^3$



## 2.4 Mixing rules

All the expressions presented in the previous section for the calculation of parameters  $a$ ,  $b$ ,  $A$ , and  $B$ , refer to the calculation of these parameters in single-component systems and consequently, must be modified in order to be applicable to multicomponent hydrocarbon mixtures as well. For this reason, this section focuses on a number of mixing rules that are essentially used in the calculation of the EoS parameters when multicomponent systems are concerned.

For the van der Waals EoS, the following mixing rules are used for the calculation of parameters  $a$  and  $b$ :

$$a_m = \sum_i^N \sum_j^N y_i y_j \sqrt{a_i a_j} \quad (2.52)$$

$$b_m = \sum_i^N y_i b_i \quad (2.53)$$

Accordingly, the parameters of a multicomponent mixture for the RK EoS are calculated as follows:

$$a_m = \sum_i^N \sum_j^N y_i y_j \sqrt{a_i a_j} \quad (2.54)$$

$$b_m = \sum_i^N y_i b_i \quad (2.55)$$

$$A_m = \sum_i^N \sum_j^N y_i y_j \sqrt{A_i A_j} \quad (2.56)$$

$$B_m = \sum_i^N y_i B_i \quad (2.57)$$

For the SRK and the PR EoS the same mixing rules are applied and are presented in the following relationships:



$$(a\alpha)_m = \sum_i^N \sum_j^N y_i y_j (a\alpha)_{ij} \quad (2.58)$$

$$(a\alpha)_{ij} = (1 - k_{ij}) \sqrt{(a\alpha)_i (a\alpha)_j} \quad (2.59)$$

$$A_m = \sum_i^N \sum_j^N y_i y_j A_{ij} \quad (2.60)$$

$$A_{ij} = (1 - k_{ij}) \sqrt{A_i A_j} \quad (2.61)$$

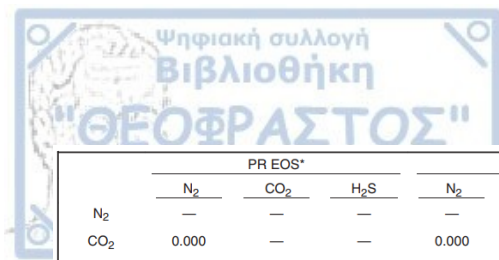
$$b_m = \sum_i^N y_i b_i \quad (2.62)$$

$$B_m = \sum_i^N y_i B_i \quad (2.63)$$

In Eqs. (2.52) - (2.63),  $a_m$ ,  $A_m$ ,  $(a\alpha)_m$ ,  $b_m$  and  $B_m$  = parameters of the mixture,  $N$  = number of components,  $y_i$  and  $y_j$  = compositions of the mixture components,  $a_i$ ,  $a_j$ ,  $A_i$ ,  $A_j$ ,  $b_i$  and  $B_i$  = parameters of the individual components.

The parameter  $k_{ij}$ , termed the Binary Interaction Coefficient (BIC), is a correction parameter which is included to characterise any binary system formed by components  $i$  and  $j$  in the hydrocarbon mixture. Binary interaction coefficients are determined empirically and are dependent on the difference in molecular size of components in a binary system (Ahmed, 2016). Therefore, it is evident that  $k_{ii} = 0$  and  $k_{ij} = k_{ji}$ .

For most hydrocarbon/hydrocarbon (HC/HC) pairs, binary interaction coefficients are regarded as zero ( $k_{ij} = 0$ ), apart from, usually, C1/C7+ pairs. On the other hand, non-HC/HC pairs are generally characterised by binary interaction coefficients that range between 0.01 to 0.15 as is indicated by Figure 2.1 (Nagy et al., 1982; Reid et al., 1987; Robinson et al., 1979; Whitson, 2000).



	PR EOS*			SRK EOS**		
	N <sub>2</sub>	CO <sub>2</sub>	H <sub>2</sub> S	N <sub>2</sub>	CO <sub>2</sub>	H <sub>2</sub> S
N <sub>2</sub>	—	—	—	—	—	—
CO <sub>2</sub>	0.000	—	—	0.000	—	—
H <sub>2</sub> S	0.130	0.135	—	0.120†	0.120	—
C <sub>1</sub>	0.025	0.105	0.070	0.020	0.120	0.080
C <sub>2</sub>	0.010	0.130	0.085	0.060	0.150	0.070
C <sub>3</sub>	0.090	0.125	0.080	0.080	0.150	0.070
i-C <sub>4</sub>	0.095	0.120	0.075	0.080	0.150	0.060
C <sub>4</sub>	0.095	0.115	0.075	0.080	0.150	0.060
i-C <sub>5</sub>	0.100	0.115	0.070	0.080	0.150	0.060
C <sub>5</sub>	0.110	0.115	0.070	0.080	0.150	0.060
C <sub>6</sub>	0.110	0.115	0.055	0.080	0.150	0.050
C <sub>7+</sub>	0.110	0.115	0.050‡	0.080	0.150	0.030‡

\*Nonhydrocarbon BIP's from Nagy and Shirkovskiy.<sup>24</sup> Use for both the original PR EOS (Ref. 7) and modified PR EOS (Ref. 25).  
 \*\*Nonhydrocarbon BIP's from Reid et al.<sup>3</sup>  
 †Not reported by Reid et al.<sup>3</sup>  
 ‡Should decrease gradually with increasing carbon number.

**Figure 2.1:** Binary Interaction Coefficients ( $k_{ij}$ ) for the SRK and PR EoS (Whitson, 2000).

### 2.4.1 Roots selection

The solution of the cubic forms of vdW, RK, SRK and PR equations of state is performed via analytical or iterative methods, which can produce one or three real roots. Generally, the largest positive root is chosen for the gas phase and the smallest positive root is selected for the liquid phase, while the middle root is discarded as the solution with no physical value. However, in order to avoid phase equilibria convergence problems in mixtures, the correct solution is better selected based on the normalised Gibbs energy function, defined mathematically for the gas and liquid phases respectively, as follows:

$$g_{gas}^* = \sum_{i=1}^n y_i \ln(f_i^V) \quad (2.64)$$

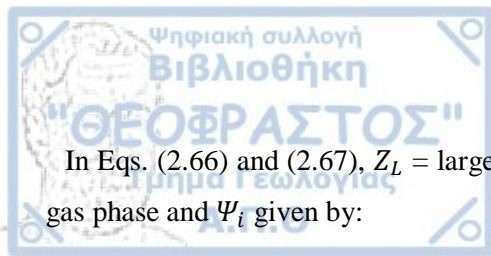
$$g_{liquid}^* = \sum_{i=1}^n x_i \ln(f_i^L) \quad (2.65)$$

In Eqs. (2.64), (2.65),  $g_{gas}^*$  and  $g_{liquid}^*$  = normalised Gibbs energy function of the gas and liquid phases respectively,  $y_i$  and  $x_i$  = mole fractions of gas and liquid and  $f_i$  = fugacity of the component in the mixture.

For each phase, after the middle root is discarded, the fugacity is calculated using the remaining two roots  $Z_{Largest}$  ( $Z_L$ ) and  $Z_{Smallest}$  ( $Z_S$ ), according to the following equations (fugacity calculation through the SRK EOS):

$$(f_i)_{Z_L} = x_i p + \exp \left\{ \frac{b_i(Z_L - 1)}{b_m} - \ln(Z_L - B) - \left( \frac{A}{B} \right) \left[ \frac{2\Psi_i}{(\alpha\alpha)_m} - \frac{b_i}{b_m} \right] \ln \left[ 1 + \frac{B}{Z_L} \right] \right\} \quad (2.66)$$

$$(f_i)_{Z_S} = x_i p + \exp \left\{ \frac{b_i(Z_S - 1)}{b_m} - \ln(Z_S - B) - \left( \frac{A}{B} \right) \left[ \frac{2\Psi_i}{(\alpha\alpha)_m} - \frac{b_i}{b_m} \right] \ln \left[ 1 + \frac{B}{Z_S} \right] \right\} \quad (2.67)$$



In Eqs. (2.66) and (2.67),  $Z_L$  = largest root of the liquid or gas phase,  $Z_S$  = smallest root of the liquid or gas phase and  $\Psi_i$  given by:

$$\Psi_i = \sum_j [x_j \sqrt{a_i a_j \alpha_i \alpha_j} (1 - k_{ij})] \quad (2.68)$$

Therefore, according to the above equations, if the normalised Gibbs energy pertaining to the smallest value is less than the one pertaining to the largest value ( $g_S^* < g_L^*$ ) then the smallest root  $Z_S$  is selected as the correct root, otherwise, the largest root  $Z_L$  is chosen.

## 2.5 Volume translation (volume shift)

Liquid density calculations performed by use of cubic EoS present a systematic deviation from experimental values of liquid density. This can be attributed to the fact that the universal critical compressibility factor,  $Z_c$ , that results from these EoS, is different from the  $Z_c$  that is obtained experimentally. As a result, cubic EoS tend to overestimate molecular volumes, hence underestimating liquid densities. Peneloux et al. (1982) were the first who introduced the concept of volume shift (or volume translation) into the SRK equation of state in order to account for this underestimation of liquid densities. They inserted a third (correction) parameter,  $c$ , in the two-parameter cubic EoS, that is component-dependent and allows for the molecular volume calculated from the EoS,  $v^{EoS}$ , to be corrected or “shifted” in a way that matches the experimental value,  $v$ :

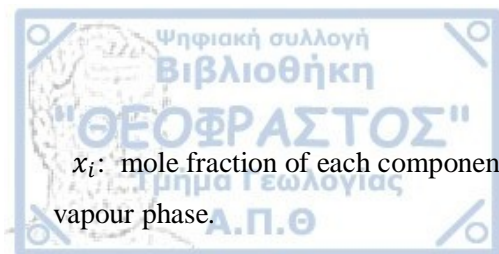
$$v = v^{EoS} - c \quad (2.69)$$

The above relationship can also be used for mixtures in the liquid and vapour phase, respectively:

$$v_L = v_L^{EoS} - \sum_{i=1}^N x_i c_i \quad (2.70)$$

$$v_v = v_v^{EoS} - \sum_{i=1}^N y_i c_i \quad (2.71)$$

where



$x_i$ : mole fraction of each component in the liquid phase and  $y_i$ : mole fraction of each component in the vapour phase.

It is evident that volume translation affects the compressibility factor,  $Z$ , therefore its value should be revised accordingly, in order to establish the calculations consistency:

$$Z = Z^{EoS} - \frac{p}{RT} \sum_{i=1}^N z_i c_i \quad (2.72)$$

On the other hand, the major advantage of the volume translation method as presented by Peneloux, is the fact that even though it improves volumetric predictions, it does not affect vapour-liquid equilibrium (VLE) calculations that were performed with the SRK EoS without volume translation. This indicates that vapour pressures of pure compounds, as well as dew and bubble points of mixtures, are all unaltered and remain equal to the ones estimated with the original SRK EoS. This is made obvious if the resulting expressions for fugacity are taken into account, when volume shift is introduced into the EoS for mixtures:

$$(f_i^L)_{modified} = (f_i^L)_{original} \exp \left[ -c_i \frac{p}{RT} \right] \quad (2.73)$$

$$(f_i^v)_{modified} = (f_i^v)_{original} \exp \left[ -c_i \frac{p}{RT} \right] \quad (2.74)$$

The above expressions demonstrate that the fugacity of each compound is multiplied by the same amount in both phases, thus resulting in the same value of fugacity ratio. In other words, the fugacity ratios remain unchanged by the volume shift:

$$\frac{(f_i^L)_{modified}}{(f_i^v)_{modified}} = \frac{(f_i^L)_{original}}{(f_i^v)_{original}} \quad (2.75)$$

The component-dependent correction parameter,  $c$ , can be estimated for non-hydrocarbons and hydrocarbons lighter than  $C_7$ , with the following expression suggested by Peneloux et al. that uses the Rackett compressibility factor,  $Z_{RA}$ , as the best correlating parameter:

$$c_i = \frac{0.40768 RT_{ci}(0.29441 - Z_{RA})}{p_{ci}} \quad (2.76)$$



where

$R$ : universal gas constant = 10.73 psi-ft<sup>3</sup>/(lb mol-°R),  $T_{ci}$ : critical temperature of component i, °R,  $p_{ci}$ : critical pressure of component i, psia

If the values of the Rackett compressibility factor are not available, they can be calculated for each component via their acentric factor,  $\omega$ , according to the equation below:

$$Z_{RA} = 0.29056 - 0.08775\omega \quad (2.77)$$

In the case of the  $C_{7+}$  pseudo-component, parameter  $c$  can be estimated with the following expression:

$$c_i = \frac{M_i}{\rho_i} - v_i^{EoS} \quad (2.78)$$

where

$M_i$ : molecular weight of component i (in this case the  $C_{7+}$  pseudo-component),  $\rho_i$ : density of i at 15 °C and 14.7 psia,  $v_i^{EoS}$ : molecular volume of i calculated from the original EoS with no volume translation.

Jhaveri & Youngren (1988) applied the work of Peneloux et al. for volume translation to the Peng-Robinson EoS. They suggested a dimensionless shift parameter,  $s_i$ , for each component expressed with the following ratio:

$$s_i = \frac{c_i}{b_i} \quad (2.79)$$

where

$b_i$ : the second parameter for component i in the unmodified PR EoS given by Eq. (2.47).

Values for  $s_i$  for pure components are provided by the authors in tables for the PR EoS (Table 2.4). If heavier hydrocarbons ( $C_{7+}$ ) are concerned, the following correlation dependent on molecular weight,  $M_i$ , should be used:

$$s_i = 1 - \frac{d}{M_i^e} \quad (2.80)$$





$d$  and  $e$  positive correlation coefficients given in Table 2.5.

In conclusion, the introduction of the correction parameter  $c$  by volume translation into a two-parameter equation of state, is proven to make any two-parameter EoS as accurate as any three-parameter EoS without altering the vapour-liquid equilibrium conditions.

**Table 2.4:** Values for the dimensionless shift parameters,  $s_i$ , for pure hydrocarbon components (Jhaveri & Youngren, 1988).

Component	Methane	Ethane	Propane	Iso-Butane	<i>n</i> -Butane	Iso-Pentane	<i>n</i> -Pentane	<i>n</i> -Hexane
$S_i$	-0.15400	-0.10020	-0.08501	-0.07935	-0.06413	-0.04350	-0.04183	-0.01478

**Table 2.5:** Positive correlation coefficients values for the estimation of dimensionless shift parameters for hydrocarbons heavier than C<sub>6</sub> (Jhaveri & Youngren, 1988).

Component Type	Correlation Coefficient		Average Error (%)
	$d$	$e$	
Paraffins	2.258	0.1823	0.19
Napthenes	3.004	0.2324	0.28
Aromatics	2.516	0.2008	0.24

## 2.6 C<sub>7+</sub> characterisation

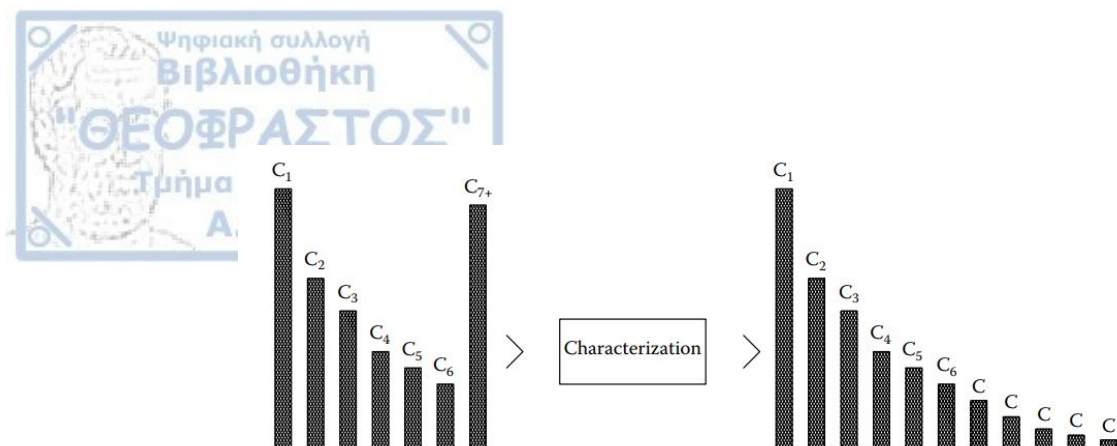
Reservoir hydrocarbon fluids contain an enormous number of different components typically belonging to one of two categories: *well-defined* components lower than C<sub>7</sub>, which include pure fractions with measured physical properties (N<sub>2</sub>, CO<sub>2</sub>, H<sub>2</sub>S, C<sub>1</sub>, C<sub>2</sub>, C<sub>3</sub>, iC<sub>4</sub>, nC<sub>4</sub>, iC<sub>5</sub>, nC<sub>5</sub>, C<sub>6</sub>), and *undefined* heavy petroleum fractions that constitute the plus fraction (usually the heptanes-plus fraction, C<sub>7+</sub>). Although there is a number of components greater than C<sub>7</sub> with defined physical properties, characterising each one of

them in a real reservoir fluid is a challenging task. All forms of cubic equations of state presented in this chapter, require the critical properties ( $p_c$ ,  $T_c$ ) and the acentric factor ( $\omega$ ) of each component that exists in the mixture in order to perform phase equilibria calculations. To make matters worse, a binary interaction parameter (BIP) is also required for each pair of the mixture's components, as well as a volume shift parameter for each component, if an equation of state with volume shift is to be used.

Therefore, the inability to fully characterise the plus fraction in terms of the physical properties of its individual components and hence, its direct use as a single component in the mixture phase behaviour calculations, is essentially responsible for the erroneous predictions of the fluid's thermodynamic and volumetric properties through the use of an equation of state. These problems associated with treating the plus fraction as a single component can be substantially reduced if the plus fraction is split into a number of pseudo-fractions. Splitting refers to the process of breaking down the plus fraction into groups of components with boiling points that fall within a certain range and are referred to as Single Carbon Number (SCN) groups ( $C_7$ ,  $C_8$ ,  $C_9$  etc.), each with a designated mole fraction, molecular weight and specific gravity (Fig. 2.2). These properties when properly combined should match the measured plus fraction properties, i.e.,  $(M)_{7+}$  and  $(\gamma)_{7+}$  (Ahmed, 2016). This way when a sufficiently large number of pseudo-components is used, an accurate PVT fluid behaviour prediction is achieved.

On the other hand, the cost and computer resources required for compositional reservoir simulation increase dramatically with the number of components used to describe the reservoir fluid. As a result, there is a limited number of components that can be used in compositional modelling and for that reason, the original split components are regrouped or lumped together into single pseudo-components in a way that the EoS predictive capability is not compromised. The lumping procedure, i.e., the reduction in the number of components used in EoS calculations, generally consists of the following two steps (Pedersen, 2014):

- Deciding what carbon number fractions to lump (group) into the same pseudo-component,
- Averaging  $p_c$ ,  $T_c$ , and  $\omega$  of the individual carbon number fractions to one  $p_c$ ,  $T_c$ , and  $\omega$  representative for the whole lumped pseudo-component.



**Figure 2.2:** Characterisation of the plus fraction (Pedersen et al. 2014).

In summary, the characterisation of the fraction (e.g.  $C_{7+}$ ), generally consists of the following steps (Ahmed 2016):

- Splitting the plus fraction into pseudo-components (e.g.  $C_7$  to  $C_{45+}$ ),
- Lumping the generated pseudo-components into an optimum number of SCN fractions,
- Characterising the lumped fraction in terms of their critical properties and acentric factors.

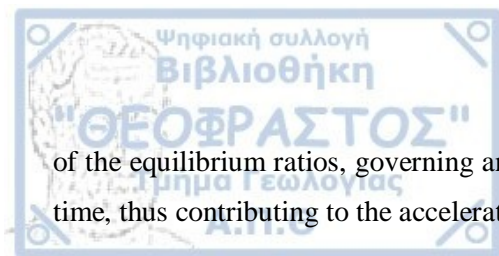
Numerous methods for the characterisation of the plus fraction have been proposed, although their description here far exceeds the purposes of this dissertation.

### 3 BASIC PRINCIPLES GOVERNING RESERVOIR SIMULATION PROCESSES

During the study of a hydrocarbon reservoir, either at an exploratory stage or especially at a later stage during production, the reservoir engineer's ultimate tool is the process of reservoir simulation. The importance of reservoir simulation is made evident if one considers the fact that the very object of our study, the reservoir itself, is buried deep underground and therefore we have no physical access to it. In fact, reservoir engineering is essentially based on gathering surface data from a hydrocarbon field and interpreting these data in a way that reveals information about the reservoir and the processes taking place within it. Hence, reservoir simulation offers a means to study the reservoir and the processes happening in it by integrating all available data from various sources into an environment that enables the evaluation of various development scenarios and procedures without interfering with the actual reservoir. In other words, reservoir simulation provides a powerful tool for evaluating alternative reservoir management strategies, thereby making it possible to select an optimum management strategy, based on existing reservoir and operating conditions (Ezekwe, 2010).

More specifically, dry gas recycling projects, as any other reservoir management project, are not automated procedures but they require careful and thorough planning and optimisation of their parameters before being put into practice in the field. There are numerous questions that need to be answered, i.e., how much of the surface dry gas must be re-injected back in the reservoir in order to ensure the success of the project? How many and which of the available injection wells must be used? Should the re-injection wells inject at the same or different rates? and so on. To accurately answer all these questions we must undeniably turn to reservoir simulation techniques. Reservoir simulation will reveal the optimum scenario that must be implemented in the reservoir under study. Nowadays, all major reservoir development and management decisions are essentially based on reservoir simulation results.

In this chapter, the basic differences between conventional black-oil modelling and compositional modelling are outlined, the main principles of the more sophisticated compositional modelling are presented, along with basic equations and various prerequisites for its use. The Stability and Flash calculation tests, which constitute a great part of the simulation process regarding vapour-liquid equilibria (VLE) calculations, are discussed next. The last section of the chapter, deals with the issue of increased computational (CPU) time that inevitably comes with the simulation process and how the prior knowledge



of the equilibrium ratios, governing an important part of VLE calculations, can reduce this computational time, thus contributing to the acceleration of the simulation process.

### 3.1 Black-oil modelling and Compositional modelling

The different types of hydrocarbon reservoirs that may be encountered, as well as the vast number of processes that take place within them, account for the necessity of numerous different reservoir simulation models, such as black-oil, compositional, dual-porosity, thermal, chemical flood etc. The black-oil model as the name refers, is mostly used during the simulation of black oil (typically an oil with the following characteristics:  $R_s < 750$  scf/stb,  $B_o < 1.4$  bbl/stb and  $API < 30$ ), as well as dry gas and immiscible recovery processes. In this considerably simpler than the fully compositional one and for many decades most widely used simulation model, the reservoir fluid is represented by two components, an oil component and a gas component (mixtures), while water exists as a third phase. The mass transfer between the two components that happens during gas solubility in oil and inversely, during liberation of gas from the oil phase, is entirely expressed by the gas solubility ( $R_s$ ), while all reservoir fluid PVT properties are determined as a function of the oil pressure and temperature. Therefore, in the black oil model the phase behaviour of both oil and gas can be adequately described by a set of tabulated PVT data, i.e.  $B_o$ ,  $B_g$ ,  $R_s$ ,  $\mu_o$  etc.

In black-oil modelling, it has been shown that the overall reservoir fluid composition remains constant throughout the simulation process. However, in case where compositional effects are important, for example when simulating volatile oil and gas condensate reservoirs, or in gas recycling projects below the dew point, where a considerable variation in the overall reservoir composition is observed, black-oil modelling appears to be inadequate to simulate all the processes and changes in phase behaviour that take place. In such circumstances, compositional simulation models are alternatively used, where each phase is defined by more than two components, one for each chemical compound present in the mixture, so that its physical properties and phase behaviour can be better represented. Of course, reservoir fluids contain thousands of components and it wouldn't be practical or even possible, to incorporate into the simulator all the individual components that exist in the mixture. For that reason, a number of pseudo-components with average physical properties are used instead (Section 2.6).

In compositional modelling simulation the phase change effects such as vaporisation and condensation cannot be described by functions of pressure and temperature as they rather depend on composition as well. Therefore, representation of the fluid phase behaviour is achieved through the use of an equation of state (EoS) and phase equilibrium relations. Consequently, as the number of components increases, so does the number of unknown variables, and this renders compositional modelling more complex and more CPU expensive than black-oil modelling, as there is a larger number of equations, along with complicated flash

calculations (section 3.4), that need to be solved in each cell of the reservoir model at each timestep. Unlike the black-oil model, a compositional model does not require experimentally derived tabulated PVT data, but a number of tuned (optimised) against experimental data parameters, that ensure the predictive capacity of the selected EoS and the reliability of its results.

In this thesis, a compositional reservoir model is used for the simulation of a number of dry gas recycling scenarios on a gas condensate reservoir and so, some basic principles of compositional modelling are presented next.

## 3.2 Basic principles of compositional modelling

### 3.2.1 Introduction

As mentioned above, compositional reservoir modelling is a complex and expensive procedure that requires a substantial amount of time and computer resources, although at the same time, it is the only way we can efficiently simulate certain types of reservoirs and processes that involve significant variations in fluids composition. The factors that basically contribute to this type of modelling being characterised as more demanding and laborious, is the intricate system of non-linear partial differential equations associated with fluid flow through the porous medium, whose number increases with the number of components used to describe the hydrocarbon system and second, the required thermodynamic equilibrium-related parameters which are derived from complicated stability and flash calculations (sections 3.3 and 3.4) that use iterative techniques to achieve convergence to a correct solution.

During the formulation of the equations that will be solved by the simulator, the basic assumptions inherent to the simulator are outlined, then these assumptions are stated in precise mathematical terms and last, they are applied to a control volume in the reservoir (Abou-Kassem et al., 2013). The result of this step is a set of non-linear, partial differential equations, that is, differential equations that contain multivariable functions and their partial derivatives, that describe fluid flow through porous media. These equations that generally constitute the compositional model are presented next. The role of the reservoir simulator is to solve these equations in space and time.

### 3.2.2 Compositional modelling equations

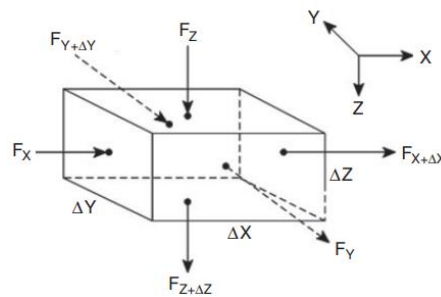
The basic conservation laws in reservoir simulation are the conservation of mass, conservation of momentum, expressed using Darcy's law of fluid flow through porous media, and conservation of energy, although the latter is usually neglected in cases where reservoir production is regarded as isothermal throughout the life of the field. The mass balance in a representative elementary volume or gridblock is

achieved by equating the accumulation of mass in the gridblock (and the resulting change of pressure) with the difference between the mass leaving the gridblock and the mass entering the gridblock (Fig. 3.1):

mass entering the gridblock – mass leaving the gridblock

= accumulation of mass in the gridblock

A material balance per fluid component is performed in each gridblock. The ability of the simulator to account for flow between gridblocks is what makes a simulator different from a reservoir engineering material balance tank model (Fanchi, 2005) where mass exchange is assumed only between the tank and surface.



**Figure 3.1:** A gridblock showing fluid flow in three directions (Ezekwe, 2010).

The mass balance equation, arriving from the mass conservation and the Darcy's law, for each hydrocarbon component and pseudo-component and for water is given by (Cao, 2002; Coats, 1980; Young & Stephenson, 1983):

$$F_i = \frac{\partial}{\partial t} [V\varphi(S_o\rho_o x_i + S_g\rho_g y_i)] - \sum_l [T(\lambda_o\rho_o x_i \Delta\Phi_o + \lambda_g\rho_g y_i \Delta\Phi_g)]_l \quad (3.1)$$

$$+ \sum_w (\rho_o x_i q_o^w + \rho_g y_i q_g^w) = 0$$

$$i = 1, \dots, n_t$$

$$F_w = \frac{\partial}{\partial t} (V\varphi S_w \rho_w) - \sum_l (T\lambda_w \rho_w \Delta\Phi_w)_l + \sum_w (\rho_w q_w^w) = 0 \quad (3.2)$$

In Eqs. (3.1) and (3.2),  $V$ : volume,  $\varphi$ : porosity,  $S_{o,g,w}$ : saturation of the oil, gas and water phases,  $\rho_{o,g,w}$ : density of the oil, gas and water phases,  $x_i$ : mole fraction of component  $i$  in the oil phase,  $y_i$ : mole fraction



of component  $i$  in the gas phase,  $T$ : transmissibility,  $\lambda_{o,g,w}$ : mobility of the oil, gas and water phases,  $\Delta\Phi_{o,g,w}$ : potential difference of the oil, gas and water phases between two individual simulator cells,  $q_o^W$ ,  $q_g^W$  and  $q_w^W$ : phase volumetric flow rates of well  $W$ ,  $n_t$ : total number of components.

Eq. (3.1) can be modified to a total hydrocarbon mass balance equation that accounts for all hydrocarbon components (h) by summing over all hydrocarbon components:

$$F_h = \frac{\partial}{\partial t} [V\varphi(S_o\rho_o + S_g\rho_g)] - \sum_l [T(\lambda_o\rho_o\Delta\Phi_o + \lambda_g\rho_g\Delta\Phi_g)]_l + \sum_W (\rho_o q_o^W + \rho_g q_g^W) = 0 \quad (3.3)$$

The phase equilibrium relationship is expressed by:

$$F_e = f_i^L - f_i^V = 0 \quad (3.4)$$

where

$f_i^L$ : fugacity of component  $i$  in the oil phase and  $f_i^V$ : fugacity of component  $i$  in the gas (vapour) phase.

The capillary pressure equations between oil and water and gas and oil phases are expressed as:

$$F_{P_{c(o,w)}} = P_{c(o,w)} - (p_o - p_w) = 0 \quad (3.5)$$

$$F_{P_{c(g,o)}} = P_{c(g,o)} - (p_g - p_o) = 0 \quad (3.6)$$

In Eqs. (3.5) and (3.6),  $P_{c(o,w)}$ : water-oil capillary pressure,  $P_{c(g,o)}$ : gas-oil capillary pressure,  $p_o$ : oil pressure,  $p_w$ : water pressure,  $p_g$ : gas pressure. Clearly, when capillarity is ignored all phases exhibit equal pressure.

Last, the saturation (or volume) constraint and component mole fraction constraints are as follows:

$$F_S = 1 - S_o - S_g - S_w = 0 \quad (3.7)$$

or

$$F_V = V_\varphi - V_t = 0 \quad (3.8)$$





$$F_o = \sum_{i=1}^{n_t} x_i - 1 = 0 \quad (3.9)$$

$$F_g = \sum_{i=1}^{n_t} y_i - 1 = 0 \quad (3.10)$$

where  $V_\varphi$ : pore volume and  $V_t$ : total fluid volume.

It is made evident that there are  $2n_t + 6$  equations and  $2n_t + 6$  unknown variables that govern reservoir fluid flow in a compositional modelling simulation (Tables 3.1 and 3.2).

**Table 3.1:** Number of equations that control hydrocarbon fluid flow through a porous medium in compositional reservoir modelling.

Equations	$F_i$	$F_w$	$F_h$	$F_e$	$F_{P_{c(o,w)}}, F_{P_{c(g,o)}}$	$F_S$ or $F_V$	$F_o, F_g$	Total
Number	$n_t - 1$	1	1	$n_t$	2	1	2	$2n_t + 6$

**Table 3.2:** Total number of selected unknown variables for equations (3.1)-(3.10).

Type	$p_o, p_g, p_w$	$S_o, S_g, S_w$	$x_i$	$y_i$	Total
Number	3	3	$n_t$	$n_t$	$2n_t + 6$

### 3.2.3 Discretisation and solution techniques of partial differential equations

If an analytical solution of the partial differential equations mentioned earlier was possible, it would produce continuous functions of space and time concerning reservoir pressure, fluid saturations, phase compositions and well flow rates. Since these equations are highly non-linear, their solution is essentially accomplished with numerical methods which provide us with values of pressure, fluid saturation and composition at discrete points in the reservoir and at discrete time steps. Therefore, through the process of discretisation, the partial differential equations are converted into algebraic equations, usually by replacing the partial derivatives with finite differences (finite difference method). The spatial finite difference interval  $\Delta x$  along the x-axis is called gridblock length and the temporal finite difference interval  $\Delta t$  is called the timestep. Indices i, j and k are ordinarily used to label grid locations along the x, y and z coordinate axes, respectively. Index n labels the present time level, so that n+1 represents a future time level (Fanchi, 2005).

The two most widely used methods in the formulation of simulator equations are the Implicit Pressure Explicit Saturation (IMPES) method and the Fully Implicit or Newton-Raphson method. The IMPES

technique combines the flow equations in a way that the unknown saturations are eliminated, thus generating a single pressure equation that is solved implicitly (simultaneously) for pressures at each gridblock at the current timestep, designated as  $n+1$ , by using parameters of the previous timestep designated as  $n$ . The next step is the explicit substitution of the pressures into the current flow equations and the saturations calculation at the current timestep ( $n+1$ ) for each gridblock (Coats, 2000; Ezekwe, 2010). In other words, the IMPES method solves for pressure at the current timestep by using saturations of the old timestep and then uses the calculated pressures to explicitly calculate saturations of the current timestep. The IMPES method has the advantages of less computing time at each timestep and reduced computer memory demands. On the other hand, it tends to be relatively unstable when applied in large timesteps.

The second method that is widely used in simulators is the Fully Implicit or Newton-Raphson method, where all primary variables at the new timestep are determined at that time. Generally, the Newton-Raphson algorithm is a method for solving simultaneously non-linear algebraic equations, which in this case have resulted from the process of discretisation, by converting the problem to a series of linear systems of equations. The Newton-Raphson technique is basically an iterative approximation procedure that is based on an initial estimate of an unknown variable and the use of Taylor's series expansion. To better understand this, let us assume a simple, one dimensional equation with the following solution:

$$f(x) = t \quad (3.11)$$

If  $x^{(0)}$  is an initial estimate of the solution, then there is probably a deviation from the correct solution denoted as  $\Delta x^{(0)}$ . This can be expressed mathematically as:

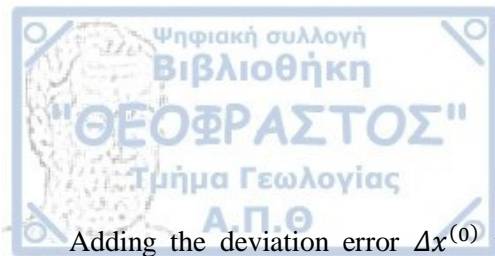
$$f(x^{(0)} + \Delta x^{(0)}) = t \quad (3.12)$$

The left hand side of Eq. (3.12) can be expanded regarding  $x^{(0)}$  using Taylor Series resulting in:

$$f(x^{(0)}) + \left(\frac{df}{dx}\right)^{(0)} \Delta x^{(0)} + \frac{1}{2!} \left(\frac{d^2f}{dx^2}\right)^{(0)} \Delta x^{(0)^2} + \dots = t \quad (3.13)$$

If the deviation error  $\Delta x^{(0)}$  is assumed small, the higher order terms can be neglected and we can consider the following equations:

$$\Delta t^{(0)} \approx \left(\frac{df}{dx}\right)^{(0)} \Delta x^{(0)} \quad (3.14)$$



$$\Delta t^{(0)} = t - f(x^{(0)}) \quad (3.15)$$

Adding the deviation error  $\Delta x^{(0)}$  to the initial estimate and taking account Eq. (3.14), the second approximation is formulated:

$$x^{(1)} = x^{(0)} + \frac{\Delta t^{(0)}}{\left(\frac{df}{dx}\right)^{(0)}} \quad (3.16)$$

Generalising the above equations we get the following relationships that constitute the core of the Newton-Raphson algorithm:

$$\Delta t^{(k)} = t - f(x^{(k)}) \quad (3.17)$$

$$\Delta x^{(k)} = \frac{\Delta t^{(k)}}{\left(\frac{df}{dx}\right)^{(k)}} \quad (3.18)$$

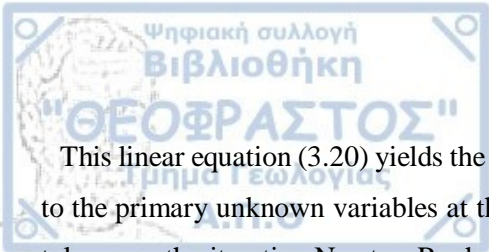
$$x^{(k+1)} = x^{(k)} + \Delta x^{(k)} \quad (3.19)$$

The above equations are by all means exceptionally simpler than the ones which we are dealing with during compositional simulation, although they serve as a great example of the way the Newton-Raphson technique operates when solving simulator equations for the calculation of unknown primary variables in each timestep. More specifically, the terms of the converted algebraic (finite difference) flow equations are expanded as the sum of each term at the current iteration level, plus a contribution due to a change of each term with respect to the primary unknown variables over the iteration as in Eq. (3.19). In order to calculate these changes, the derivatives of the flow equations must be calculated first, which are then stored in a matrix called acceleration or Jacobian matrix. The Newton-Raphson method ultimately leads to a linear matrix equation:

$$\mathbf{J} \cdot \delta \mathbf{X} = \mathbf{R} \quad (3.20)$$

where

$\mathbf{J}$ : Jacobian (acceleration) matrix,  $\delta \mathbf{X}$ : column vector of changes to the primary unknown variables and  $\mathbf{R}$ : column vector of residuals.



This linear equation (3.20) yields the changes to the primary unknown variables,  $\delta \mathbf{X}$ , which are then added to the primary unknown variables at the beginning of the iteration. If the changes are less than a specified tolerance, the iterative Newton-Raphson technique is considered complete and the simulator proceeds to the next timestep (Fanchi, 2005).

The Fully Implicit or Newton-Raphson formulation is used in this thesis during the simulation of dry gas recycling scenarios on a gas condensate reservoir, through the environment of Petroleum Experts' Reveal software and for that reason it was presented more extensively. This method is considerably more stable than the IMPES method, especially concerning flow problems with large compositional changes in the gridblocks (Ezekwe, 2010). However, it also has higher requirements of computer memory and computational time which is a major drawback, especially when one considers other fundamental simulation processes that also require a large amount of CPU time like the stability and flash calculation problems presented next.

### 3.3 Phase-stability analysis

During compositional reservoir simulation there are certain requirements that need to be fulfilled like the various conservation laws presented in section 3.2.2, concerning mass, momentum, etc. Another requirement is that of thermodynamic equilibrium between the existing phases which is essentially accomplished with the assistance of two algorithms that determine the number of phases present in the hydrocarbon mixture (Stability algorithm) and the percentage and composition of each phase (Phase Split algorithm).

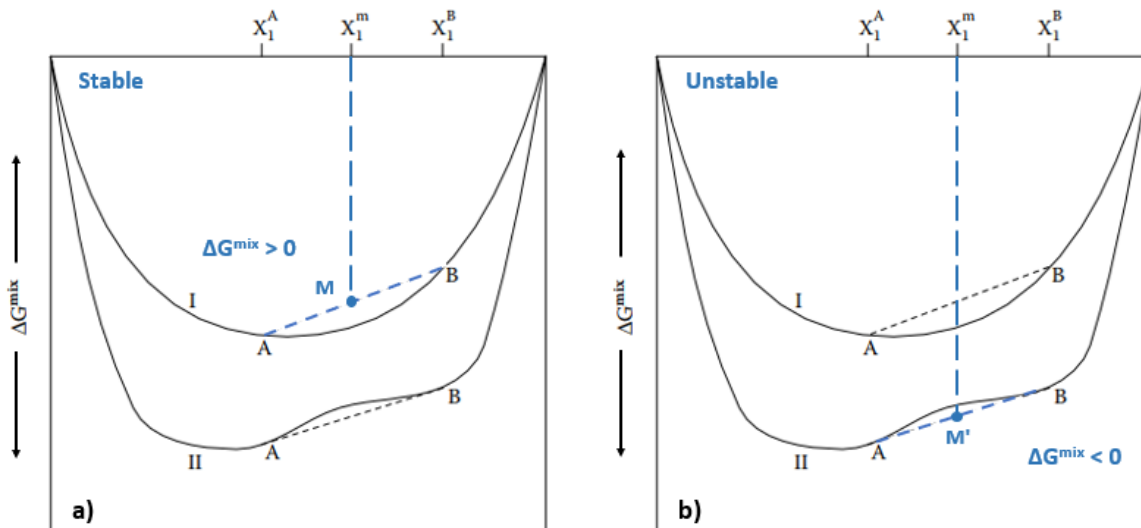
When conducting vapour-liquid equilibria (VLE) calculations with an equation of state, an important issue is the determination of the number of phases present in the mixture, i.e. if the mixture will split into two or more phases in equilibrium, or if it will remain as a single phase at specific temperature and pressure. Performing saturation pressure calculations is a means to solve this problem however, it is an expensive and yet not entirely reliable method. For that reason, the problem of stability, that has been addressed by Michelsen (1982) and basically determines the number of phases present in each cell of the simulator at each timestep, is used instead. Stability analysis is a major part of the simulation process because it defines whether or not a phase split calculation will also be performed.

#### 3.3.1 Graphical interpretation of phase stability

A closed system at a given temperature and pressure is said to be in equilibrium if the Gibbs free energy of the system is at its minimum with respect to all possible changes. This fundamentally means that any given closed system will try to arrange its molecules in a position that minimises its Gibbs free energy,  $G$ ,

either by forming one homogeneous phase, or by splitting into two or more different phases (Pedersen et al., 2014). Therefore, the problem of phase stability essentially deals with the question of whether a given composition has a lower energy remaining as a single phase (stable) or whether the mixture Gibbs energy will decrease by splitting the mixture into two or more phases (Whitson, 2000). This can be demonstrated graphically if we assume a binary mixture containing components 1 and 2, with a mole fraction of component 1 equal to  $x_1^m$ , plotted against the mixture's Gibbs free energy curve (Fig. 3.2). If the mixture splits into two phases A and B with mole fractions of component 1 denoted as  $x_1^A$  in phase A and  $x_1^B$  in phase B respectively, then the Gibbs energy of mixing of the total system will be the one shown by point M (Fig. 3.2a). In this case, it can be seen that the phase split leads to an increase in  $\Delta G$  of mixing (point M lies above the Gibbs plot), contrary to the Gibbs energy minimisation requirement for equilibration, and will therefore not take place. In such case, the mixture is considered to be stable.

Let's assume a second mixture equivalent to the previous one, although this time after the phase split, the Gibbs energy of mixing of the total system is determined by point M' (Fig. 3.2b). Here, the splitting leads to a reduction of  $\Delta G$  of mixing (point M' lies below the Gibbs energy line) and this means that such a binary mixture containing a mole fraction of  $x_1^m$  of component 1, will split into two phases A and B thus establishing equilibrium.



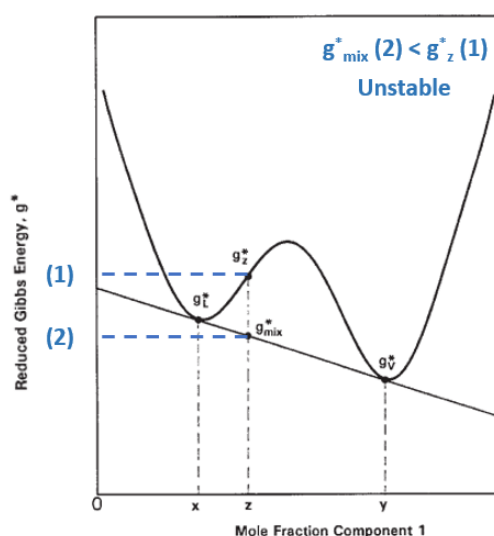
**Figure 3.2:** Principle of stability analysis for a binary mixture (Pedersen et al. 2014).

It is usually the normalised (or reduced) Gibbs energy,  $g^*$ , that is plotted against the mole fraction of one of the components in a binary mixture (Fig. 3.3):



$$g_z^* = \sum_{i=1}^N z_i \ln f_i(z) \quad (3.21)$$

where  $g_z^*$ : normalised Gibbs energy for the mixture composition,  $z_i$ : mole fraction of component  $i$  and  $f_i(z)$ : fugacity of component  $i$ . The equilibrium condition of the system, is then graphically established by drawing a straight line tangent to two (or more) compositions of the Gibbs energy surface curve (Fig. 3.3). The difference between the Gibbs energy curve and the tangent line at the points of composition is called the Tangent Plane Distance (TPD(x)). Provided that the Gibbs free energy of the mixture (point (2)) is lower than the Gibbs free energy of the initial feed composition (point (1)), the original mixture is unstable and will split into two phases. Otherwise, the original mixture is stable and appears as a homogeneous single-phase mixture.



**Figure 3.3:** Gibbs energy surface for a binary system (Whitson, 2000).

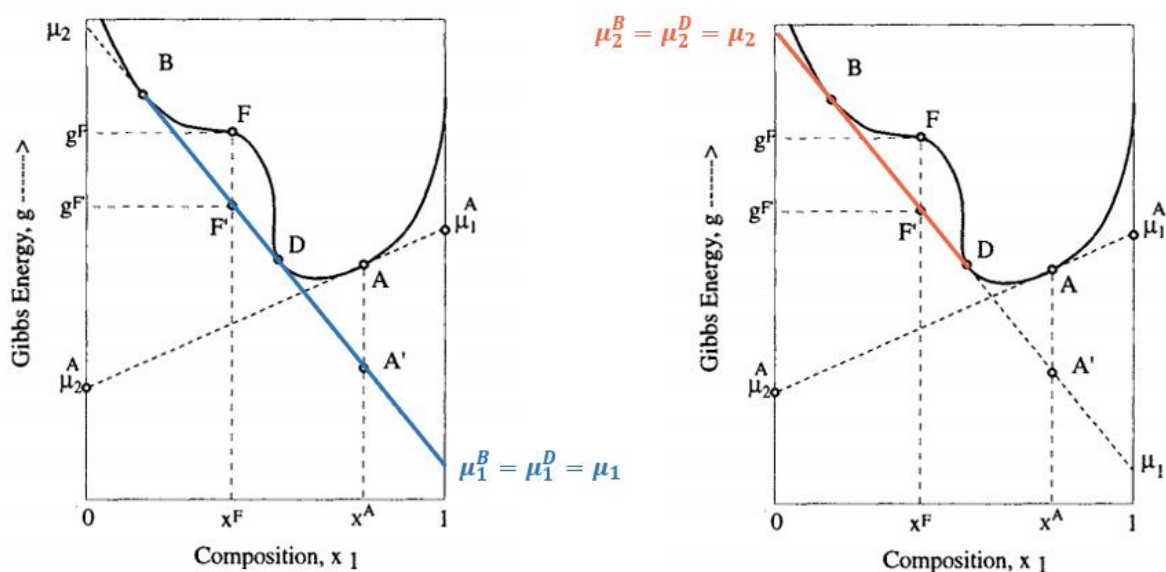
Another example that demonstrates the achievement of thermodynamic equilibrium by phase splitting through minimisation of the Gibbs free energy, is shown in Figure 3.4. A binary system is again considered, containing components 1 and 2 with an initial feed composition of  $F$ . The x-axis of Figure 3.4 demonstrates the mole fraction of the first component, ranging between 0, in which case the mixture fully consists of the second component, and 1 where, accordingly, the mixture fully consists of the first component. It can be shown that a line tangent to a point belonging to the Gibbs energy curve, intersects the Gibbs energy axis (y-axis) at a value that is equal to the chemical potential of component 2 (i.e.,  $\mu_2$  at  $x_1 = 0$ ) and to the chemical potential of component 1 (i.e.,  $\mu_1$  at  $x_1 = 1$ ) at the point of tangency. What makes this observation interesting, is the fact that if a line simultaneously tangent to points B and D is considered, then this line

intersects the y-axis in two points indicating equal values of chemical potential for the same component existing in both the separated phases B and D:

$$\mu_1^B = \mu_1^D = \mu_1 \quad (3.22)$$

$$\mu_2^B = \mu_2^D = \mu_2 \quad (3.23)$$

Eqs. (3.22) and (3.23) show that the chemical potential of component 1 is equal in both phases B and D and the same is true for component 2 in both phases. This fundamentally means that the two phases B and D in which the original binary mixture has been split into, are in thermodynamic equilibrium, since the criterion of thermodynamic equilibrium is that the chemical potential of component  $i$  in phase 1 equals the chemical potential of component  $i$  in phase 2. Another observation is that splitting of the initial feed composition, F, into the two separate phases of B and D, leads to a reduction in the system's Gibbs free energy, denoted in Fig. 3.4 as  $gF'$ . Therefore both conditions, equality of chemical potential and minimisation of Gibbs free energy, demonstrate the system's tendency for thermodynamic equilibrium through separation of the mixture into two different phases.

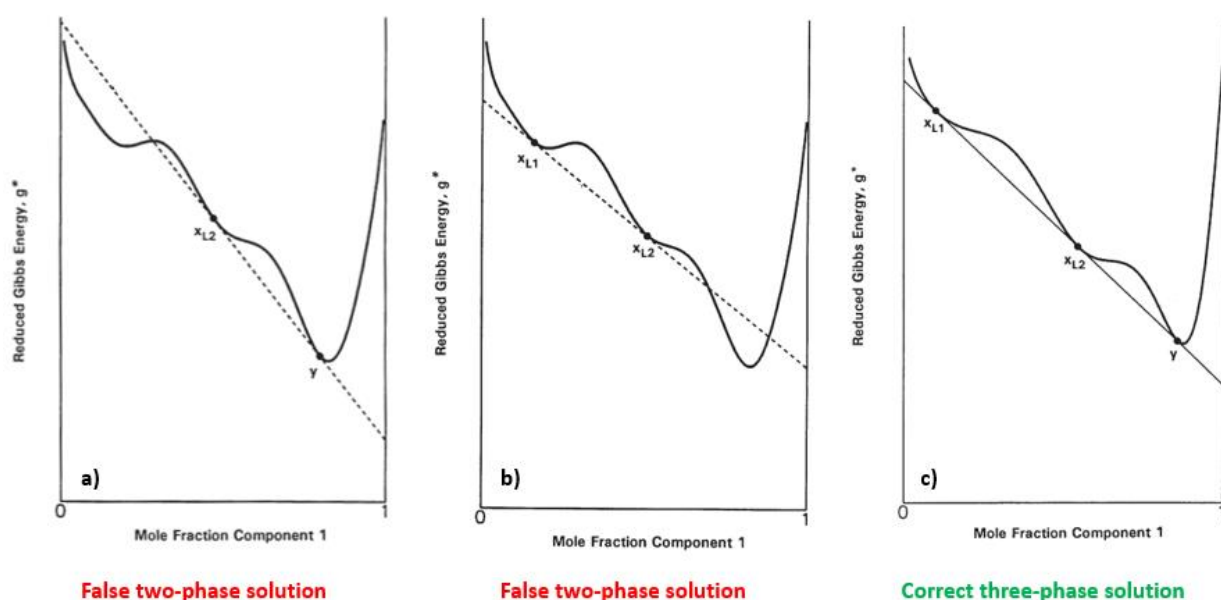


**Figure 3.4:** The feed composition F is separated into the two equilibrated phases B and D characterised with equal chemical potential values, resulting in reduced Gibbs energy (Danesh, 1998).

Another important consideration is that only phase changes that ensure the global minimisation of the Gibbs free energy will eventually take place, as opposed to changes that only result in simple reduction of Gibbs energy. This is better illustrated in Fig. 3.5 where three Gibbs energy plots against the concentration



of the first component are provided. The first two plots (Fig. 3.5a and 3.5b) do not represent valid solutions of a two-phase split as they only yield a local minimum in the mixture Gibbs energy. The correct solution is given in the third diagram (Fig. 3.5c) where a three-phase split ensures a universal minimum, the lowest possible value, in the mixture Gibbs energy. False two-phase solutions are difficult to detect unless one has a priori knowledge of the actual equilibrium condition. Low-temperatures and high CO<sub>2</sub> concentrations are conditions associated with three-phase behaviour that may be susceptible to false two-phase solutions (Whitson, 2000).



**Figure 3.5:** Gibbs energy plots illustrating two false two-phase solutions yielding only a local minimum in the mixture Gibbs energy and the correct three-phase solution (Baker et al., 1982; Whitson, 2000).

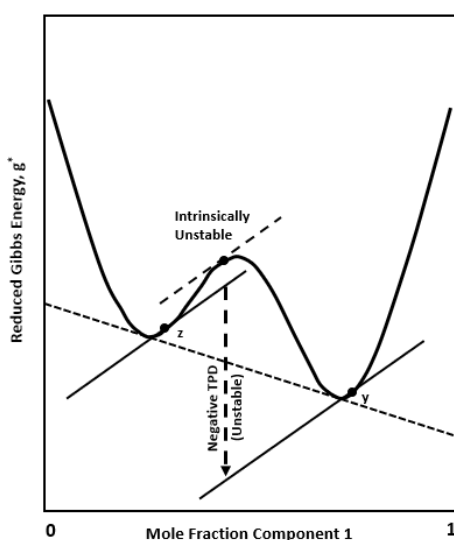
All the above examples lead to the conclusion that a mixture remains a stable single-phase if the Gibbs energy surface is concave upward at all concentrations. Otherwise, the mixture may split into equilibrated phases indicated by the points on the Gibbs energy curve with a common tangent. Amongst all the tangent points, only those by the tangent which identifies the lowest energy level at the mixture composition correspond to the true solution (Danesh, 1998). This graphical stability analysis presented in this section for binary mixtures, can also be used for multicomponent mixtures where the Gibbs energy curve is extended to a Gibbs energy surface and the tangent line to a tangent plane.

### 3.3.2 Michelsen's stability test algorithm

The graphical interpretation of stability analysis presented in the previous section, although convenient for describing the Gibbs tangent plane criterion, is practically impossible to implement as it entails a thorough examination of all the possible compositions that could lead to a reduction of the system's free



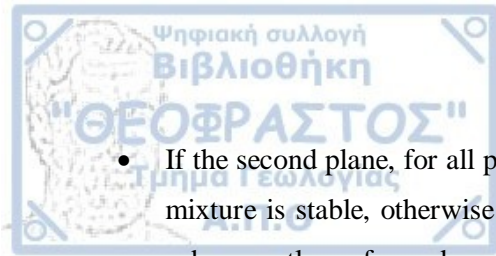
Gibbs energy and consequently, it cannot be implemented as a numerical algorithm through which phase stability will be determined. For that reason in 1982, Michelsen suggested a different approach that basically consists of locating second-phase compositions with tangent planes parallel to the tangent plane of the mixture composition which he proved that they correspond to the minima of the TPD. This way if the parallel tangent planes are located below that of the mixture composition then the mixture is unstable and it will split into two or more phases (Fig. 3.6). On the other hand, if the parallel tangent planes are lying above the mixture tangent plane, or even if a parallel plane does not exist in the first place, then the mixture is stable and will remain as a homogeneous single-phase. In the third case, where a composition that is not equal to the original mixture composition is found to shape the same tangent plane as the original mixture, this is an indication of a mixture at its bubble or dew point (saturation point), with the second phase consisting of an infinitesimal equilibrium phase (incipient phase).



**Figure 3.6:** Michelsen's parallel tangent plane criterion for phase stability. The figure illustrates the case of an unstable mixture with the parallel tangent plane of the second phase composition located below the tangent plane of the original mixture composition (Whitson, 2000).

This method developed by Michelsen, can be successfully applied to various multiphase equilibria problems. The method can be summarised in the following three steps (Danesh, 1998):

- A plane is drawn tangent to the Gibbs energy surface at the feed composition.
- A second phase is assumed to be present. Its composition is so determined that the tangent plane at that point on the Gibbs energy surface becomes parallel to the first plane.



- If the second plane, for all possible compositions, is found to lie above the first one, the original mixture is stable, otherwise it is considered to split into two phases, and flash calculations are subsequently performed.

Based on the above, Michelsen developed a successive substitution stability test algorithm, which constitutes the standard approach to treat phase stability during reservoir simulation processes. The procedure usually requires two tests, one that assumes the second phase as vapour-like and a second test, that assumes the second phase as liquid-like. Each test is conducted separately, converging the vapour-like search first and then converging the liquid-like search. The algorithm is as follows (Gaganis, 2020):

1. Compute fugacity of each component of the feed  $f_i^{(z)}$  using the EoS model
2. Initialise  $K_i$  using Wilson's (1968) correlation (Section 4.1):

$$K_i = \frac{\exp[5.37(1 + \omega_i)(1 - T_{ri}^{-1})]}{p_{ri}} \quad (3.24)$$

where  $\omega_i$ : acentric factor,  $T_{ri}$ : pseudo-reduced temperature,  $p_{ri}$ : pseudo-reduced pressure.

3. Assume feed is a liquid and look for a bubble composition, i.e., compute:

$$Y_i = K_i z_i \quad (3.25)$$

4. Compute trial bubble composition sum:

$$S_V = \sum Y_i \quad (3.26)$$

5. Normalise composition and compute its fugacity  $f_i^{(y)}$ :

$$y_i = Y_i / S_V \quad (3.27)$$

6. Compute correction factor:

$$R_i = \frac{1}{S_V} \frac{f_i^{(z)}}{f_i^{(y)}} \quad (3.28)$$



7. Check for convergence by evaluating:

$$\sum (R_i - 1)^2 < \varepsilon \quad (3.29)$$

where  $\varepsilon < 1 \times 10^{-12}$

8. If convergence has not been achieved, update the equilibrium coefficients by applying:

$$K_i^{(n+1)} = K_i^{(n)} R_i^{(n)} \quad (3.30)$$

where the superscripts  $(n + 1)$  and  $(n)$  indicate the iteration level.

9. After convergence has been achieved check if the algorithm has converged to a “trivial solution”, i.e., a solution corresponding to a second phase composition same to the original fluid composition, by evaluating:

$$\sum (\ln K_i)^2 < \delta \quad (3.31)$$

where  $\delta = 1 \times 10^{-4}$

The algorithm needs to be repeated, this time by assuming that the feed is a gas and the second phase is a drop. In that case, the following changes apply:

3. Assume feed is a liquid and look for a drop composition, i.e., compute:

$$X_i = z_i / K_i \quad (3.32)$$

4. Compute drop composition sum:

$$S_L = \sum X_i \quad (3.33)$$

5. Normalise composition and compute its fugacity  $f_i^{(x)}$ :

$$x_i = X_i / S_L \quad (3.34)$$

6. Compute correction factor:



$$R_i = \frac{1}{S_L} \frac{f_i^{(x)}}{f_i^{(z)}} \quad (3.35)$$

Continue with steps 7-9 as before. As soon as both calculations have been completed, Table 3.3 can be used for the interpretation of the stability test results.

The initial estimation of the equilibrium coefficients in the algorithm presented above, is performed with Wilson's correlation, which even though is a quick means of attaining initial estimates of the K-values, does not necessarily provide reliable results as it is bound by a number of limitations (Section 4.1). However, Michelsen points out that the initial estimate of the new phase composition in the stability algorithm is not crucial as is the case when performing flash calculations. If the stability test indicates the presence of an unstable mixture, then flash calculations are performed next.

**Table 3.3:** Stability test result selection.

Vapour phase test	Liquid phase test	Result
Trivial solution	Trivial solution	Stable
$S_V \leq 1$	Trivial solution	Stable
Trivial solution	$S_L \leq 1$	Stable
$S_V \leq 1$	$S_L \leq 1$	Stable
$S_V > 1$	Trivial solution	Unstable
Trivial solution	$S_L > 1$	Unstable
$S_V > 1$	$S_L > 1$	Unstable
$S_V > 1$	$S_L \leq 1$	Unstable
$S_V \leq 1$	$S_L > 1$	Unstable

### 3.4 Phase split

Flash (or phase split) calculations refer to the determination of the molar amounts and compositions of the equilibrium phases in a hydrocarbon system, given the pressure, temperature and overall composition. Usually, a two-phase flash calculation is performed, considering a biphasic mixture that consists of a vapour phase and a liquid phase existing in equilibrium, which determines:

- the molar fraction of the gas phase ( $n_v$  or  $\beta$ ),
- the moles of the liquid phase ( $n_L$ ),
- the composition of the gas phase ( $y_i$ ) and
- the composition of the liquid phase ( $x_i$ ).

Generally, the two-phase split calculation, as any other phase behaviour calculation, depends on equations that represent i) the material balance for each component and ii) the equality of component fugacity in each phase. Consequently, the first constraint for component and phase material balance, essentially describes that  $n_t$  moles of feed with composition  $z_i$  will distribute into  $n_v$  moles of vapour with composition  $y_i$  and  $n_L$  moles of liquid with composition  $x_i$ , without any loss of matter or chemical alteration. Hence, the total material balance for the system is:

$$n_t = n_v + n_L \quad (3.36)$$

Since usually  $n_t = 1$ , Eq. (3.36) can be expressed as:

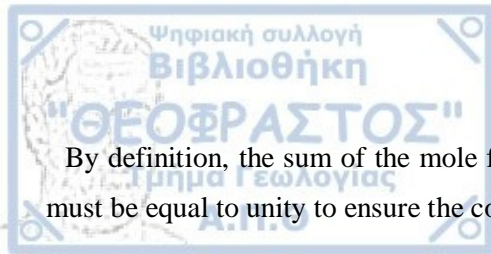
$$n_v + n_L = 1 \quad (3.37)$$

or

$$n_L = 1 - \beta \quad (3.38)$$

The material balance for each component,  $i$ , considering  $n_t = 1$  is:

$$z_i = y_i \beta + x_i (1 - \beta) \quad (3.39)$$



By definition, the sum of the mole fractions of the equilibrated phases and that of the original mixture, must be equal to unity to ensure the compositional consistency of each equilibrated phase:

$$\sum_{i=1}^N z_i = \sum_{i=1}^N y_i = \sum_{i=1}^N x_i = 1 \quad (3.40)$$

where  $N$ : number of components. Note that  $\sum z_i = 1$  is supposed to be satisfied by definition. It can be shown that  $\sum x_i = 1$  also implies that  $\sum y_i = 1$ , thus reducing the equations in (3.40) to one only.

Therefore, the following equation can be obtained:

$$\sum_{i=1}^N y_i - \sum_{i=1}^N x_i = 0 \quad (3.41)$$

The second criterion of equifugacity is fulfilled with the following equation that applies for two phases in equilibrium (definition of the equilibrium coefficient,  $K_i$ ):

$$K_i = \frac{y_i}{x_i} = \frac{\varphi_i^L}{\varphi_i^V} \quad (3.42)$$

Eqs. (3.39) and (3.42) may be combined to give:

$$z_i = x_i K_i \beta + x_i (1 - \beta)$$

or solving for  $x_i$ :

$$x_i = \frac{z_i}{\beta(K_i - 1) + 1} \quad (3.43)$$

and accordingly for  $y_i$ :

$$y_i = \frac{z_i K_i}{\beta(K_i - 1) + 1} = K_i x_i \quad (3.44)$$



The material balance equations, Eqs. (3.39), (3.41), and the equilibrium requirement, Eq. (3.42) provide the required  $2n+1$  equations to solve the phase split problem and determine the  $2n+1$  unknowns, i.e.,  $y_i$ ,  $x_i$  and  $\beta$ . However, the number of variables can be reduced by the combination of Eqs. (3.40), (3.43) and (3.44) that result in:

$$\sum_{i=1}^N x_i = \sum_{i=1}^N \frac{z_i}{\beta(K_i - 1) + 1} = 1 \quad (3.45)$$

$$\sum_{i=1}^N y_i = \sum_{i=1}^N \frac{z_i K_i}{\beta(K_i - 1) + 1} = 1 \quad (3.46)$$

Therefore:

$$\sum_{i=1}^N \frac{z_i K_i}{\beta(K_i - 1) + 1} - \sum_{i=1}^N \frac{z_i}{\beta(K_i - 1) + 1} = 0 \quad (3.47)$$

And finally:

$$f(\beta) = \sum_{i=1}^N \frac{z_i(K_i - 1)}{\beta(K_i - 1) + 1} = 0 \quad (3.48)$$

Eq. (3.48) is the famous Rachford-Rice equation which can be solved by root solving techniques, such as successive substitution or the Newton-Raphson method, for the vapour phase molar fraction  $\beta$ . This way, the phase split problem is reformulated in terms of the K-values and the vapour phase mole fraction,  $\beta$ , while the number of equations is reduced to  $n+1$  that is, Eqs. (3.42) and (3.48) with  $n+1$  unknowns, i.e.,  $K_i$  and  $\beta$ . Therefore, it is more than evident the degree at which simplifies the problem the in advance knowledge by any means of the equilibrium coefficients.

### 3.4.1 Two-phase flash algorithm

The above mentioned set of equations are the key equations used in two-phase split calculations. The phase split algorithm for the computation of the vapour phase mole fraction,  $\beta$  and the compositions of the vapour and liquid phases  $y_i$  and  $x_i$  respectively, is presented next.

**Step 1: Estimation of initial K-values.** If a stability analysis has been performed indicating a biphasic mixture, the converged K-values resulting from the stability test, provide the most reliable K-value estimates for the initialization of the two-phase split. In a direct two-phase split calculation, Wilson's (1968) correlation can be used instead (Section 4.1):

$$K_i = \frac{\exp[5.37(1 + \omega_i)(1 - T_{ri}^{-1})]}{p_{ri}} \quad (3.24)$$

**Step 2: Calculation of  $\beta$ .** The vapour phase mole fraction,  $\beta$ , is calculated through the Rachford-Rice equation, Eq. (3.48), which is a non-linear equation, yet monotonically decreasing, and its solution requires iterative techniques, like the Newton-Raphson method, until convergence is achieved at a set tolerance. An arbitrary value of  $\beta$  is first assumed between 0 and 1, usually 0.5. Ahmed (2013) suggests a relationship for the calculation of a more reliable initial value of  $\beta$ . This assumed value of  $\beta$  is evaluated in Eq. (3.48) along with the initial estimates of the K-values. If the absolute value of the function  $f(\beta)$  is less than the preset tolerance, e.g.,  $f(\beta) < 10^{-6}$ , then the assumed value of  $\beta$  is kept as the correct solution. Otherwise, a new value is provided from the following expression:

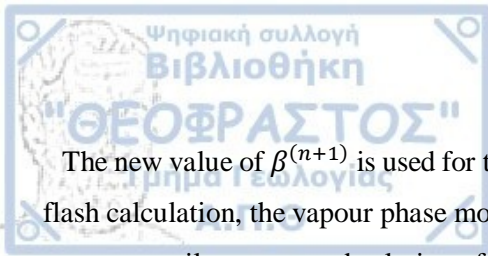
$$\beta^{(n+1)} = \beta^n - \frac{f(\beta)}{f'(\beta)} \quad (3.49)$$

where the superscripts  $(n + 1)$  and  $(n)$  indicate the iteration level.

The first derivative of function  $f(\beta)$  is given by:

$$f'(\beta) = - \sum_{i=1}^N \frac{z_i(K_i - 1)^2}{[\beta(K_i - 1) + 1]^2} \quad (3.50)$$





The new value of  $\beta^{(n+1)}$  is used for the next iteration, and hence, during this second step of the two-phase flash calculation, the vapour phase mole fractions are updated at each iteration, while the K-values are kept constant until a converged solution of  $\beta$  has been reached.

**Step 3: Calculation of liquid and gas phase composition.** Having determined  $\beta$  corresponding to the assumed K-values, the composition of the liquid and gas phases can be calculated from Eqs. (3.43) and (3.44) respectively.

**Step 4: Calculation of  $Z_L$ ,  $Z_v$ ,  $f_i^L$  and  $f_i^v$  from an EoS.** The previously calculated compositions are used for the re-evaluation of the K-values with the assistance of an EoS, that will be substituted in Eq. (3.48) for the next round of iteration. The compressibility factors of the liquid,  $Z_L$ , and vapour,  $Z_v$ , phases, as well as the fugacity of each component in the liquid,  $f_i^L$ , and vapour,  $f_i^v$ , phases are calculated with one of the following equations of state (EoS):

SRK EoS:

$$Z^3 - Z^2 + (A - B - B^2)Z - AB = 0 \quad (2.34)$$

$$\ln \varphi_i = \frac{B_i}{B} (Z - 1) - \ln(Z - B) + \frac{A}{B} \left[ \frac{B_i}{B} - \frac{2}{\alpha a} \sum_j x_j (\alpha a)_{ij} \right] \ln \left( 1 + \frac{B}{Z} \right) \quad (3.51)$$

PR EoS:

$$Z^3 - (1 - B)Z^2 + (A - 3B^2 - 2B)Z - (AB - B^2 - B^3) = 0 \quad (2.42)$$

$$\ln \varphi_i = \frac{B_i}{B} (Z - 1) - \ln(Z - B) + \frac{A}{2.828B} \left[ \frac{B_i}{B} - \frac{2}{\alpha a} \sum_j x_j (\alpha a)_{ij} \right] \ln \left( \frac{Z + 2.414B}{Z - 0.414B} \right) \quad (3.52)$$

where  $\varphi_i$ : partial component fugacity (fugacity coefficient) for the calculation of component fugacity from Eqs. (2.9) and (2.10),  $A$ ,  $B$ ,  $\alpha$  and  $a$ : equation of state parameters presented in Chapter 2.

**Step 5: Evaluation of the fugacity constrain.** In this step, the equality of the individual component fugacities for each phase calculated at the previous step, is checked to a set tolerance level (i.e.,  $\varepsilon = 1 \times 10^{-13}$ ):

$$\sum_{i=1}^N \left( \frac{f_i^L}{f_i^V} - 1 \right)^2 < \varepsilon \quad (3.53)$$

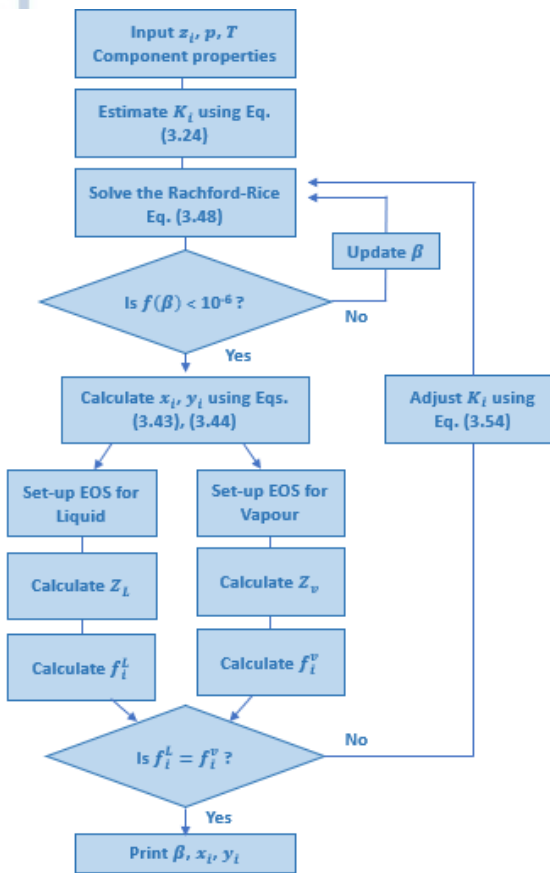
**Step 6: Convergence check.** If convergence is reached at step 5 then the process is completed. If convergence has not been reached, the K-values must be updated and the new values are used for the next iteration starting again at step 2. A new set of K-values can be obtained with successive substitution:

$$K_i^{(n+1)} = K_i^{(n)} \frac{f_i^{L(n)}}{f_i^{V(n)}} \quad (3.54)$$

**Step 7: Trivial solution check.** If a stability analysis has not been performed a trivial solution might arise that needs to be confirmed with a stability test. Convergence at a trivial solution can be checked with the following condition:

$$\sum_{i=1}^N (\ln K_i)^2 < 10^{-4} \quad (3.55)$$

In summary, the following figure (Fig. 3.7) is the flowchart of the phase split algorithm which consists of an inner loop that solves the Rachford-Rice equation for the calculation of the vapour phase mole fraction,  $\beta$ , by keeping the K-values constant, and updating the value of  $\beta$  at each iteration step and an outer loop that uses the previously estimated  $\beta$ ,  $x_i$  and  $y_i$ , to acquire a new set of K-values to be used for the next outer loop iteration. The algorithm is completed when the correct  $\beta$  has been determined that corresponds to the set of K-values that properly characterise the vapour-liquid equilibria of the hydrocarbon system.



**Figure 3.7:** Flow chart of the flash calculation algorithm using an EoS.

The solution of Eq. (3.48) should always be limited to the region  $\beta_{min} \leq \beta \leq \beta_{max}$  which is the only physically meaningful solution where compositions  $x_i$  and  $y_i$  are positive.  $\beta = 0$  corresponds to a biphasic mixture consisting of a liquid, in equilibrium with an infinitesimal amount of gas (bubble point condition), while  $\beta = 1$  corresponds to a biphasic mixture consisting of a gas, in equilibrium with an infinitesimal amount of liquid (dew point condition). The values of  $\beta_{min}$  and  $\beta_{max}$  are determined from:

$$\beta_{min} = \frac{1}{1 - K_{i(max)}} \quad (3.51)$$

$$\beta_{max} = \frac{1}{1 - K_{i(min)}} \quad (3.52)$$

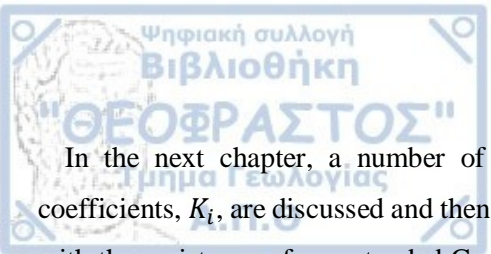
However, there are two other types of converged solutions that can be obtained. When  $\beta < 0$  or  $\beta > 1$  we come up with a physically unacceptable solution that is referred to as a negative flash, which still

satisfies the equifugacity and material balance constraints and fundamentally indicates that the mixture is thermodynamically stable as a single phase and thus will not split into two phases. The second possible solution is a so-called “trivial” solution that corresponds to liquid and gas compositions identical to the initial feed composition and K-values equal to unity ( $x_i = y_i = z_i$ ,  $K_i = 1$ ). These last two solutions apparently arise when a stability analysis has not been previously performed and they should always be checked with the phase stability test to verify that the mixture is indeed single phase. A valid trivial solution occurs when two-phase solutions do not exist (Whitson, 2000).

### 3.5 CPU time requirements and importance of the in advance knowledge of K-values

In compositional reservoir simulation processes, the reservoir is divided into an enormous number of cells where each cell contains either a single-phase or a multi-phase fluid that is considered to be in equilibrium at the cell's prevailing pressure and temperature conditions. The equilibrium conditions within each cell at each timestep, are determined by complex phase split calculations whose iterative nature calls for more than one calculation per gridblock at any timestep. It can be realised therefore, that in a compositional reservoir simulator a considerable amount of computational time is taken up because of these iterative calculations at each cell. In fact, for a large reservoir, the total number of equilibrium flashes may exceed millions or even billions, consuming a large computational time and resulting of course, in expensive computation. Hence, the reduction of flash calculation time is an important consideration in compositional reservoir simulation projects.

In this section it was shown that with the assistance of the Rachford-Rice equation, Eq. (3.48), the number of equations consisting the two-phase split problem is reduced to  $n+1$  equations that need to be solved for the determination of  $n+1$  unknowns, i.e.,  $K_i$  and  $\beta$ . This indicates that if the K-values are known by any means, then the phase split calculation problem is further simplified to exclusively the calculation of the vapour phase mole fraction,  $\beta$ , since the only iterative process would be the solution of the Rachford-Rice equation. Once the correct  $\beta$  is calculated, then compositions  $x_i$  and  $y_i$  would be directly determined from Eqs. (3.43) and (3.44). Therefore, the importance of the in advance knowledge of the equilibrium coefficients,  $K_i$ , cannot be stressed enough, as it provides a means to an extremely reduced number of computations and subsequently, to a substantially reduced amount of computational time. This is of great importance considering that in compositional simulation, phase split calculations constitute a very significant part as was previously mentioned, and can account for up to 30% of the total running time. This is further justified by the fact that the successive substitution methods used in phase split calculations can be very slow in converging to a solution, especially for near critical mixtures for which all the K-values approach unity.



In the next chapter, a number of conventional methods for the determination of the equilibrium coefficients,  $K_i$ , are discussed and then the chapter focuses on a new method for the calculation of K-values with the assistance of an extended Constant Volume Depletion test, which is basically a generalisation of the classic Constant Volume Depletion laboratory test, that was developed for the purposes of this thesis and specifically for accelerating the gathering of characteristic K-values, necessary for the simulation of gas condensate reservoirs undergoing dry gas recycling procedures.



## 4 SOURCES OF K-VALUES

Equilibrium coefficients constitute a great part of phase equilibria calculations, which in turn are necessary in several reservoir engineering applications. During the previous decades, the oil industry relied broadly upon empirical correlations as the only means of acquiring equilibrium coefficient data, even though they mostly provide rough approximations of the required K-values and are further conditioned by various assumptions and limitations. More recently, advancements in computational power have created a shift towards the more complex and time consuming, yet more efficient and accurate method of deriving K-values with the assistance of Equations of State. Despite the fact that estimation of K-values through empirical correlations might appear as a rather obsolete method compared to the more sophisticated EoS approach, correlations are still used widely today as a quick and economic way of gathering the desired K-value data. By all means, there is also an increasing number of new methods with the ability to produce accurate values of equilibrium ratios, while reducing the computational time.

In this chapter, several methods of gathering equilibrium coefficient values are presented, starting with empirical correlations proposed by various authors, including correlations for the plus fraction and for the non-hydrocarbon components. The following section deals with EoS-derived equilibrium coefficients, focusing on the increased time requirements that characterise this method. Next, two classic PVT studies for the analysis of reservoir fluids are presented, namely the Constant Composition Expansion (CCE) or Constant Mass study, and the Constant Volume Depletion (CVD) study which is later used in this thesis to acquire equilibrium coefficient values for comparison with K-values derived from EoS-based, compositional reservoir simulation scenarios of a gas condensate system. In the last section of the chapter, a new experimental method is presented that was developed for the purposes of this thesis, as a modification of the classic CVD study, that provides an accurate and accelerated estimation of K-values corresponding to a gas condensate system undergoing the process of dry gas recycling.

### 4.1 Determination of equilibrium ratios using empirical correlations

In section 2.1 it was stated that the equilibrium ratio can be expressed in terms of vapour pressure and system pressure, based on Raoult's law according to the following relationship:

$$K_i = \frac{y_i}{x_i} = \frac{p_{vi}}{p} \quad (2.4)$$

The simplicity of this equation, which of course is bound by a number of assumptions, encourages the idea of estimating the equilibrium coefficients of a hydrocarbon system, solely by the use of component vapour pressure and system pressure. Even though this might be applicable to low pressures, in higher pressures, this approach is proved to be erroneous as it results in inaccurate predictions, since it assumes that K-values are only a function of the hydrocarbon system temperature and pressure and not overall composition. In real mixtures, the influence of the composition is of great significance. Therefore, since prediction of equilibrium coefficients is necessary in several phase equilibria calculations, numerous methods have been developed through the years that involve empirical relationships for the estimation of K-values of hydrocarbon mixtures utilizing both approaches, that is both depending and being independent of the mixture composition. Some of these methods are presented next.

#### 4.1.1 A simplified method for the determination of K-values

This method can be applied to light hydrocarbon mixtures that exist at a low pressure (< 1000 psia) and correlates the equilibrium ratios of C<sub>2</sub> to C<sub>7</sub> with that of methane. First, the K-value for the methane fraction is estimated with the following relationship:

$$K_{C_1} = \frac{\exp\left(A - \frac{B}{T}\right)}{p} \quad (4.1)$$

with

$$A = 2.0 \times 10^{-7}p^2 - 0.0005p + 9.5073 \quad (4.2)$$

$$B = 0.0001p^2 - 0.456p + 865 \quad (4.3)$$

where

$T$ : system temperature, °R,  $p$ : system pressure, psia.

The following equation (4.4) correlates the K-value of the methane fraction with the K-values of C<sub>2</sub> – C<sub>7</sub>:

$$K_i = \frac{K_{C_1} R_i}{\ln(p K_{C_1})} \quad (4.4)$$

where  $R_i$ , the component characterisation parameter given by:



$$R_i = a_i T - b_i \quad (4.5)$$

The values for coefficients  $a_i$  and  $b_i$  are given in Table 4.1 for pure components  $C_2 - C_7$ . The K-value for the plus fraction ( $C_{7+}$ ) can be found by the Katz et al. (1959) expression presented in Section (4.2.1). It is evident that this method only serves as a rough estimate of the K-values for light hydrocarbon mixtures at pressures below 1000 psia.

**Table 4.1:** Values for the coefficients  $a_i$  and  $b_i$  for the  $C_2 - C_7$  fractions (Ahmed, 2010).

Component	$a_i$	$b_i$
$C_2$	0.00665	1.29114
$C_3$	0.00431	1.269876
i- $C_4$	0.00327	1.206566
n- $C_4$	0.00245	1.1002
i- $C_5$	0.00203	0.910736
n- $C_5$	0.00147	0.737
$C_6$	0.00094	0.528
$C_7$	0.00091	0.516263

#### 4.1.2 Wilson's method (1968)

The correlation proposed by Wilson is one of the most well-known methods for the determination of K-values as it is still used widely today as a means to provide initial estimates of K-values that are necessary in Stability and Phase split algorithms (discussed in Chapter 3). Wilson's correlation has the following form:

$$K_i = \frac{p_{c_i}}{p} \exp \left[ 5.37(1 + \omega_i) \left( 1 - \frac{T_{c_i}}{T} \right) \right] \quad (4.6)$$



where  $p_{ci}$ : critical pressure of component i, psia,  $p$ : system pressure, psia,  $T_{ci}$ : critical temperature of component i, °R,  $T$ : system temperature, °R,  $\omega_i$ : acentric factor of component i. The Wilson equation generally provides reliable estimation of K-values for subcritical components when applied in low pressures that do not exceed 500 psia (Danesh, 1998; Michelsen, 1993).

#### 4.1.3 Hoffman et al. correlation (1953)

Any hydrocarbon or non-hydrocarbon component can be uniquely characterised by combining its boiling point temperature, critical temperature and critical pressure, into a characterisation parameter which is defined by the following expression (Ahmed, 2010):

$$F_i = b_i [1/T_{bi} - 1/T] \quad (4.7)$$

where

$$b_i = \frac{\log(p_{ci}/14.7)}{[1/T_{bi} - 1/T_{ci}]} \quad (4.8)$$

In Eqs. (4.7) and (4.8),  $F_i$ : component characterisation factor,  $T_{bi}$ : normal boiling point of component i, °R.

Hoffman et al. observed that plots of  $\log(K_i p)$  vs  $F_i$  at a given pressure, often form straight lines for components  $C_1 - C_6$  and correlate well with the measured K-values that characterise a gas condensate reservoir. Based on the above observation they proposed the following equation for the calculation of K-values for light hydrocarbons ( $C_1 - C_6$ ):

$$\log K_i p = A_0 + A_1 F_i \quad (4.9)$$

or equivalently,

$$K_i = \frac{10^{(A_0 + A_1 F_i)}}{p} \quad (4.10)$$

where

$A_0$ : intercept of the  $\log(K_i p)$  vs  $F_i$  plot and  $A_1$ : slope of the  $\log(K_i p)$  vs  $F_i$  plot. The parameters values depend on the fluid composition and Hoffman et al. did not provide a method to estimate them. As a result, this method is mostly used to validate experimentally obtained K-values by evaluating whether they lie closely enough on a straight line.

#### 4.1.4 Standing's method (1979)

Based on the above method of Hoffman et al., Standing proposed a low pressure K-value correlation that can be used at pressures < 1000 psia and temperatures < 200 °F and is mainly applied to surface separator calculations. Standing produced a set of equations that fit the graphical presentations of the experimental K-values derived from samples of Oklahoma City crude oil/natural gas, generated by Katz and Hachmuth (1937). The proposed equations correlate coefficients  $A_0$  and  $A_1$  of Eq. (4.9) with pressure to give:

$$A_0 = 1.2 + 0.00045p + 15 \times 10^{-8}p^2 \quad (4.11)$$

$$A_1 = 0.89 - 0.00017p - 3.5 \times 10^{-8}p^2 \quad (4.12)$$

Standing proposed optimised modified values of the correlating parameter  $b_i$  and the boiling point  $T_{bi}$  of Eq. (4.7) for the following components  $N_2$ ,  $CO_2$ ,  $H_2S$  and  $C_1 - C_6$  which are shown in Table 4.2, that considerably improve the predicted K-values.

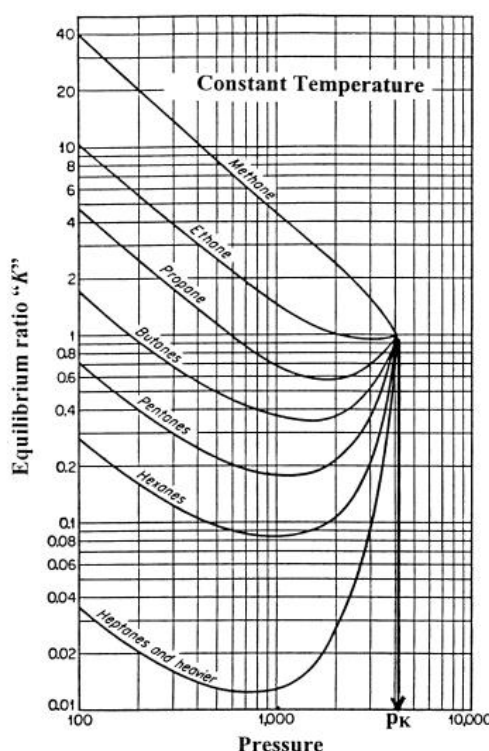
**Table 4.2:** Optimised values of  $b_i$  and  $T_{bi}$  from Eqs. (4.7) and (4.8) for use in Standing's low pressure K-value correlation (Ahmed, 2010).

Component	$N_2$	$CO_2$	$H_2S$	$C_1$	$C_2$	$C_3$	i- $C_4$	n- $C_4$	i- $C_5$	n- $C_5$	$C_6^*$	n- $C_6$	n- $C_7$	n- $C_8$	n- $C_9$	n- $C_{10}$
$b_i$	470	652	1136	300	1145	1799	2037	2153	2368	2480	2738	2780	3068	3335	3590	3828
$T_{bi}$ (°R)	109	194	331	94	303	416	471	491	542	557	610	616	616	718	763	805
*Lumped Hexanes fraction																

#### 4.1.5 The Convergence Pressure method

In a multicomponent hydrocarbon mixture it can be shown that as the pressure increases isothermally, while the overall mixture composition remains fixed, the plot of experimentally determined K-values vs pressure illustrates a tendency of the equilibrium coefficients of all components to converge towards unity at a certain pressure defined as the convergence pressure,  $p_k$ , of the hydrocarbon mixture (Fig. 4.1). Since all components exhibit the same equilibrium coefficient value of unity at the convergence pressure, this suggests that all existing phases must have the same composition. As the above condition only occurs for hydrocarbon mixtures that are characterised by their critical temperature, then the convergence pressure should be the critical pressure. In any other temperature, the convergence pressure is a non-physical value because the mixture reaches its saturation pressure (bubble or dew point pressure) long before it reaches the convergence pressure.

In log-log plots of K-values vs pressure as in Figure 4.1, for light components (where  $T > T_{ci}$ ), K-values decrease monotonically toward the convergence pressure, while for heavier components (where  $T < T_{ci}$ ), K-values initially decrease as a function of pressure at low pressures, reaching a minimum, and finally increasing toward unity at the convergence pressure (Whitson, 2000). It has been observed that K-values generally reach this minimum at pressures  $> 1000$  psia, implying that for low pressures, K-values are independent of composition because they have a linear relationship with pressure and therefore are only dependent on system pressure. In addition, it has been shown that for mixtures of various composition with convergence pressures of 4000 psia or greater and system pressures of less than 1000 psia, equilibrium ratios present essentially the same values, thus providing yet another indication that the overall mixture composition has a minor effect on K-values if the system pressure is  $< 1000$  psia. However, each hydrocarbon system may exhibit a different convergence pressure, since two sets of equilibrium coefficients for example, do not necessarily present the same values at particular pressures and temperatures, proving that at least in high pressures, there is a compositional influence on K-values.



**Figure 4.1:** Equilibrium ratios for a hydrocarbon system on a K-value/Pressure log-log diagram converging to unity at the convergence pressure,  $p_K$  (Ahmed, 2010).

The convergence pressure method provides a useful parameter for correlating the effect of composition on equilibrium ratios. The convergence pressure can fairly describe this compositional dependency at high pressures and for that reason equilibrium ratios are usually correlated as functions of pressure, temperature

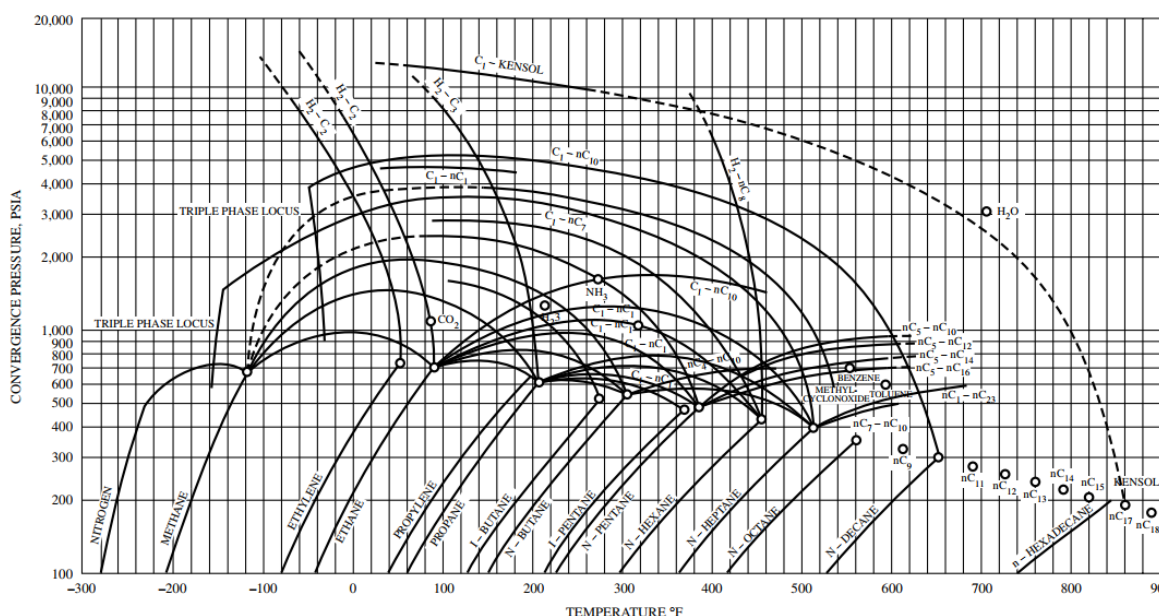
and convergence pressure. There are a number of different methods in the literature for the calculation of convergence pressure and three of these methods are discussed next:

- Hadden's method (1953)

This iterative procedure considers a binary system, that is assumed to describe the entire hydrocarbon mixture, consisting of the lightest fraction in the hydrocarbon system and a pseudo-component that lumps all the remaining fractions. This binary system then uses the binary system convergence pressure chart (Fig. 4.2) to determine the convergence pressure of the hydrocarbon mixture at a specific temperature. Convergence pressure is determined as follows (Ahmed, 2010):

**Step 1:** Estimate a value for the convergence pressure.

**Step 2:** From appropriate equilibrium ratio charts, read the K-values of each component present in the mixture by entering the charts with the system pressure and temperature.

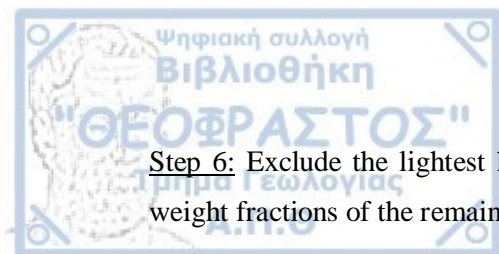


**Figure 4.2:** Convergence pressures for binary systems. (Gas Processors Suppliers Association, Engineering Data Book, 10th Ed., 1978).

**Step 3:** Perform flash calculations using the calculated K-values and system composition to determine liquid phase composition.

**Step 4:** Identify the lightest hydrocarbon component that comprises of at least 0.1 mol % in the liquid phase.

**Step 5:** Convert the liquid mole fraction to a weight fraction.



Step 6: Exclude the lightest hydrocarbon component, as identified in Step 4 and normalise the weight fractions of the remaining components.

Step 7: Calculate the weight average critical temperature and pressure of the pseudo-component.

Step 8: Enter Figure 4.2 with the critical properties of the pseudo-component and trace the critical locus of the binary system consisting of the light component and the pseudo-component.

Step 9: Read the new convergence pressure from the point at which the locus crosses the temperature of interest.

Step 10: If the calculated new convergence pressure is not reasonably close to the assumed value, repeat Steps 2 through 9.

- Standing's method (1977)

The convergence pressure can be approximately correlated with the molecular weight of the  $C_{7+}$  fraction,  $M_{(C_{7+})}$ , with the following linear equation proposed by Whitson and Torp (1981):

$$p_k = 60M_{(C_{7+})} - 4200 \quad (4.13)$$

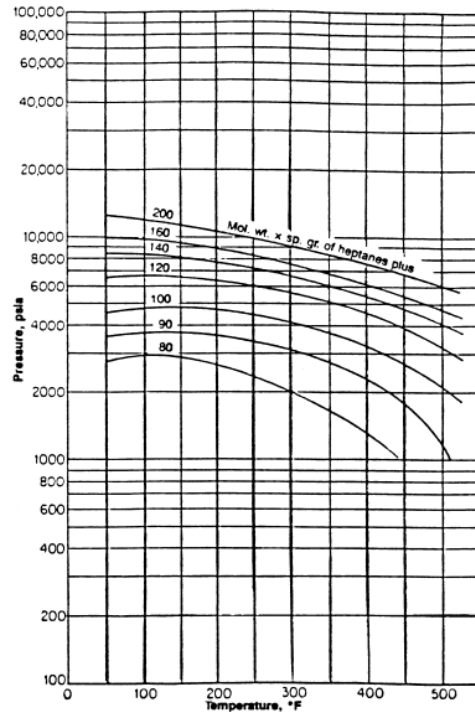
- Rzasa et al.'s method (1952)

This method provides a simplified graphical correlation for the prediction of convergence pressure in light hydrocarbon mixtures (Fig. 4.3). It is expressed mathematically as a function of temperature and the product of the molecular weight and specific gravity of the heptanes-plus fraction and can be used for hydrocarbon mixtures at temperatures in the range of 50 to 300 °F as follows:

$$p_k = -2381.8542 + 46.341487M_{(C_{7+})} \cdot \gamma_{(C_{7+})} + \sum_{i=1}^3 a_i \left[ \frac{M_{(C_{7+})} \cdot \gamma_{(C_{7+})}}{T - 460} \right]^i \quad (4.14)$$

where

$M_{(C_{7+})}$ : molecular weight of  $C_{7+}$ ,  $\gamma_{(C_{7+})}$ : specific gravity of  $C_{7+}$ ,  $T$ : temperature, °R,  $a_1 = 6124.3049$ ,  $a_2 = -2753.2538$ ,  $a_3 = 415.42049$ .



**Figure 4.3:** Rzaa et al.'s convergence pressure correlation (American Institute of Chemical Engineers).

#### 4.1.6 Whitson & Torp's correlation (1981)

Whitson and Torp modified Wilson's equation (Eq. 4.6) in order to achieve accurate results in higher pressures by incorporating the convergence pressure into the equation and introducing a pressure dependent parameter,  $A_1$ :

$$K_i = \left( \frac{p_{ci}}{p_k} \right)^{A_1 - 1} \frac{\exp[5.37 A_1 (1 + \omega_i)(1 - T_{ri}^{-1})]}{p_{ri}} \quad (4.15)$$

with

$$A_1 = 1 - \left( \frac{p}{p_k} \right)^{0.7} \quad (4.16)$$

where  $p_{ci}$ : critical pressure of component i,  $p_k$ : convergence pressure,  $\omega_i$ : acentric factor of component i,  $T_{ri}$ : pseudo-reduced temperature ( $T_{ci}/T$ ) of component i,  $p_{ri}$ : pseudo-reduced pressure ( $p_{ci}/p$ ) of component i, pressures  $p$  and  $p_k$  are given in psig.

## 4.2 Equilibrium coefficients of the Plus Fraction

All the previously presented correlations for the determination of equilibrium ratios for hydrocarbon mixtures are based on the critical properties of well-defined pure components. However, when performing phase equilibria calculations the equilibrium ratio for all components, including the plus fraction, must be known. For this reason, the following correlations developed for the determination of equilibrium ratios of the plus fraction, are discussed next.

### 4.2.1 Katz & Hachmuth's correlation (1937)

These authors proposed a simple relationship that gives a reasonable approximation of the K-value of the heptanes-plus fraction, when applied in light hydrocarbon mixtures. They suggested that the K-value of  $C_{7+}$  is equal to the 15% of the K-value of the heptanes component:

$$K_{C_{7+}} = 0.15K_{C_7} \quad (4.17)$$

### 4.2.2 Standing's method (1979)

Standing extended his method to the calculation of K-values for the plus fraction by imposing experimental K-values for the  $C_{7+}$  on Eq. (4.10), thus calculating the corresponding characterisation factors,  $F_i$ , for the plus fraction. He suggested the following equations, where initially, the number of carbon atoms,  $n$ , of the normal paraffin hydrocarbon that has the same K-value as the  $C_{7+}$  fraction, is calculated as a function of system temperature and pressure:

$$n = 7.30 + 0.0075(T - 460) + 0.0016p \quad (4.18)$$

Next, the estimated number of carbon atoms is used to calculate the correlating parameter,  $b$ , and the boiling point,  $T_b$ , required in Eq. (4.7) by using the following relationships:

$$b = 1013 + 324n - 4.256n^2 \quad (4.19)$$

$$T_b = 301 + 59.85n - 0.971n^2 \quad (4.20)$$

Last, the characterisation factor of the plus fraction is calculated from Eq. (4.7) and the desirable equilibrium coefficient value of the  $C_{7+}$  is estimated from Eq. (4.10). It should be pointed out that Standing's correlation, as was previously mentioned, can only be applied to low pressures of less than 1000 psia and temperatures that do not exceed 200 °F. These conditions make Standing's correlations suitable for



application in separator flash calculations, as they provide accurate estimations for crude oils with GORs ranging from 300 to 1500 scf/STB and oil gravities ranging from 26 to 48 °API (Glaso & Whitson, 1980).

#### 4.2.3 Winn's correlation (1954)

Winn proposed a relationship that estimates the equilibrium ratio of the plus fraction, as a function of the K-values of n-heptane and ethane and a volatility exponent:

$$K_{C_+} = \frac{K_{C_7}}{(K_{C_2}/K_{C_7})^b} \quad (4.21)$$

where  $K_{C_+}$ : K-value of the plus fraction,  $K_{C_7}$ : K-value of n-heptane at system pressure, temperature and convergence pressure,  $K_{C_2}$ : K-value of ethane and  $b$ : volatility exponent. The volatility exponent can be calculated from the following expression:

$$b = a_1 + a_2(T_b - 460) + a_3(T_b - 460)^2 + a_4(T_b - 460)^3 + \frac{a_5}{T - 460} \quad (4.22)$$

where  $T_b$ : atmospheric boiling point, °R,  $a_1 = 1.6744337$ ,  $a_2 = -3.4563079 \cdot 10^{-3}$ ,  $a_3 = 6.1764103 \cdot 10^{-6}$ ,  $a_4 = 2.4406839 \cdot 10^{-9}$ ,  $a_5 = 2.9289623 \cdot 10^2$ .

#### 4.2.4 Campbell's method (1976)

According to Campbell, the plot of  $\log(K_i)$  vs  $(T_{ci})^2$  for each component is a linear relationship in any hydrocarbon system. Based on this observation, he proposed that extrapolation of the best fit straight line passing through propane to hexane components, can provide a value for the equilibrium coefficient of the plus fraction.

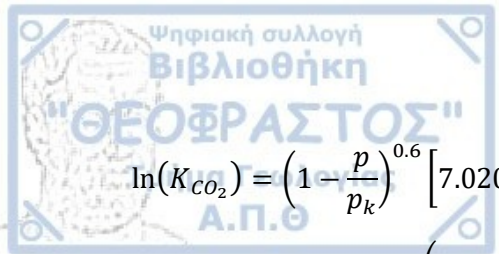
### 4.3 Correlations for non-hydrocarbon components

#### 4.3.1 Lohrenze et al.'s correlations (1963)

The following correlations are used for the estimation of K-values of non-hydrocarbon components ( $N_2$ ,  $CO_2$  and  $H_2S$ ) as a function of system pressure, temperature and convergence pressure:

$$\ln(K_{N_2}) = \left(1 - \frac{p}{p_k}\right)^{0.4} \left[ 11.294748 - \frac{1184.2409}{T} - 0.90459907 \ln(p) \right] \quad (4.23)$$





$$\ln(K_{CO_2}) = \left(1 - \frac{p}{p_k}\right)^{0.6} \left[ 7.0201913 - \frac{152.7291}{T} - \ln(p) \left( 1.8896974 - \frac{1719.2856}{T} + \frac{644740.69}{T^2} \right) \right] \quad (4.24)$$

$$\ln(K_{H_2S}) = \left(1 - \frac{p}{p_k}\right)^{0.8} \left[ 6.3992127 + \frac{1399.2204}{T} - \ln(p) \left( 0.76885112 + \frac{18.215052}{T} \right) - \frac{1112446.2}{T^2} \right] \quad (4.25)$$

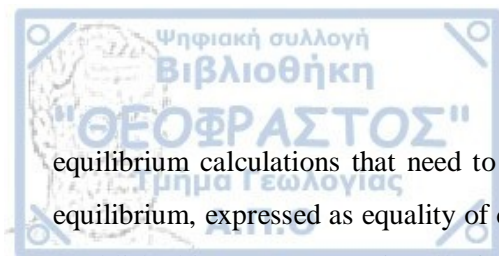
where  $T$ : temperature, °R,  $p$ : pressure, psia,  $p_k$ : convergence pressure, psia.

#### 4.4 Equilibrium coefficients based on an EoS

So far a number of empirical correlations have been presented that incorporate basic parameters of component characterisation, along with pressure, temperature and sometimes convergence pressure, and can produce in a short amount of time equilibrium ratio values for hydrocarbon mixtures. These methods are based on simplified equations that yield approximate K-value estimates and even though they have been widely used in the past decades, their accuracy is not sufficient when dealing with challenging vapour-liquid phase equilibria calculations. This is due to the fact that these empirical correlations were developed based on various assumptions and limitations and they are mostly used for equilibrium ratio calculations in low pressure situations resembling ideal behaviour.

Consequently, when conducting vapour-liquid equilibria calculations that involve large scale pressure and compositional variations, as is the case during the compositional simulation of a gas condensate reservoir undergoing dry gas injection, equilibrium coefficients derived from empirical correlations are not representative and can lead to major inaccuracies in the model. As a result, the generated K-values should be based on a suitable Equation of State that can fully describe the thermodynamic fluid behaviour corresponding to all the phenomena that take place in the reservoir.

As explained in Chapter 3, the use of an Equation of State in compositional hydrocarbon reservoir simulation, although greatly improves the simulation process and offers greater accuracy by taking into account the total fluid composition, on the other hand, it is responsible for a large increase in computational time that can take days or even weeks for the simulation to complete when complex fluids are incorporated. This time delay is partly due to an enormous number of complex equations concerning thermodynamic



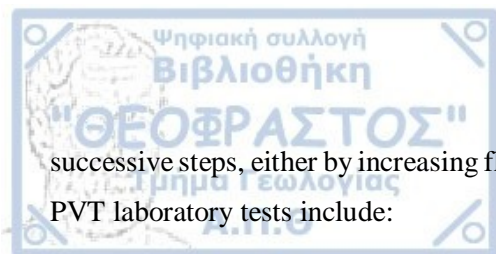
equilibrium calculations that need to be performed throughout the simulation process. Thermodynamic equilibrium, expressed as equality of component fugacity in both existing phases ( $f_i^L - f_i^V = 0$ ), must be established in every reservoir cell of the simulation model and at each timestep of the simulation process. More specifically, thermodynamic equilibrium between two phases essentially means that the fugacity of each component of the multicomponent hydrocarbon mixture in the liquid phase, must be equal to the fugacity of the same component of the mixture in the vapour phase. Thus, verification of thermodynamic equilibrium is performed by calculation of each component's fugacity in both phases and comparison of the individual component fugacity between the two phases. Once this criterion of equifugacity is fulfilled, an accurate set of the desired K-values for each cell at each timestep can be produced.

Estimation of component fugacity is a laborious task as there is the need to resort to a series of methods than involve iterative techniques, starting with Phase Stability calculations (Section 3.3.2) that will reveal whether the fluid exists as a single- or two-phase at the specific temperature and pressure, and continuing with the equally complex Phase Split calculations (Section 3.4.1) in case the fluid proves to be bi-phasic. The phase split calculation will determine the fugacities of each component in both phases and subsequently the establishment of thermodynamic equilibrium, that will eventually provide the desired set of K-values. To make things worse, one should realise that the forementioned process for the derivation of K-values via an Equation of State, must be performed in every cell of the reservoir model at any timestep throughout the whole simulation process. Considering the size and complexity of an actual hydrocarbon reservoir that could potentially require simulation for a thirty or more years production period, along with the entire number of management procedures that might follow production, it is obvious that the gathering of large sets of representative K-values, cannot be performed through compositional reservoir simulation via an Equation of State, but it rather requires the use of alternative methods.

In the next sections of this chapter, two of these alternative methods are presented, the Constant Mass (CCE) study that can satisfactorily simulate the process of pressure depletion in a hydrocarbon reservoir, and a new experimental method based on the conventional Constant Volume Depletion (CVD) study that efficiently simulates the extraction of liquid condensate from the produced gas, before its reinjection during a gas recycling process in a gas condensate reservoir. Both of these methods are used for the derivation of representative sets of K-values corresponding to the above mentioned production scenarios.

#### 4.5 Introduction to routine laboratory PVT tests

PVT laboratory tests are routinely performed on reservoir fluids to study and quantify their properties and phase behaviour, as well as evaluate their volumetric performance at various pressure conditions. Most of these tests are depletion experiments where the pressure of the single-phase test fluid is lowered in



successive steps, either by increasing fluid volume or removing part of it (Danesh, 1998). The most common PVT laboratory tests include:

- Compositional analysis of the reservoir fluid,
- Constant Composition Expansion (CCE) or Constant Mass Expansion (CME) test,
- Constant Volume Depletion (CVD) test
- Differential Liberation (DL) test
- Separator tests.

In this section, the Constant Composition Expansion and the Constant Volume Depletion tests are presented. Both of these processes are used as the basis for the new suggested experimental procedure, the extended Constant Volume Depletion (eCVD) test, which is later used for the derivation of K-values of a gas condensate system undergoing dry gas recycling.

#### 4.5.1 Constant Composition (Constant Mass) Expansion test

A hydrocarbon fluid sample is inserted into a PVT cell and heated to the desired temperature, usually the reservoir temperature, which remains constant throughout the experimental procedure. The fluid is stabilised at an initial pressure sufficiently high to ensure single-phase conditions. After equilibration, the fluid volume is noted as the initial experimental volume. The cell pressure is then reduced at successive predetermined steps by increasing the cell volume and at each step the fluid is equilibrated and the total hydrocarbon volume is measured. This process is continued until a low pressure is reached, somewhere in the interval of 100 to 50 bar (~1400 to 700 psi) (Pedersen, 2014). During the CCE test no gas or liquid is removed from the cell throughout the experiment, and the second phase generated below the saturation pressure is considered to be in equilibrium with the other existing phase. Therefore, the overall composition of the total hydrocarbon mixture remains constant since no mass is taken out of the cell (Fig. 4.4).

Constant composition expansion tests are conducted for both oil and gas condensate samples. In a crude oil sample, the CCE test will reveal basic PVT parameters like bubble point pressure ( $p_b$ ), relative volume ( $V_{rel}$ ), isothermal compressibility coefficient ( $c_o$ ) above the bubble point, oil density ( $\rho_o$ ) above the bubble point and two-phase volumetric behaviour below the bubble point. A visual detection of a gas bubble in the PVT cell indicates that the fluid has reached its saturation pressure (bubble point pressure). At the saturation pressure the recorded volume is appointed as the reference volume ( $V_{sat}$ ) and is used in combination with the total hydrocarbon volume for the calculation of the reference volume at each pressure step, according to the following relationship:



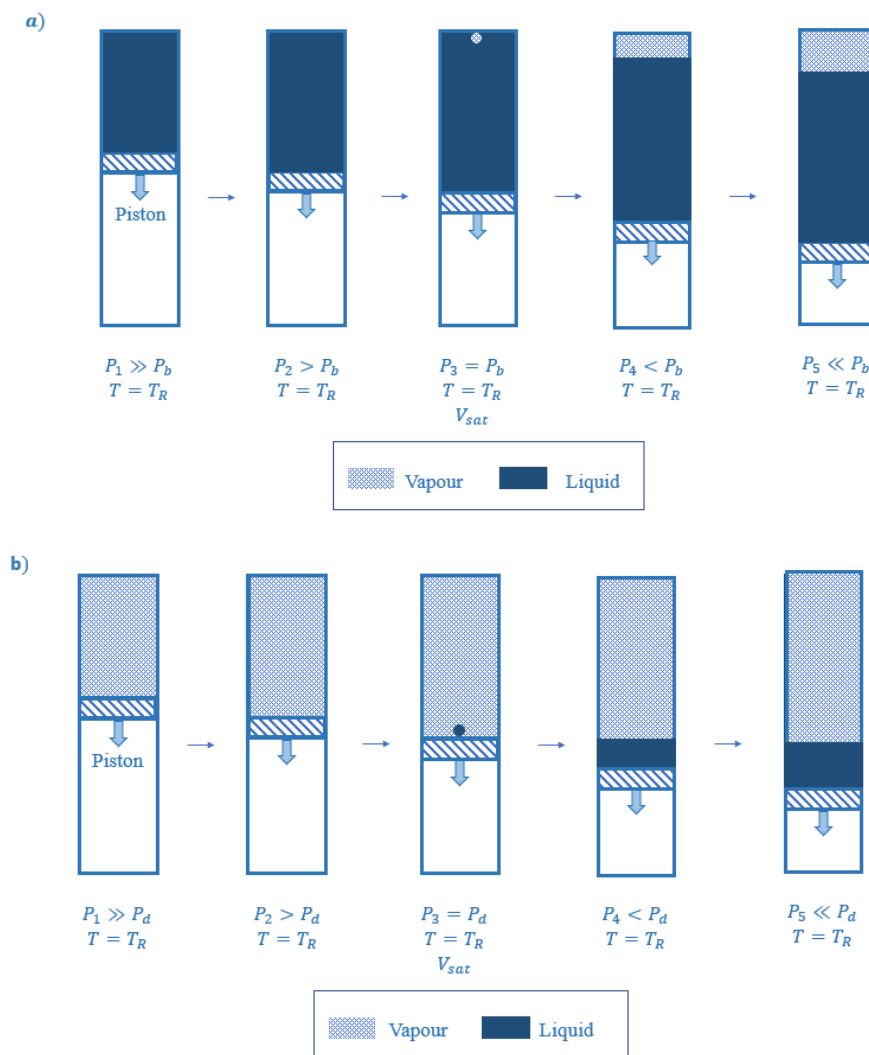
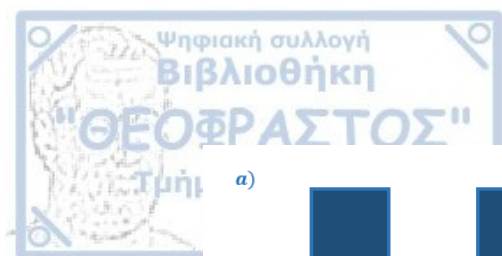
$$V_{rel} = \frac{V_{tot}}{V_{sat}} \quad (4.26)$$

where  $V_{rel}$ : relative volume,  $V_{tot}$ : total hydrocarbon volume at each pressure step,  $V_{sat}$ : volume at the saturation pressure. Usually, the relative volumes derived from the CCE are plotted as a function of pressure, where the saturation pressure can also be identified by the point of discontinuity on the relative volume/pressure curve (Fig. 4.5). However, this change in slope cannot be easily defined in the case of light or volatile oils and gas condensates, where a break in volumetric behaviour is not evident (Fig. 4.6) due to the larger compressibility of the gas phase, so determination of the saturation pressure is entirely based on visual observation of the first gas bubble/liquid drop.

In gas condensate samples the same process is performed as explained for oil mixtures, starting from a high pressure with a known volume of single-phase gas and reducing the pressure, past the dew point, to a final pressure of about 50 bar (Pedersen, 2014). The dew point is visually measured with the appearance of the first drop of liquid in the PVT cell and the reference volume is recorded at this point, through which the relative volume is calculated at all pressures. The CCE for gas condensates will provide the following parameters: dewpoint pressure ( $p_d$ ), gas compressibility factors ( $Z$ ) above the dew point, and oil relative volume below the dewpoint, a parameter commonly known as the “liquid dropout curve” given by the following expression:

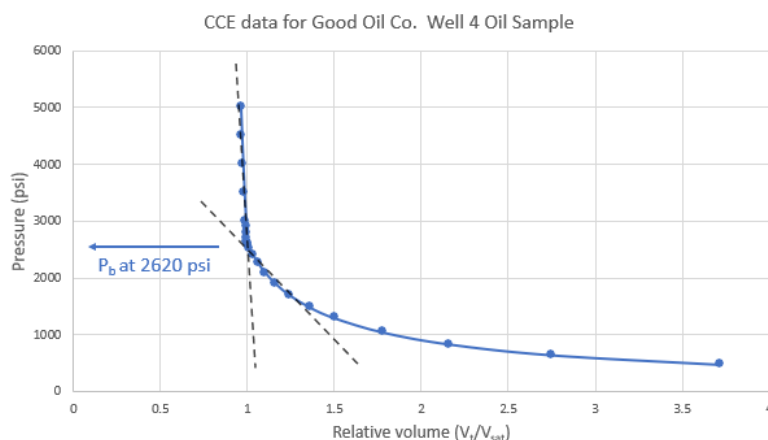
$$\% \text{ Liquid dropout} = 100 \times \frac{V_{liq}}{V_{sat}} \quad (4.27)$$

where  $V_{liq}$ : liquid volume at each pressure step.

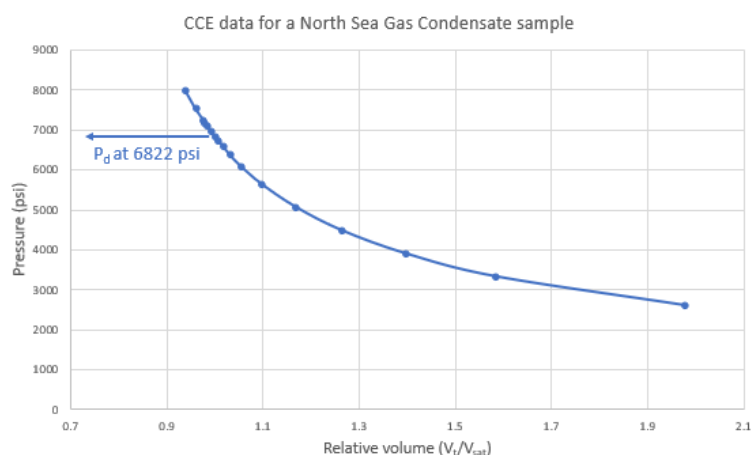


**Figure 4.4:** CCE laboratory test for a) a crude oil sample and b) a gas condensate sample.

It is assumed here that the hydrocarbon system remains constant below the saturation pressure, an assumption that is not true in an actual reservoir, since increased mobility of the gas causes it to move away from its associated oil. However, even though this method cannot offer entirely accurate results, the CCE test might be used for a simplified simulation of production by pressure depletion.



**Figure 4.5:** Pressure/Relative volume diagram for a black oil sample showing an apparent discontinuity and a change in slope at the bubble point pressure, representing the transition from the single-phase to the two-phase system (“Core Laboratories Good Oil Company Oil Well No. 4 PVT Study,” Core Laboratories, Houston).



**Figure 4.6:** Pressure/Relative volume diagram for a gas condensate sample showing no apparent change in slope at the dew point pressure (Danesh, 1998).

#### 4.5.2 Constant Volume Depletion (CVD) test

This test is performed on gas condensate mixtures and rarely on volatile oils. A representative sample of the original single-phase reservoir fluid of known volume and initial overall composition of  $z_1$  is placed in a visual PVT cell at the saturation pressure and reservoir temperature (Fig. 4.7a). The temperature is maintained constant throughout the experimental procedure. At these initial conditions, the cell volume is recorded and is used as the reference volume,  $V_{sat}$ . At this point the gas compressibility factor can be calculated from the real gas equation, corresponding to the initial saturation pressure conditions:

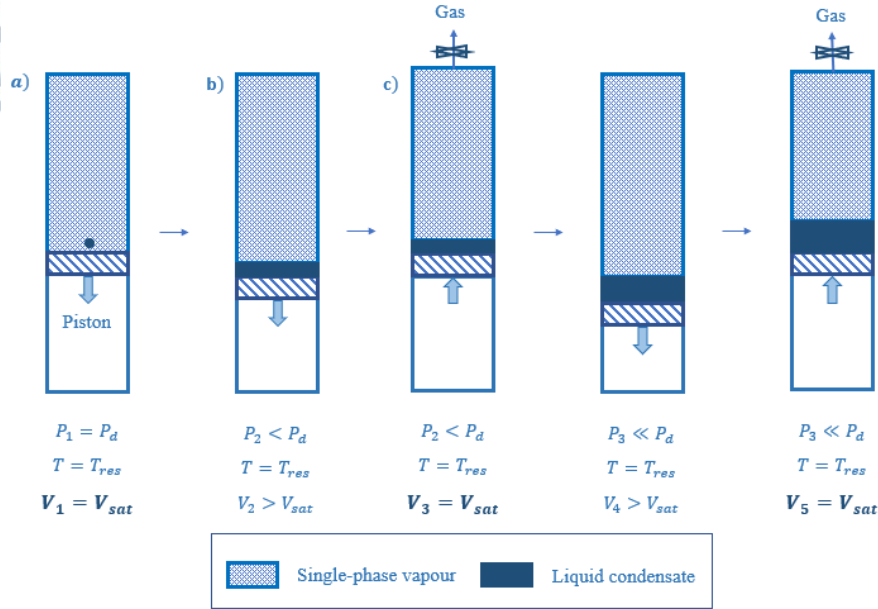


$$Z_d = \frac{p_d V_{sat}}{n_i RT} \quad (4.28)$$

where  $Z_d$ : gas compressibility factor at the dew point,  $p_d$ : dew point pressure, psia,  $V_{sat}$ : reference volume at the dew point,  $n_i$ : initial number of gas moles,  $R$ : gas constant = 10.73,  $T$ : temperature, °R. The cell pressure is reduced by volume expansion to a predetermined lower pressure (Fig. 4.7b). This expansion causes the condensation of the gas and the appearance of a second phase (retrograde liquid) in the PVT cell. After equilibration, the total cell volume is recorded. Next, the cell volume is reduced to the original reference volume by removing the excess amount of gas through a valve at the top of the cell, while the pressure is kept constant (Fig. 4.7c). The volumes of the generated liquid and of the removed gas are recorded. This step is designed to resemble the characteristics of the pressure depletion process in retrograde gas reservoirs, where the retrograde liquid remains immobile in the reservoir and the equilibrium gas is the only producing phase (Ahmed, 2016). This process is repeated for successive pressure steps until a minimum test pressure is reached of approximately 50 bar (Pedersen, 2014) and the quantity and composition of the remaining gas and liquid in the cell are measured. The CVD test provides five important laboratory measurements that can be used in a variety of reservoir engineering predictions (Ahmed, 2016):

- Dew point pressure,
- Compositional changes of the gas phase with pressure depletion,
- Gas compressibility factor at reservoir pressure and temperature,
- Recovery of original-in-place hydrocarbons at any pressure,
- Retrograde condensate accumulation, i.e., liquid saturation.





**Figure 4.7:** CVD laboratory test procedure for a gas condensate sample.

The retrograde liquid saturation (liquid dropout) is measured at each step and expressed as the ratio of the volume of the retrograde liquid ( $V_L$ ) divided by the reference volume at the saturation pressure ( $V_{sat}$ ). As in the CCE experiment, it is given by Eq. (4.27). Another property that is calculated is the two-phase compressibility factor that represents the total compressibility of gas and condensate liquid in the cell and is given by:

$$Z_{two-phase} = \frac{pV_{sat}}{(n_i - n_p)(RT)} \quad (4.29)$$

where  $Z_{two-phase}$ : two-phase compressibility factor,  $n_p$ : cumulative gas moles removed,  $n_i - n_p$ : remaining moles of fluid in the cell. The CVD test is commonly used to simulate the actual behaviour of a gas condensate reservoir undergoing pressure depletion, as well as the compositional variations in the produced gas, under the assumption that during production the condensed liquid saturation does not exceed its critical value and so the liquid phase remains immobile in the reservoir.

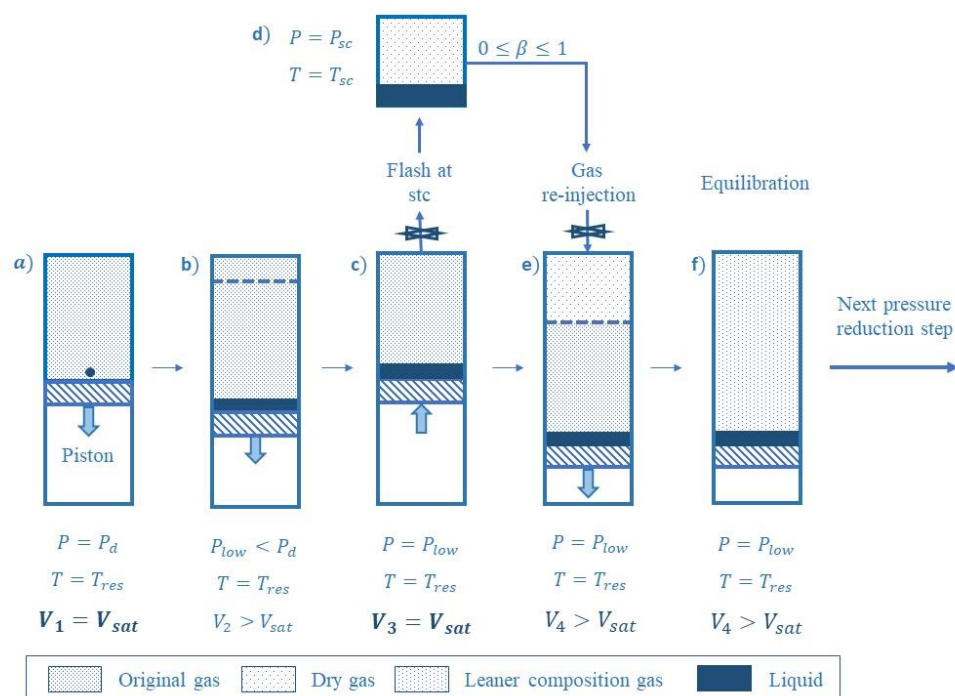


#### 4.6 The extended Constant Volume Depletion (eCVD) experimental method

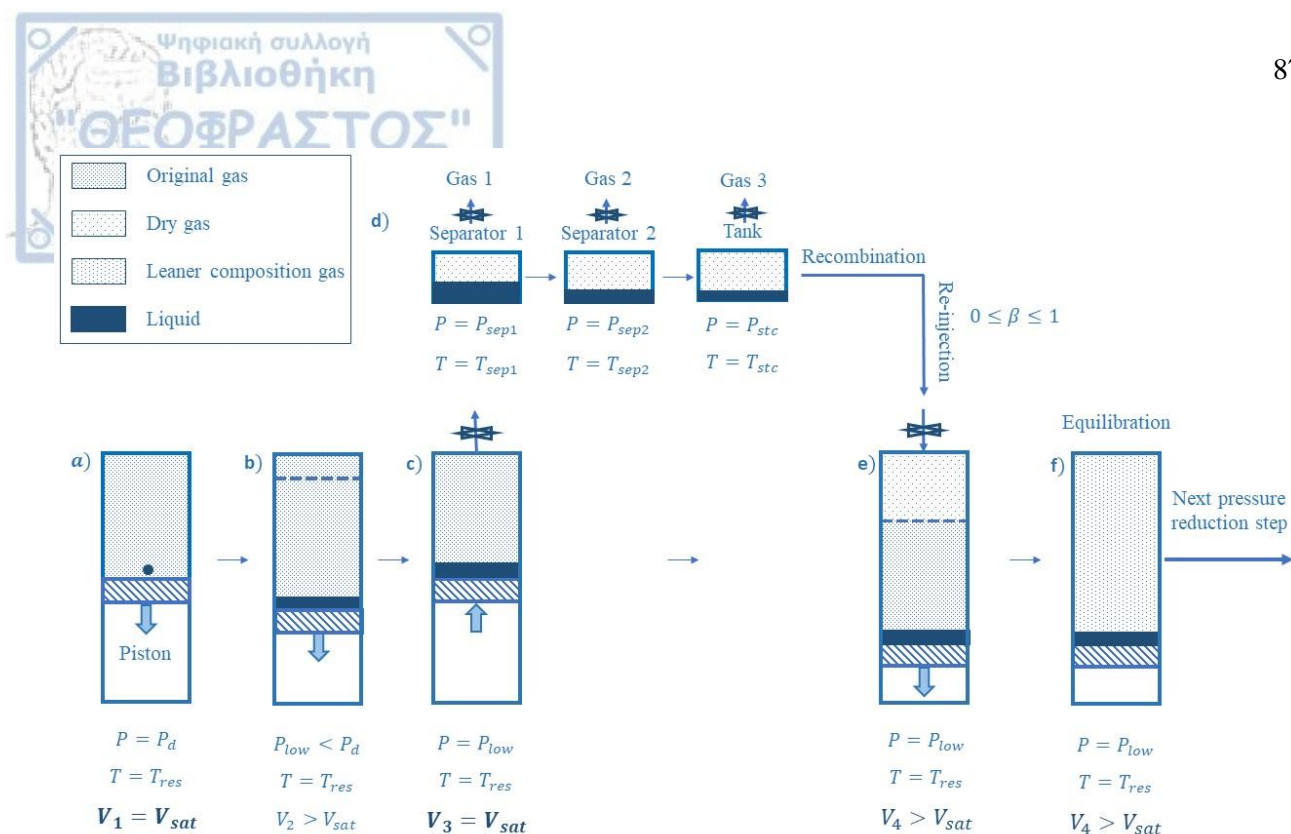
The above mentioned conventional experimental PVT methods can offer great results concerning crude oil and gas condensate systems, under the condition that reservoir production is performed by pressure depletion. However, these methods fail to thoroughly represent other production and management techniques that might be used during the operational period of a hydrocarbon reservoir, leading to erroneous results that will impact the accuracy of all other calculated properties and parameters. Since the main object of this thesis is gas condensate reservoirs subjected to lean gas recycling processes, there was a need for the development of a new experimental method with the ability to provide accurate PVT results concerning this type of reservoirs.

The new method is essentially based on the typical Constant Volume Depletion laboratory procedure and it also borrows some elements from the typical Constant Composition Expansion laboratory procedure used for gas condensate mixtures. These procedures have been extended so as to take into account the composition and quantity of the reinjection gas and can therefore efficiently reproduce the processes of gas production, gas separation at the surface facilities, dry gas reinjection in the reservoir and revaporisation of the liquid condensate in the reservoir. The process is as follows. A representative gas condensate sample with a known overall composition is placed in a PVT cell at the reservoir temperature and saturation pressure (Fig. 4.8a). The cell volume at this step is marked as the reference (saturation) volume. The cell pressure is reduced by increasing the cell volume, causing condensation of liquid in the PVT cell (Fig. 4.8b). The excess gas volume is released through a valve at the top of the cell at a constant pressure in order to reset the cell to its previous reference volume (Fig. 4.8c). Up to this point all steps are identical to the classic CVD experiment. The removed gas volume is then flashed at standard conditions (Fig. 4.8d) and stripped from its intermediate and heavy components. At this step, a number of separators can also be introduced instead of performing a direct flash of the released gas at standard conditions (Fig. 4.9). In that case, before its reinjection in the PVT cell, the separated dry gas from each separation stage must be recombined according to its composition and the number of moles present. After the separation process into dry gas and liquid condensate, an amount equal to  $\beta$  of the dry gas is reinjected back into the PVT cell at a constant cell pressure (Fig. 4.8e). After the reinjection, the new leaner fluid composition is left to equilibrate (Fig. 4.8f). The new overall fluid composition in the PVT cell at this last stage is calculated and is used as the initial composition for the next pressure reduction step. The composition of the gas phase and the composition of the liquid phase present in the cell are also determined and used for the calculation of the K-values at this reduced pressure step. This procedure is repeated for a number of successive pressure reduction steps until a predetermined low pressure is achieved where the experiment is completed. It is

evident that any dry gas with a known composition can be used as reinjection gas as for example, a dry gas originating from an adjacent field.

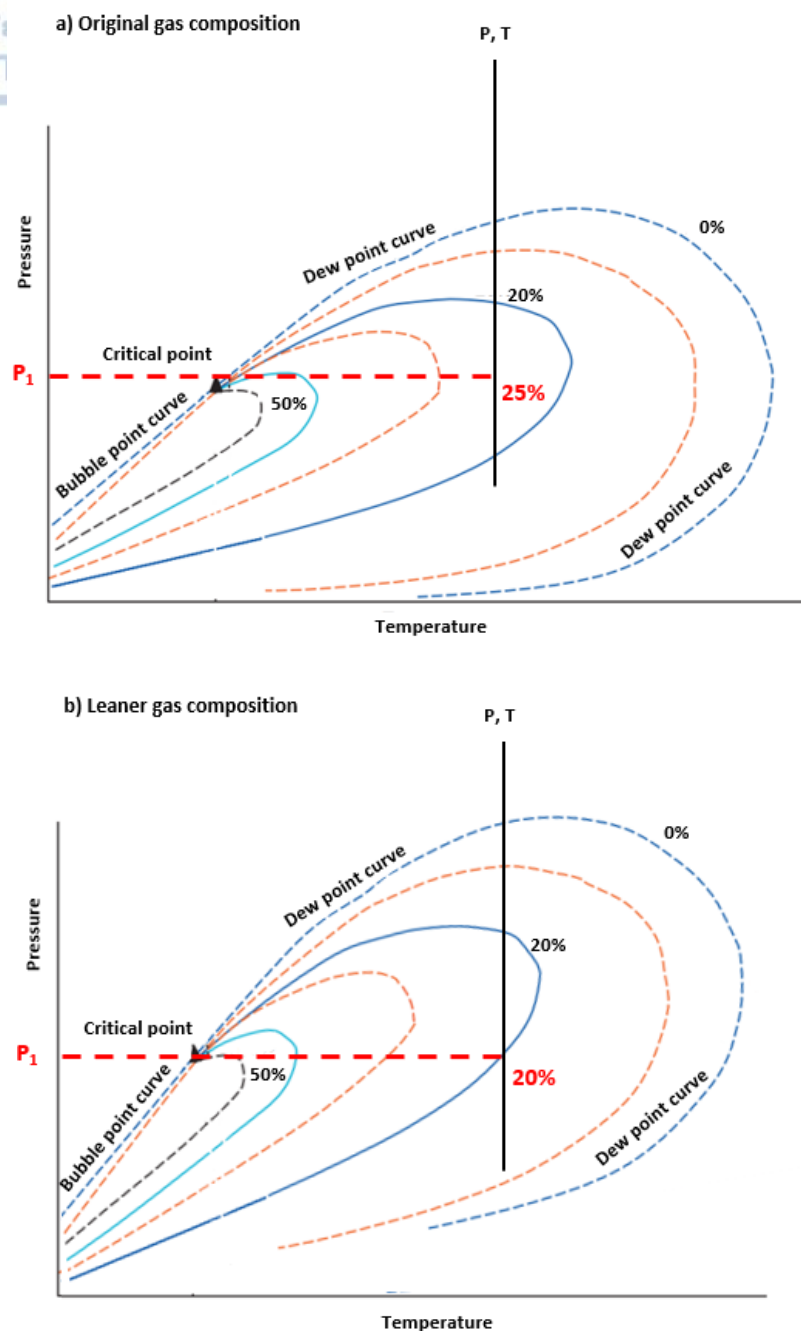


**Figure 4.8:** Schematic illustration of the new suggested extended CVD experimental procedure for a gas condensate sample with direct flash of the released gas at standard conditions.



**Figure 4.9:** Schematic illustration of the new suggested extended CVD experimental procedure for a gas condensate sample with the introduction of a series of separators before flashing of the released gas at standard conditions.

Bearing in mind that the ultimate goal of this process is the revaporisation of the liquid condensate trapped in the pores of the reservoir rock, and subsequently its production to the surface, it is remarkable to notice that dry gas reinjection at each pressure step progressively leads to a leaner overall fluid composition in the PVT cell, or accordingly in the reservoir, which in turn causes the phase envelope of the gas condensate mixture (Chapter 1) to shift in a counter-clockwise manner (Fig. 4.10). This is an important observation because at the same pressure, the shifted phase envelope displays a reduced percentage of liquid condensate, past the point of maximum liquid condensation, than the phase envelope of the original composition, indicating that the overall leaner composition causes the revaporisation of the generated liquid. Another factor that benefits this process is of course the partial pressure maintenance due to the gas reinjection, provided that the dry gas is injected at sufficient amounts.



**Figure 4.10:** Schematic illustration of the counter-clockwise shift of a phase envelope for a gas condensate system as a result of lighter fluid composition. Along the isothermal production path at the same pressure  $P_1$ , the phase envelope belonging to the leaner composition shows a reduced liquid percentage due to revaporisation.

#### 4.6.1 Gathering of K-value data from the extended CVD test

The above presented procedure can be used to obtain representative sets of K-values corresponding to various pressures, either by running it at the lab or by simulating with the assistance of an appropriate EoS,

the processes of gas production, gas surface separation, dry gas reinjection and liquid revaporisation that take place in a gas condensate reservoir during gas recycling. Any available software that can provide phase equilibria calculations based on an EoS, as for example CMG's WinProp software, is suitable to fulfil this task. The stepwise computational process for the determination of K-values is presented next.

Step 1: An initial amount,  $N_G^{(0)}$ , of the original gas condensate fluid with a known composition of  $\mathbf{z}^{(0)}$  is flashed at a pressure equal to the mixture saturation pressure and reservoir temperature (Fig. 4.8a). The temperature inside the PVT cell remains constant throughout the whole process and equal to the reservoir one. Since the mixture is at its dew point, the amount of liquid present can be practically regarded as zero.

$$N_G^{(0)} = a \quad (4.30a)$$

$$N_L^{(0)} = 0 \quad (4.30b)$$

where  $N_G^{(0)}$ : number of gas moles at the saturation pressure and  $N_L^{(0)}$ : number of liquid moles at the saturation pressure. The phase split calculation will provide the molecular volumes of gas,  $V_{G_m}^{(0)}$ , and liquid,  $V_{L_m}^{(0)}$ , to be used for the calculation of the gas and liquid phase volumes, and the liquid (drop),  $\mathbf{x}^{(0)}$ , and gas phase,  $\mathbf{y}^{(0)}$ , compositions at the dew point. Because the mixture is at the dew point, the gas phase composition is equal to the initial fluid composition and the total cell volume is practically equal to the gas phase volume.

$$V_G^{(0)} = N_G^{(0)} \cdot V_{G_m}^{(0)} \quad (4.30c)$$

$$V_L^{(0)} = N_L^{(0)} \cdot V_{L_m}^{(0)} \quad (4.30d)$$

$$V_{tot}^{(0)} = V_G^{(0)} \quad (4.30e)$$

$$\mathbf{x}^{(0)} = f(\mathbf{z}^{(0)}, p_d) \quad (4.30f)$$

$$\mathbf{y}^{(0)} = \mathbf{z}^{(0)} \quad (4.30g)$$

where  $V_G^{(0)}$ : gas phase volume at the saturation pressure,  $V_L^{(0)}$ : liquid phase volume at the saturation pressure,  $V_{tot}^{(0)}$ : total cell volume at the saturation pressure (reference volume),  $p_d$ : saturation pressure.

Step 2: The initial composition is flashed at a lower pressure,  $p_{low}$ , to achieve liquid condensation (Fig. 4.8b). The phase split calculation will provide the gas phase molar fraction,  $n_g^{(1)}$  at  $p_{low}$ , which is used for the calculation of the number of moles present in the gas,  $N_G^{(1)}$ , and liquid,  $N_L^{(1)}$ , phases:

$$N_G^{(1)} = N_G^{(o)} \cdot n_g^{(1)} \quad (4.31a)$$

$$N_L^{(1)} = N_G^{(o)} \cdot (1 - n_g^{(1)}) \quad (4.31b)$$

The molar volumes of gas,  $V_{G_m}^{(1)}$ , and liquid,  $V_{L_m}^{(1)}$  at  $p_{low}$  are also determined from the phase split and used as previously for the calculation of the gas and liquid phase volumes at  $p_{low}$ . The total volume,  $V_{tot}^{(1)}$ , is also calculated:

$$V_G^{(1)} = N_G^{(1)} \cdot V_{G_m}^{(1)} \quad (4.31c)$$

$$V_L^{(1)} = N_L^{(1)} \cdot V_{L_m}^{(1)} \quad (4.31d)$$

$$V_{tot}^{(1)} = V_G^{(1)} + V_L^{(1)} \quad (4.31e)$$

The excess gas volume to be removed from the cell,  $V_G^{(r)}$ , is calculated as follows:

$$V_G^{(r)} = V_{tot}^{(1)} - V_{tot}^{(o)} \quad (4.31f)$$

The gas phase,  $\mathbf{y}^{(1)}$ , and liquid phase,  $\mathbf{x}^{(1)}$ , compositions at  $p_{low}$  are also determined from the EoS, while the overall fluid composition at this step,  $\mathbf{z}^{(1)}$ , remains constant (Eq. 4.31i):

$$\mathbf{y}^{(1)} = f(\mathbf{z}^{(o)}, p_{low}) \quad (4.31g)$$

$$\mathbf{x}^{(1)} = f(\mathbf{z}^{(o)}, p_{low}) \quad (4.31h)$$

$$\mathbf{z}^{(1)} = \mathbf{z}^{(o)} \quad (4.31i)$$

Step 3: The excess amount of gas volume is removed from the cell at a constant pressure and flashed at surface conditions (Fig. 4.8c and d) where its intermediate and heavy components are separated from the lean dry gas by forming condensate. The gas phase molar fraction at standard conditions,  $n_g^{(2)}$ , is estimated from the EoS and used to calculate the following parameters:



$$N_G^{(r)} = V_G^{(r)} / V_{Gm}^{(1)} \quad (4.32a)$$

$$N_G^{(2)} = N_G^{(r)} \cdot n_g^{(2)} \quad (4.32b)$$

$$N_L^{(2)} = N_G^{(r)} \cdot (1 - n_g^{(2)}) \quad (4.32c)$$

where  $N_G^{(r)}$ : number of moles of the removed gas volume,  $N_G^{(2)}$ : number of moles of the gas phase at standard conditions and  $N_L^{(2)}$ : number of moles of the liquid phase at standard conditions. The gas,  $\mathbf{y}^{(2)}$ , and liquid,  $\mathbf{x}^{(2)}$ , compositions at standard conditions ( $p_{sc}, T_{sc}$ ) are given from the EoS and at this step the overall fluid composition that is flashed at the surface,  $\mathbf{z}^{(2)}$ , is equal to the gas phase composition of Step 2:

$$\mathbf{z}^{(2)} = \mathbf{y}^{(1)} \quad (4.32d)$$

$$\mathbf{y}^{(2)} = f(\mathbf{y}^{(1)}, p_{sc}, T_{sc}) \quad (4.32e)$$

$$\mathbf{x}^{(2)} = f(\mathbf{y}^{(1)}, p_{sc}, T_{sc}) \quad (4.32f)$$

Step 4: An amount  $\beta$  ( $0 \leq \beta \leq 1$ ) of the lean dry gas is reinjected in the cell at a constant pressure by increasing the cell volume (Fig. 4.8e). At this stage the fluids present in the cell are not in equilibrium as the overall composition is changed but temperature, pressure and volume remain unaltered. The injected gas causes an alteration in composition, hence there is a number of parameters that need to be calculated before the equilibration process, concerning numbers of moles and composition of the existing phases. These parameters are calculated as follows.

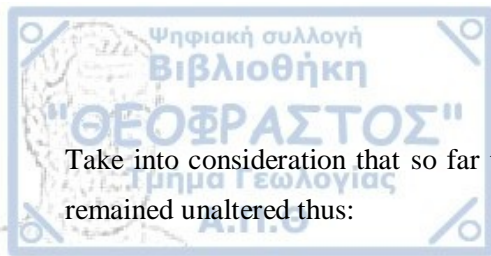
Number of gas moles present in the cell before gas reinjection:

$$N_G^{(3)} = N_G^{(1)} - N_G^{(r)} \quad (4.33a)$$

Total number of gas moles present in the cell after gas reinjection without phase equilibrium:

$$N_G^{(4)} = N_G^{(3)} + \beta \cdot N_G^{(2)} \quad (4.33b)$$





Take into consideration that so far the liquid phase present in the PVT cell as generated at Step 2 has remained unaltered thus:

$$N_L^{(1)} = N_L^{(3)} = N_L^{(4)} \quad (4.33c)$$

and

$$\mathbf{x}^{(1)} = \mathbf{x}^{(3)} = \mathbf{x}^{(4)} \quad (4.33d)$$

also

$$\mathbf{y}^{(3)} = \mathbf{y}^{(1)} \quad (4.33e)$$

since the same is true for the composition of the remaining gas phase in the PVT cell between Steps 2 and 4 before reinjection. In Eqs. (4.33c) – (4.33e),  $N_L^{(3)}$ : number of liquid moles before gas reinjection,  $\mathbf{x}^{(3)}$ : liquid phase composition before gas reinjection,  $N_L^{(4)}$ : number of liquid moles after gas reinjection without equilibration between the phases,  $\mathbf{x}^{(4)}$ : liquid phase composition after gas reinjection without equilibration between the phases and  $\mathbf{y}^{(3)}$ : gas phase composition before gas reinjection.

Therefore, the total number of moles (gas and liquid) in the cell after gas reinjection without equilibrium between the phases is:

$$N_{tot}^{(4)} = N_G^{(4)} + N_L^{(4)} \quad (4.33f)$$

The gas phase composition,  $\mathbf{y}^{(4)}$ , as well as the overall fluid composition,  $\mathbf{z}^{(4)}$ , in the PVT cell after the reinjection and before equilibration of the two phases must be also calculated using the following material balance expressions:

$$\mathbf{y}^{(4)} = \frac{N_G^{(3)} \cdot \mathbf{y}^{(3)} + \beta \cdot N_G^{(2)} \cdot \mathbf{y}^{(2)}}{N_G^{(3)} + \beta \cdot N_G^{(2)}} \quad (4.33g)$$

$$\mathbf{z}^{(4)} = \frac{N_G^{(4)} \cdot \mathbf{y}^{(4)} + N_L^{(4)} \cdot \mathbf{x}^{(4)}}{N_G^{(4)} + N_L^{(4)}} \quad (4.33h)$$



**Step 5:** Equilibration of the phases after gas reinjection in the PVT cell is achieved by flashing the overall fluid composition calculated at the previous step,  $\mathbf{z}^{(4)}$ , at the cell prevailing pressure established at Step 2. The cell temperature remains fixed. The following parameters are calculated for the two equilibrated phases:

Total number of gas moles after equilibration:

$$N_G^{(5)} = N_{tot}^{(4)} \cdot n_g^{(5)} \quad (4.34a)$$

Number of liquid moles after equilibration:

$$N_L^{(5)} = N_{tot}^{(4)} \cdot (1 - n_g^{(5)}) \quad (4.34b)$$

Total number of moles present (gas and liquid) in the cell after equilibration:

$$N_{tot}^{(5)} = N_G^{(5)} + N_L^{(5)} \quad (4.34c)$$

Volume of the gas phase in the PVT cell:

$$V_G^{(5)} = N_G^{(5)} \cdot V_{Gm}^{(5)} \quad (4.34d)$$

Volume of the liquid phase in the PVT cell:

$$V_L^{(5)} = N_L^{(5)} \cdot V_{Lm}^{(5)} \quad (4.34e)$$

Total volume of the PVT cell after equilibration:

$$V_{tot}^{(5)} = V_G^{(5)} + V_L^{(5)} \quad (4.34f)$$

The gas,  $\mathbf{y}^{(5)}$ , and liquid,  $\mathbf{x}^{(5)}$ , compositions after equilibration are estimated from the EoS while the overall fluid composition after equilibration,  $\mathbf{z}^{(5)}$ , remains fixed:



$$\mathbf{y}^{(5)} = f(\mathbf{z}^{(4)}, p_{low}) \quad (4.34g)$$

$$\mathbf{x}^{(5)} = f(\mathbf{z}^{(4)}, p_{low}) \quad (4.34h)$$

$$\mathbf{z}^{(5)} = \mathbf{z}^{(4)} \quad (4.34i)$$

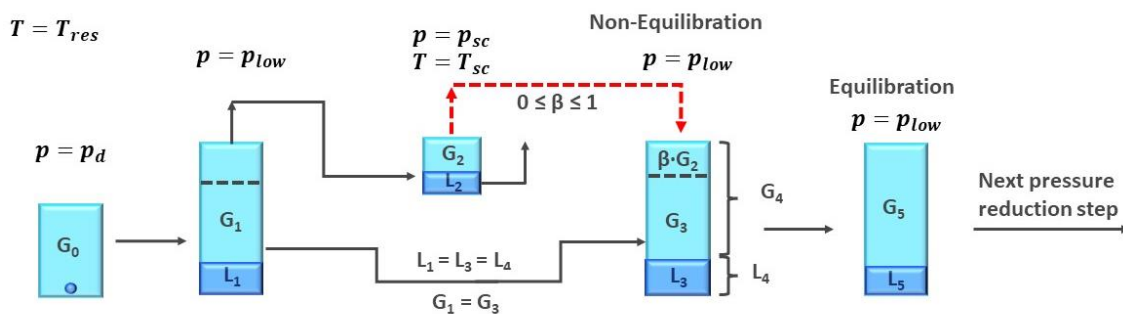
In Eqs. (4.34a) – (4.34i),  $n_g^{(5)}$ : gas phase molar fraction after equilibration,  $V_{Gm}^{(5)}$  and  $V_{Lm}^{(5)}$ : molar volume of the gas and liquid phases respectively, after equilibration.

**Step 6:** The equilibrium coefficients that characterise the system at the last equilibration stage are calculated through the estimated gas,  $\mathbf{y}^{(5)}$ , and liquid,  $\mathbf{x}^{(5)}$ , compositions of Step 5.

**Step 8:** The estimated composition of  $\mathbf{z}^{(5)}$  is selected as the initial overall fluid composition and the process is repeated from Step 2 for the next reduced pressure value. The experiment is completed when all sets of K-values have been gathered for all the predetermined pressure reduction steps.




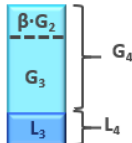
The following figure (Fig. 4.11) in combination with Table 4.3 summarise the above presented process.  $G_0 - G_5$  and  $L_0 - L_5$  denote the changes in gas phase and liquid phase compositions respectively, that take place at each stage of the experimental process.


All methods introduced in this chapter, excluding the empirical correlations of Sections 4.1 – 4.3, are later used in this thesis for the derivation and comparison of representative sets of K-values corresponding to pressure depletion and gas recycling scenarios for a gas condensate reservoir.



**Figure 4.11:** Schematic illustration of the extended CVD experimental process for the simulation of dry gas recycling in a gas condensate reservoir.

**Table 4.3:** Outline of the extended CVD experimental process with a summary of the related parameters at each step.

		Phase split input	Phase split output	Calculations	Comments
$p = p_d$ 	<b>Step 1:</b> Phase split at $p_d$ .	$\mathbf{z}^{(0)}, p_d, T_{res}$ (Constant temperature in the cell throughout the process)	$V_{G_m}^{(0)}$ , $V_{L_m}^{(0)}$ , $\mathbf{y}^{(0)}$ , $\mathbf{x}^{(0)}$	i) phase volumes, ii) total cell volume (reference volume at $p_d$ )	Initial composition at the dew point $\rightarrow$ $\mathbf{y}^{(0)} = \mathbf{z}^{(0)}$
$p = p_{low}$ 	<b>Step 2:</b> Reduce pressure below saturation point. Phase split at $p_{low}$ .	$\mathbf{z}^{(0)}, p_{low}$	$n_g^{(1)}$ $V_{G_m}^{(1)}$ , $V_{L_m}^{(1)}$ , $\mathbf{y}^{(1)}$ , $\mathbf{x}^{(1)}$	i) number of gas and liquid moles, ii) phase volumes, iii) total cell volume, iv) excess gas volume to be removed	Overall composition equal to the initial overall composition: $\mathbf{z}^{(1)} = \mathbf{z}^{(0)}$
$p = p_{sc}$ $T = T_{sc}$ 	<b>Step 3:</b> Flash of the excess gas volume at standard conditions.	$\mathbf{y}^{(1)}, p_{sc}, T_{sc}$	$n_g^{(2)}$ , $\mathbf{y}^{(2)}$ , $\mathbf{x}^{(2)}$	i) number of removed gas moles, ii) number of gas and liquid moles at stc.	The overall composition at stc is equal to the gas composition of the previous step: $\mathbf{z}^{(2)} = \mathbf{y}^{(1)}$
<b>Non-Equilibration</b> $p = p_{low}$ 	<b>Step 4:</b> Dry gas reinjection ( $0 \leq \beta \leq 1$ ) at constant pressure without phase equilibration.			i) number of gas moles before and after reinjection, ii) number of total (gas + liquid) moles, iii) gas composition and overall fluid composition	The injected gas modifies the fluid overall composition and makes it lighter. The injection gas may not originate from the produced reservoir.

				before equilibration.	
<p>Equilibration <math>p = p_{low}</math></p> 	<p><b>Step 5:</b> Equilibration of the phases after gas reinjection. Phase split at <math>p_{low}</math>.</p>	<p><math>\mathbf{z}^{(4)}, p_{low}</math></p>	<p><math>n_g^{(5)}</math> <math>V_{Gm}^{(5)},</math> <math>V_{Lm}^{(5)},</math> <math>\mathbf{y}^{(5)},</math> <math>\mathbf{x}^{(5)}</math></p>	<p>i) number of gas and liquid moles and total (gas + liquid) moles,  ii) phase volumes and total cell volume</p>	<p>The overall fluid composition between Steps 4 and 5 remains fixed and is used as the initial composition for the next reduction pressure step.</p>
<p><b>Step 7:</b> Collect K-values corresponding to the gas and liquid phase compositions calculated at Step 5.</p> <p>The equilibrium coefficients characterise the equilibrated gas condensate system composition after lean gas reinjection at the last stage of the specific pressure reduction step.</p>					
<p><b>Step 8:</b> Return to Step 2 using as an initial composition the overall fluid composition calculated at Step 5 and proceed with the next reduced pressure step. Complete the process when a low predetermined pressure has been reached.</p>					

## 5 METHODOLOGY – RESULTS

A total of eight different production scenarios were set up with the assistance of IPM Petroleum Experts' Reveal reservoir simulator, in order to study the effects of production with dry gas recycling on liquid condensation and revaporisation in the reservoir, in terms of the corresponding equilibrium coefficient values (K-values). The collected equilibrium coefficient values from all eight production scenarios were later compared to the results of a Constant Mass study (CCE). In addition, the results of three of the gas recycling scenarios, the ones with reinjection of 80% of the amount of the produced gas with and without separators and the one with reinjection of 60% of the amount of the produced gas without separators, were also compared against the results of the extended Constant Volume Depletion study (eCVD).

A 10x10x1 block was designed as a simplistic representation of a gas condensate reservoir with uniform porosity of 0.2 and varying permeability across both the x and y directions. The initial reservoir pressure was set at 3,000 psia for all the scenarios and the reservoir temperature was maintained fixed throughout the process at 220 °F. The saturation pressure for all scenarios was estimated to be approximately 2,950 psia.

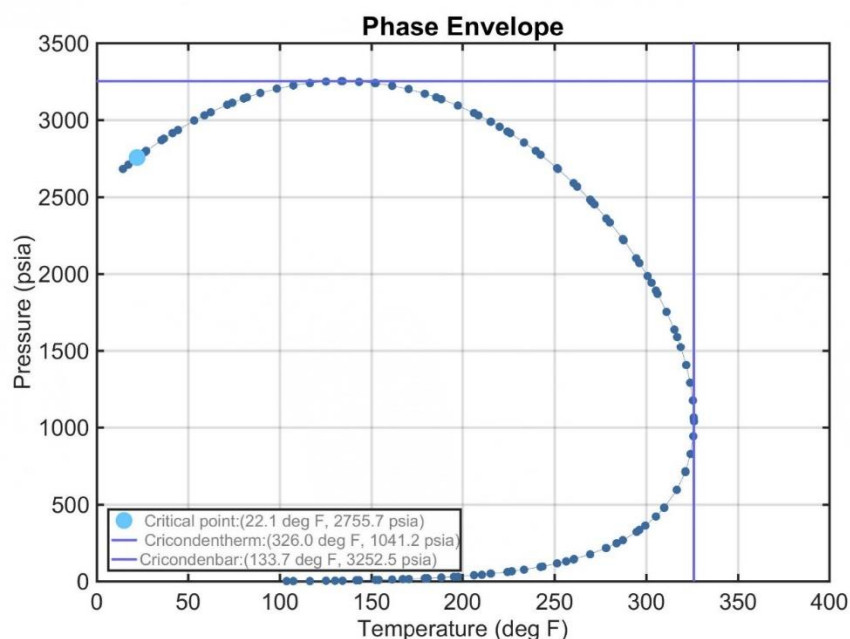
The reservoir fluid had an initial overall composition rich in methane that is typical of a retrograde gas condensate system (Table 5.1). It consisted of a total of 20 components, two of which were non-hydrocarbon components (nitrogen and carbon dioxide), while ten of the heavier components were pseudo-components. The phase envelope of the reservoir fluid is given in Figure 5.1.

**Table 5.1:** Initial reservoir fluid composition.

Component	N <sub>2</sub>	CO <sub>2</sub>	C1	C2	C3	iC4	nC4	iC5	nC5	C6
(%)	3.79998	0.349998	67.9096	11.3599	5.42997	1.14999	2.02999	0.749996	1.00999	1.14999
Component	C6C6	C7C7	C8C8	C9C9	C10C10	C11C11	C12C12	C13C13	C14C14	C15C15
(%)	0.830954	0.731419	0.653924	1.6269	0.698846	0.300194	0.12895	0.055391	0.023794	0.010221

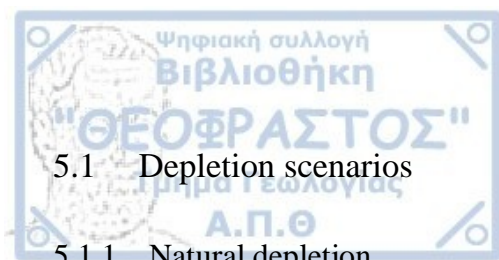
Firstly, a natural depletion scenario was run and the equilibrium coefficient values were collected for each component at each reservoir cell, throughout the 10 year production period. Secondly, a water flooding scenario was set up in which the well positions were randomly picked. This scenario was built with the

purpose of examining whether water injection, as well as well positioning have any impact on the equilibrium coefficient values compared with the first natural depletion scenario. Next, a number of gas recycling scenarios were designed with varying amounts of reinjection gas. The reinjection dry gas, stripped from its heavy components at the surface, originated from the reservoir itself. More specifically, the produced gas was either flashed directly at standard conditions, where it was separated into reinjection dry gas and liquid condensate, or it was driven through a series of separators before being flashed at standard conditions, in which case the maximum amount of condensate was produced and consequently, the reinjection gas had the leanest possible composition.



**Figure 5.1:** Phase envelope of the reservoir fluid typical of a retrograde gas condensate system.

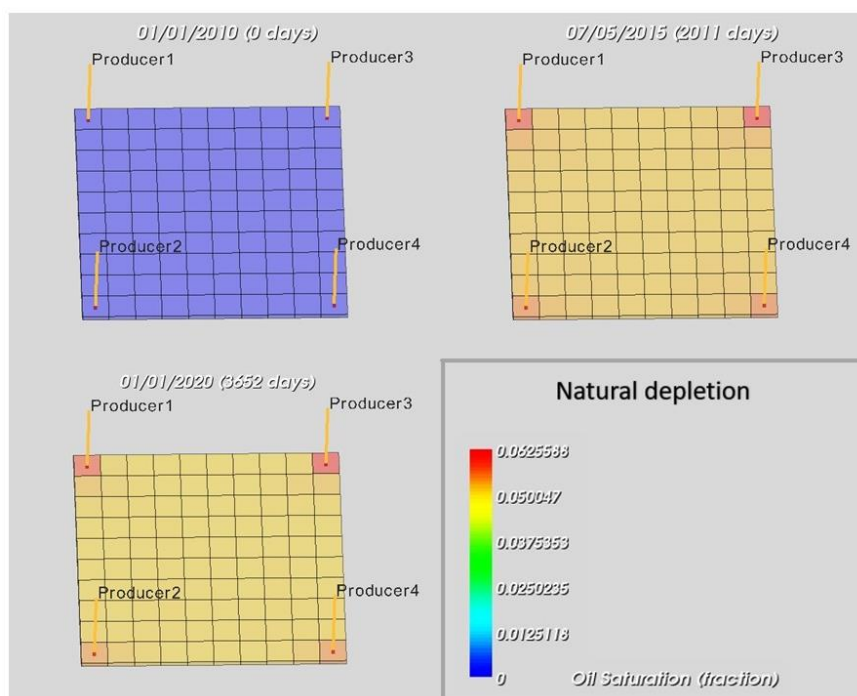
Two experiments were developed, the Constant Composition Expansion (CCE) test using CMG's WinProp software and an extended Constant Volume Depletion (eCVD) test in MATLAB code, for the collection of equilibrium coefficient values at various pressures equivalent to the reservoir pressures during simulation. Pressure/K-values diagrams were later constructed for the comparison of the simulation and the experimental data.



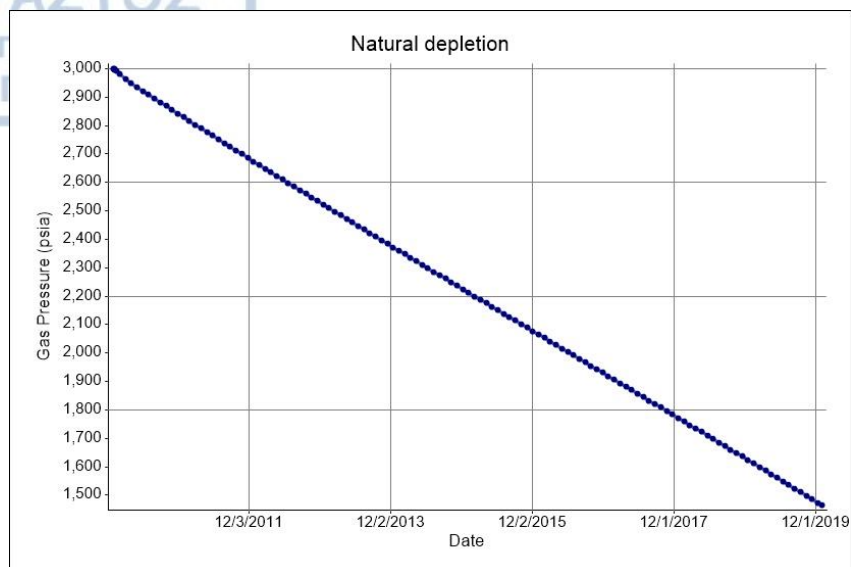
## 5.1 Depletion scenarios

### 5.1.1 Natural depletion

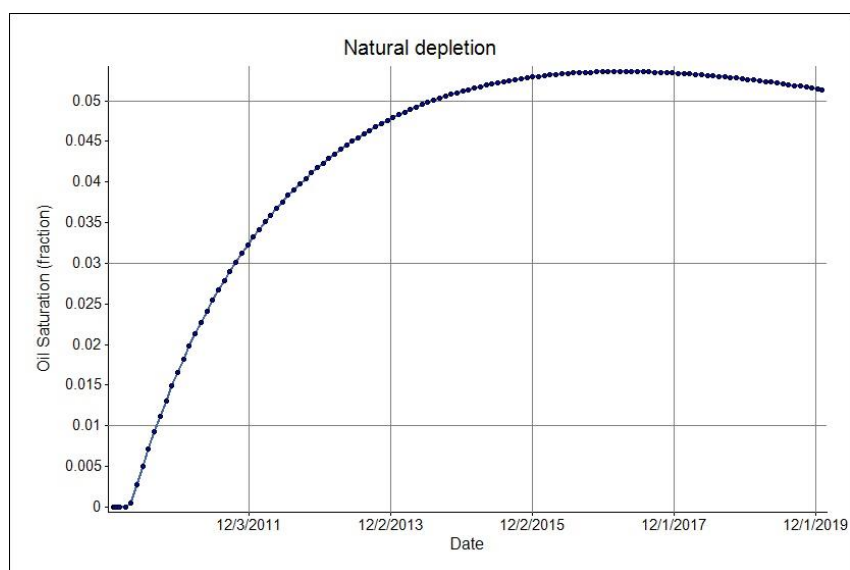
In the first scenario of natural depletion, the reservoir was depleted by pressure reduction caused by four production wells operating at a fixed rate of 3 MMscf/day each, for a period of ten years (Fig. 5.2). The initial reservoir pressure was set at 3,000 psia, while the dew point pressure was approximately 2,950 psia. The reservoir pressure exhibited a steady decline and reached almost 1,500 psia at the end of the production period (Fig. 5.3). As a result of the reduction in pressure, generation of liquid condensate initiated in the reservoir and its saturation began to increase, reaching a maximum average value of 0.05 (5%) before starting to slightly decrease again as a response to the reduced reservoir pressure at the later years of production (Fig. 5.4). In other words, the reduced reservoir pressure at the last years of production marked the beginning of retrograde condensation and some revaporisation was observed in the reservoir as the lower dew point was approached. The phenomenon of condensate blockage can be observed in Fig. 5.2 around the wellbore regions, which experienced the greatest pressure decline, where the red colour indicates increased liquid condensate saturation. The pressure/K-values plot for the natural depletion scenario indicates an excellent match between the K-values derived from the simulation scenario and the CCE experiment (Fig. 5.5). It also verifies that the K-values in depleting reservoirs are simply a function of pressure rather than composition.



**Figure 5.2:** Natural depletion scenario by pressure reduction. The variation in oil saturation throughout the years is evident.

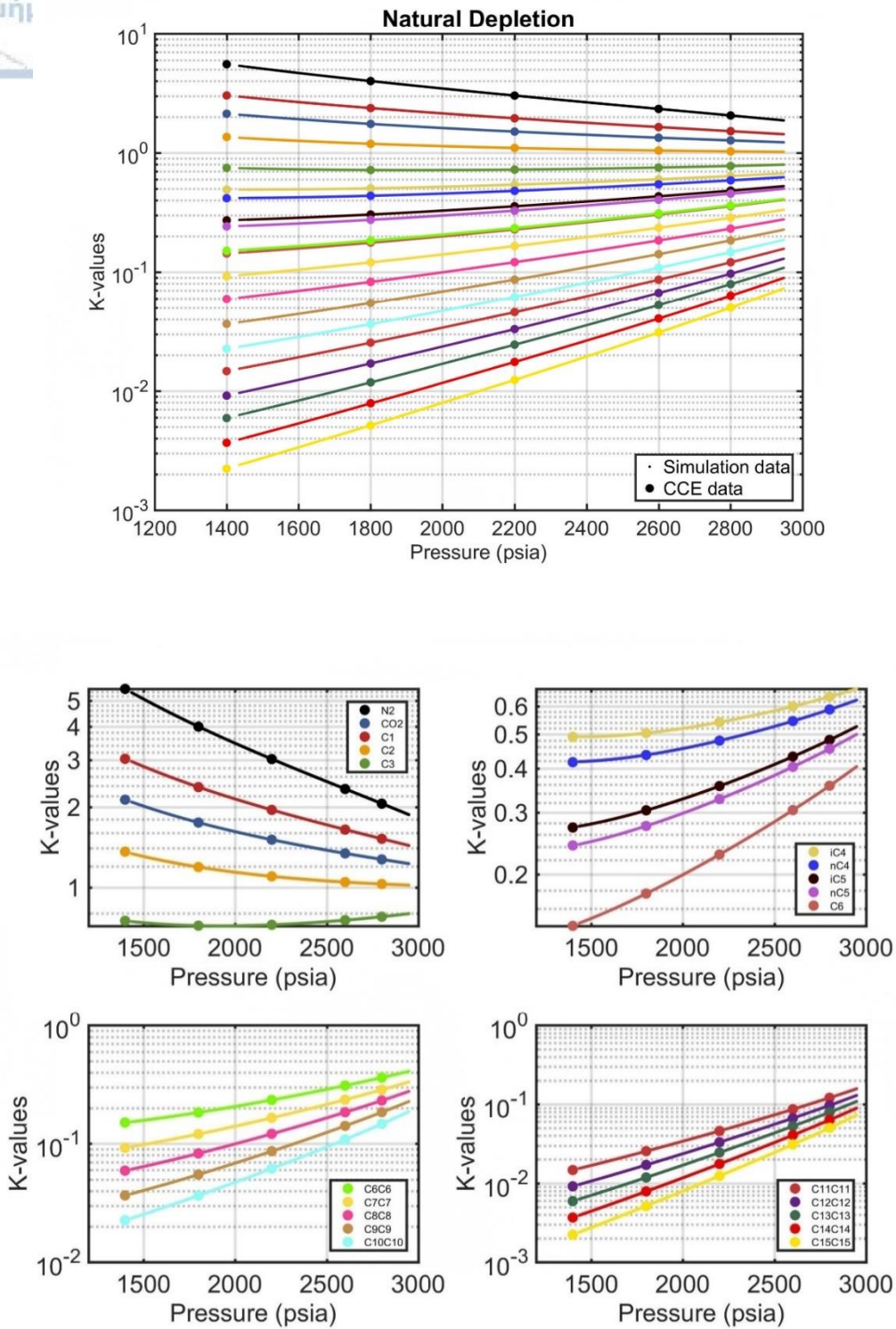


**Figure 5.3:** Average reservoir pressure (psia) for the ten year production period of the natural depletion scenario.



**Figure 5.4:** Average liquid condensate saturation (fraction) for the ten year production period of the natural depletion scenario.

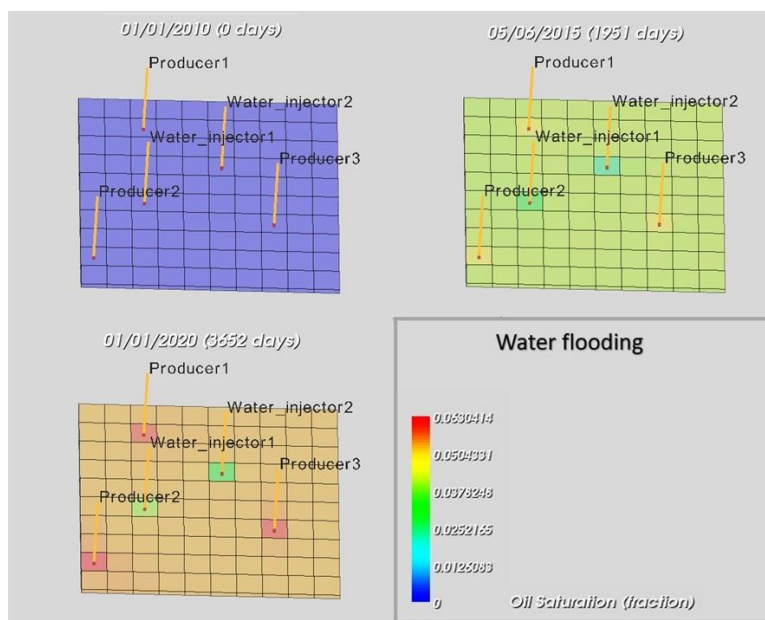




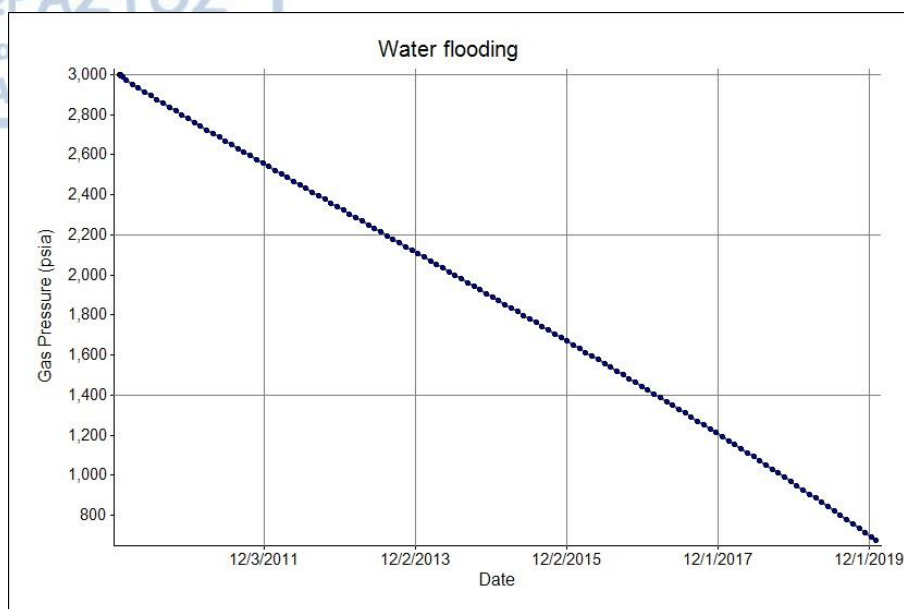
**Figure 5.5:** Pressure/K-values plots for the natural depletion scenario showing an exact match between the simulation derived and CCE derived data.

### 5.1.2 Water flooding

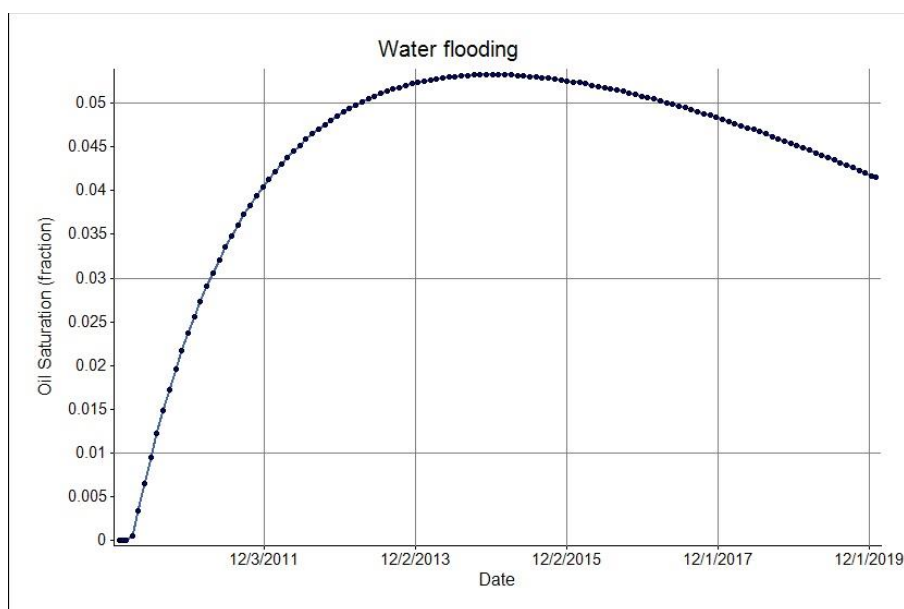
The water flooding scenario was created in an attempt to verify that water injection in the reservoir does not interfere with the K-values, as it has been proven that water is thermodynamically non-reactive with hydrocarbons. Three production wells were producing at a fixed rate of 6 MMscf/day each, for a ten year period. Two water injection wells were introduced injecting water at a fixed rate, the first one 300 STB/day and the second 500 STB/day for the same time period of ten years. The location of the wells was randomly picked to test whether it affects in any way the computed equilibrium coefficient values (Fig. 5.6). The initial reservoir pressure was again set at 3,000 psia, while the dew point pressure was approximately 2,950 psia. The reservoir pressure exhibited a constant decline, since the amount of the injected water was not sufficient to provide pressure maintenance (i.e. the voidage replacement ratio was less than unity), and reached almost 700 psia at the end of the production period (Fig. 5.7). The generation of liquid condensate began as a response to the reduction in pressure and as in the previous scenario, reached a maximum value of 0.05 (5%), although in this case, retrograde condensation was observed at a greater extent as a result of the much more reduced reservoir pressure at the later years of production (Fig. 5.8). The effect of condensate blockage can also be observed around the production wells (Fig. 5.6), while around the water injection wells, liquid saturation appears to be reduced, since at these regions the saturation of water was constantly increasing at the expense of the remaining phases' saturation.



**Figure 5.6:** The water flooding scenario was designed to check whether water injection and well positioning have an impact on the equilibrium coefficient values.

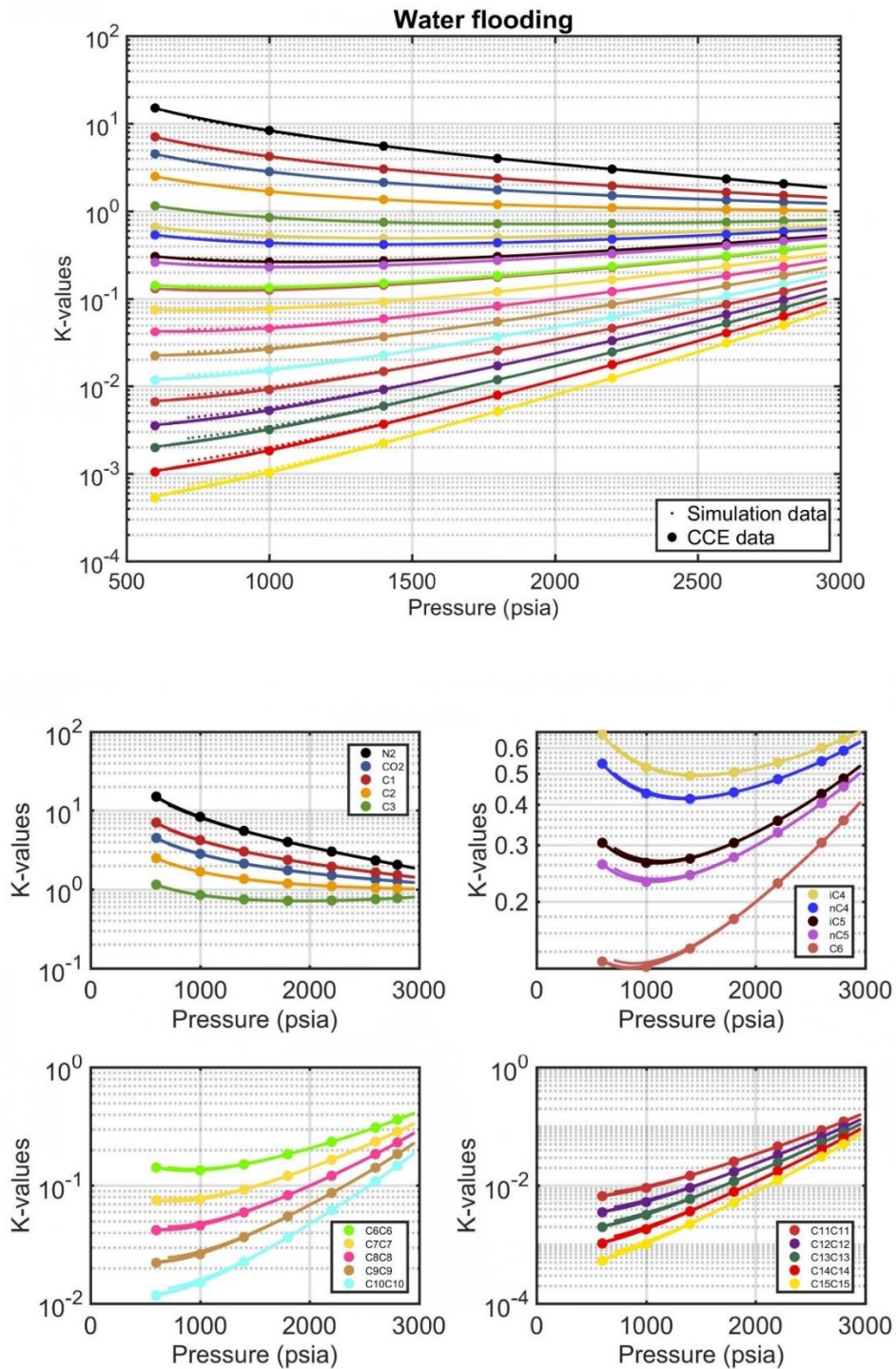


**Figure 5.7:** Average reservoir pressure (psia) for the ten year production period of the water flooding scenario. The amount of the injected water is not sufficient to provide pressure maintenance.



**Figure 5.8:** Average liquid condensate saturation (fraction) for the ten year production period of the water flooding scenario. The retrograde condensation is more pronounced compared to the natural depletion scenario because of the much more reduced reservoir pressure at the last years of the production period.

The pressure/K-values plots for this scenario of water flooding, exhibit a perfect match between the simulation derived and the CCE derived data, exactly like the natural depletion scenario, proving that neither water injection nor well positioning affect the resulting equilibrium coefficient values (Fig. 5.9).



**Figure 5.9:** Pressure/K-values plots for the water flooding scenario showing an exact match between the simulation and CCE data demonstrating that water injection in the reservoir and well positioning do not affect the derived K-values.

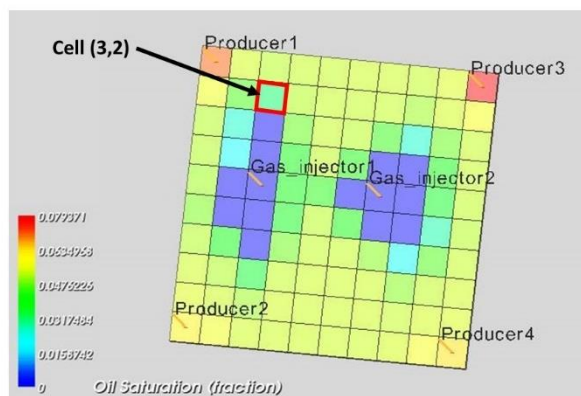


## 5.2 Gas recycling scenarios

In the following gas recycling scenarios, the produced gas was stripped from its heavy components at surface and the remaining dry gas was reinjected back in the reservoir in various amounts through gas injection wells. Two sets of experiments were designed: i) four gas recycling scenarios where the produced gas was directly flashed at standard conditions and ii) two gas recycling scenarios where the produced gas was successively flashed through a series of separators before being finally flashed at surface conditions.

In all recycling scenarios, the composition of the reinjection gas was initially calculated from the initial overall composition of the reservoir fluid. During the ten years of the production period, the reinjection composition was updated once, five years after the production began, based on the composition of a cell of the reservoir model that was regarded as representative of the reservoir's average overall composition at that time. The cell that was selected was cell (3,2) in the 10x10 block reservoir, as it is located close to a production well (Producer1) and therefore has an equivalent composition to the fluid that is produced at the surface, without being affected by the pressure drop that the near wellbore region experiences and second, it is also close to an injection well (Gas\_injector1) in way that the recycled dry gas has managed to reach that region and therefore modify its composition by making it leaner (Fig. 5.10).

The only scenario with an extended production period of twenty years is the one where 80% of the produced gas is reinjected in the reservoir after been treated through a series of separators at the surface. In this scenario, the reinjection gas was updated three times in total, once every five years, again based on the composition of cell (3,2).



**Figure 5.10:** Cell (3,2) in the 10x10 block of the simplistic gas condensate reservoir whose composition was regarded as representative of the average overall reservoir composition at the times of recalculation of the injection gas composition.

For the direct flash scenarios, the composition of the reinjection dry gas was calculated with the assistance of CMG's WinProp software by performing a two-phase flash of the initial reservoir fluid composition at

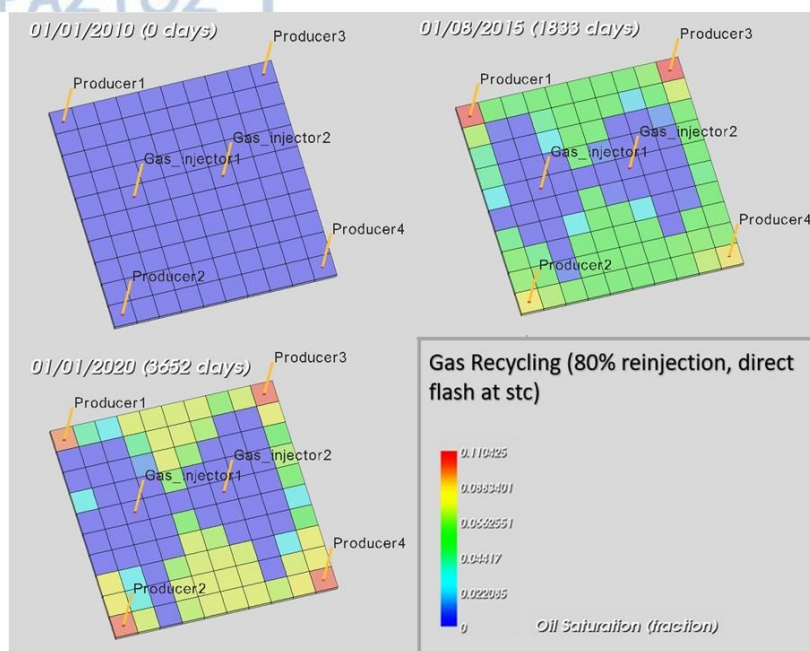
standard conditions (60 °F and 14.7 psia). The initial reinjection gas composition for the direct flash scenarios can be seen in Table 5.2.

**Table 5.2:** Reinjection dry gas composition at the start of the production period based on the initial overall reservoir fluid composition for the gas recycling scenarios with a direct flash at stc.

Component	N <sub>2</sub>	CO <sub>2</sub>	C1	C2	C3	iC4	nC4	iC5	nC5	C6
(%)	3.96145	0.3647	70.78466	11.82712	5.62955	1.18121	2.07061	0.73654	0.97138	0.92263
Component	C6C6	C7C7	C8C8	C9C9	C10C10	C11C11	C12C12	C13C13	C14C14	C15C15
(%)	0.69336	0.4244	0.20323	0.19683	0.02747	0.00423	0.00056	0.00008	0.00001	0.00000

### 5.2.1 Gas recycling 80% (direct flash at stc)

In this scenario, the produced gas was flashed directly at surface conditions and after its separation into liquid condensate and dry gas, 80% of the produced gas was reinjected in the reservoir as dry gas with a composition shown in Table 5.2. Four production wells were operating at a fixed rate of 7 MMscf/day each, throughout the production period. The gas injectors for the first five years had a fixed injection rate of 11.2 MMscf/day each and during the last 5 years an increased fixed rate of 12 MMscf/day each (Fig. 5.11). After five years of production the composition of cell (3,2) was used as a feed one that was directly flashed at standard conditions to provide the updated reinjection composition for the last five years of production (Table 5.3). The reservoir pressure exhibited a constant decline that reached 2,300 psia at the end of the production period, although a partial pressure maintenance at the second period of production can be observed, due to the increased amount of the injected gas (Fig. 5.12). The plot of liquid saturation versus time exhibits a reduced amount of liquid condensate in the reservoir (~0.038, i.e. 3.8%) compared to the depletion scenarios (Fig. 5.13). In addition, some revaporisation is observed during the last three years, even though the reservoir pressure has been kept at 2,450 psia. Both observations are indications that the gas recycling process contributes to the reduced amount of liquid condensate in the reservoir by modifying the overall reservoir composition and making it leaner.



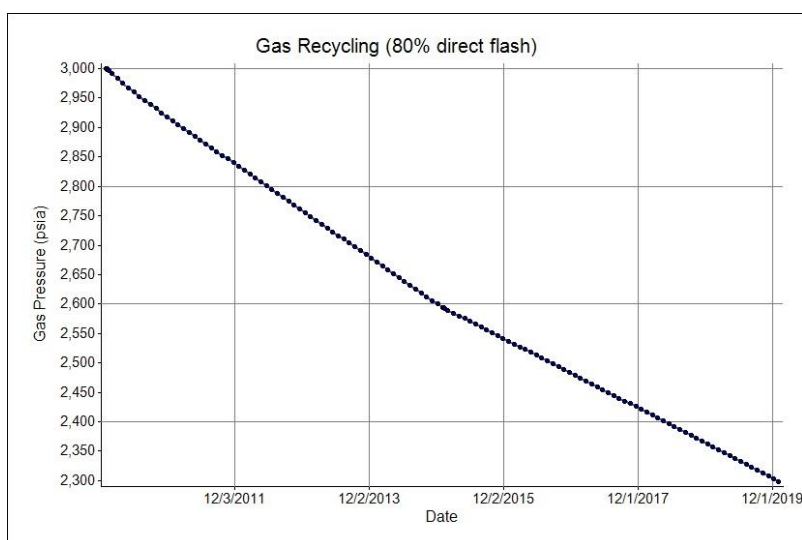
**Figure 5.11:** Gas recycling scenario where 80% of the produced gas is reinjected in the reservoir as dry gas after its direct flash at surface conditions and its separation from the heavy components.

**Table 5.3:** Composition of the injected gas after five years of production calculated based on the composition of cell (3,2) that was considered as representative of the average reservoir fluid composition after five years of production and the process of dry gas recycling.

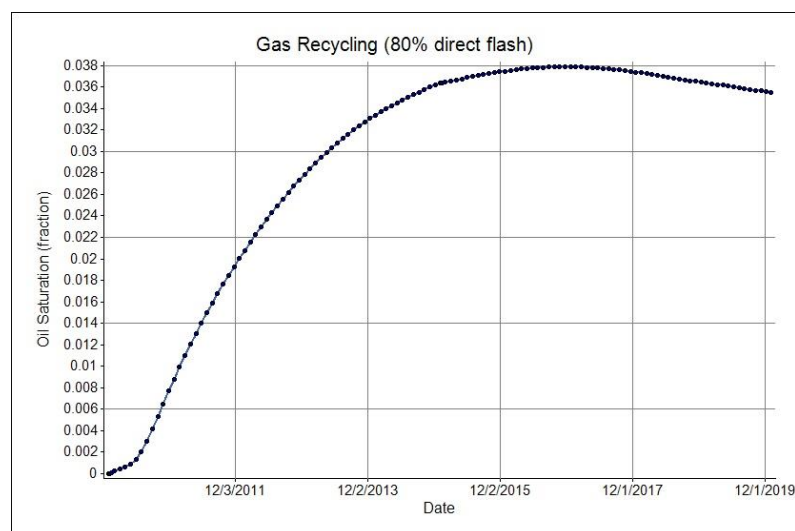
Component	N <sub>2</sub>	CO <sub>2</sub>	C1	C2	C3	iC4	nC4	iC5	nC5	C6
(%)	3.96999	0.36732	70.84241	11.8106	5.6082	1.17531	2.05986	0.73326	0.96091	0.91754
Component	C6C6	C7C7	C8C8	C9C9	C10C10	C11C11	C12C12	C13C13	C14C14	C15C15
(%)	0.69169	0.42657	0.20455	0.19957	0.0274	0.00419	0.00052	0.00009	0.00001	0.00000

A common characteristic of all pressure versus K-values plots in the gas recycling scenarios is the deviation that is observed at various degrees at the light and heavy components and especially at low pressures. This deviation becomes more pronounced as the stripping of the gas from its intermediate and heavy components increases. In general, the pressure/K-values plots for this scenario exhibit a good match between the simulation and the CCE data although, some scattering is observed at the lower pressures, especially for the heavier components, where the CCE data seem to underestimate the K-values (Fig. 5.14). On the other hand, the extended CVD derived K-values appear to have a better match against the simulation derived K-values. The first plot of Figure 5.15 shows the simulation-derived K-values versus pressure for

the total of 20 components compared against the extended CVD-derived K-values, where it is made evident that the extended CVD is not an appropriate method to describe the phase behaviour of heavy fractions greater than C11C11 as well as of CO<sub>2</sub>. On the other hand, the second plot of Figure 5.15 depicts the rest of the fluid's components which exhibit a perfect match, implying that the extended CVD can efficiently describe the phase behaviour for the majority of the fluid's components.

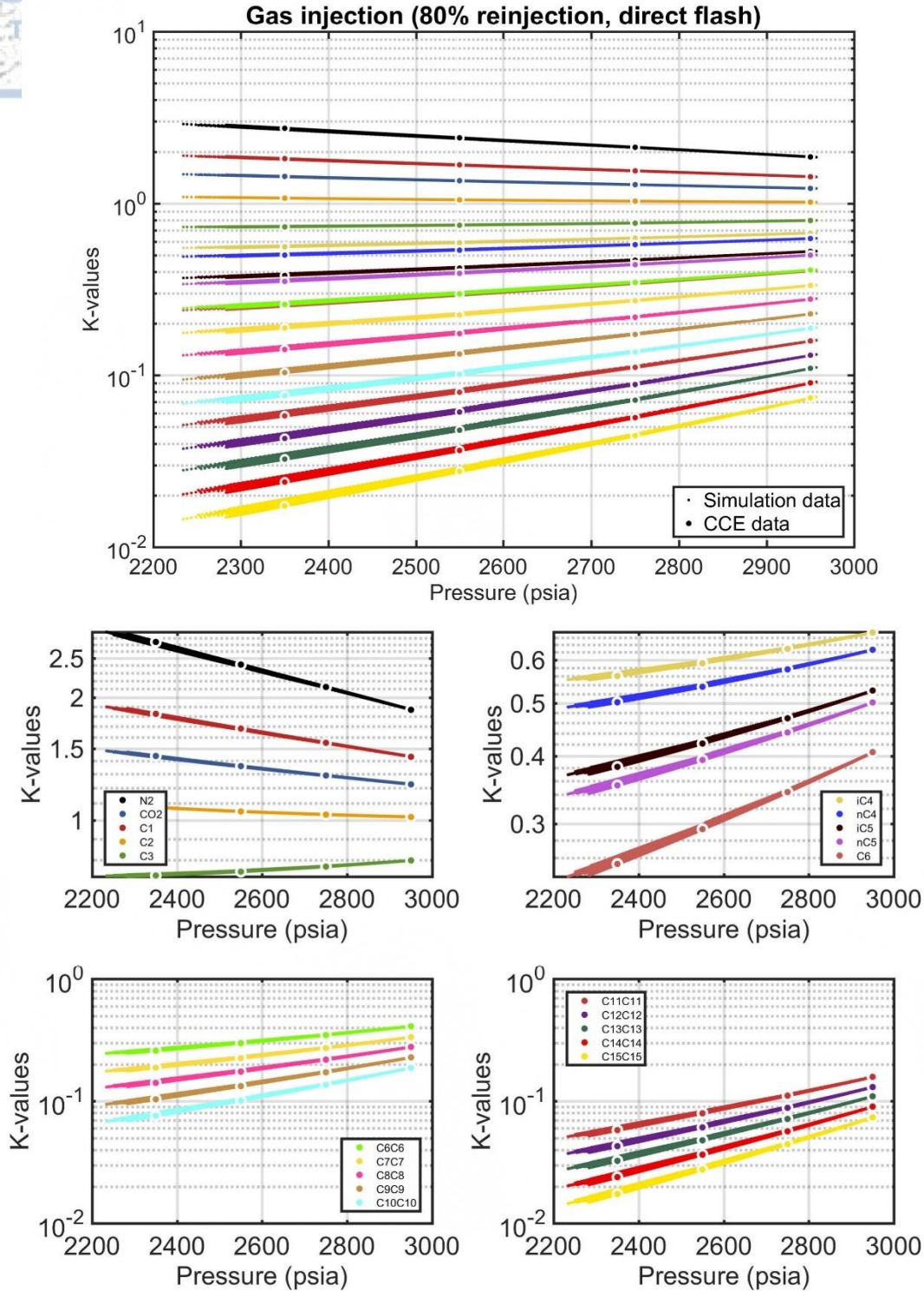


**Figure 5.12:** Average reservoir pressure (psia) for the ten year production period of the gas recycling scenario with reinjection of 80% of the produced gas after its direct flash at surface conditions and its separation from the heavy components. A change in slope at five years of production indicates a partial pressure maintenance, owing to the increased amount of reinjection gas during the last five years of production.

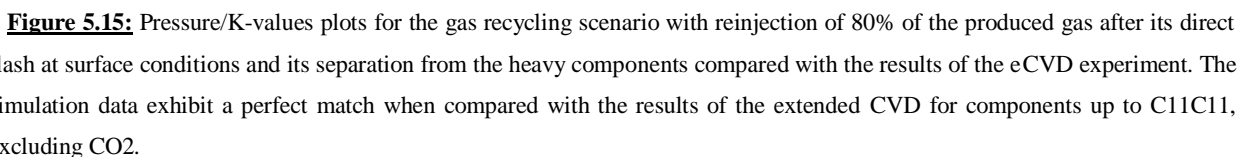


**Figure 5.13:** Average liquid condensate saturation (fraction) for the ten year production period of the gas recycling scenario with reinjection of 80% of the produced gas after its direct flash at surface conditions and its separation from the heavy components. The observed revaporisation happens due to a change in the reservoir fluid's composition as a result of the gas recycling process and not because of a reduced reservoir pressure.





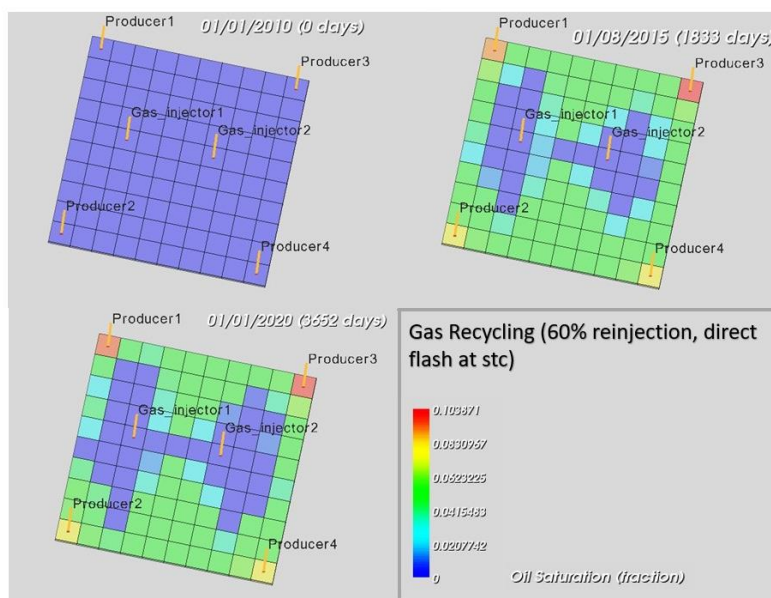
**Figure 5.14:** Pressure/K-values plots for the gas recycling scenario with reinjection of 80% of the produced gas after its direct flash at surface conditions and its separation from the heavy components compared with the results of the CCE experiment. The diagrams show a good match between the simulation and the CCE derived data although some scattering is observed at lower pressures where the CCE underestimates the K-values.



### 5.2.2 Gas recycling 60% (direct flash at stc)

In this scenario the injection wells operated at a dry gas injection rate that corresponds to 60% of the amount of the produced gas and initial injection composition given in Table 5.2. Four production wells were producing at a fixed rate of 7 MMscf/day each and two injection wells were injecting dry gas at a fixed rate of 8.4 MMscf/day each for a period of ten years (Fig. 5.16). The composition of the injected gas was updated as previously at five years of production, again based on the composition of cell (3,2) (Table 5.4). The reservoir pressure was constantly reduced, since the amount of the reinjection gas did not provide pressure maintenance, and it reached 1,500 psia at the end of the production period (Fig. 5.17). The liquid saturation reached a maximum average value of 0.036 (3.6%) and was then reduced, due to revaporisation caused by both the change in reservoir fluid's composition as a result of gas recycling, as well as the further reduction in reservoir pressure (Fig. 5.18).

The pressure/K-values charts exhibit a good match between the simulation derived and CCE derived data, although the CCE derived K-values tend to slightly underestimate the K-values of the heavy components. In addition, the heavy components exhibit some scattering of their values, although this scattering is less pronounced than in the previous 80% scenario (Fig. 5.19). On the other hand, comparison of the simulation data against the results of the eCVD experiment, exhibit a perfect match of their values for components up to C11C11, excluding CO<sub>2</sub> (Fig. 5.20). Consequently, the simulation data in this scenario can be better represented by the results of the eCVD experiment where it is applicable.

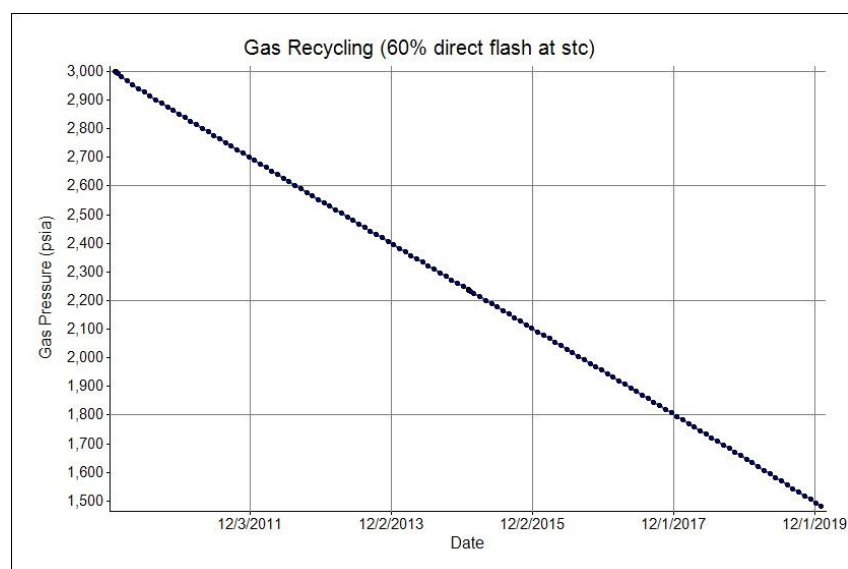


**Figure 5.16:** Gas recycling scenario where 60% of the produced gas is reinjected in the reservoir as dry gas after its direct flash at surface conditions and its separation from the heavy components.

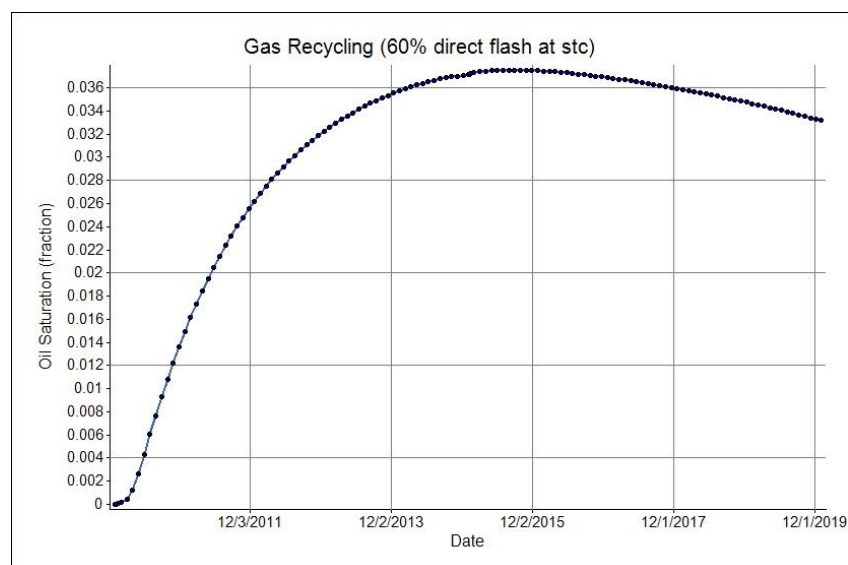


**Table 5.4:** Composition of the injected gas after five years of production calculated based on the composition of cell (3,2) that was regarded as representative of the average reservoir fluid composition after five years of production and the process of dry gas recycling.

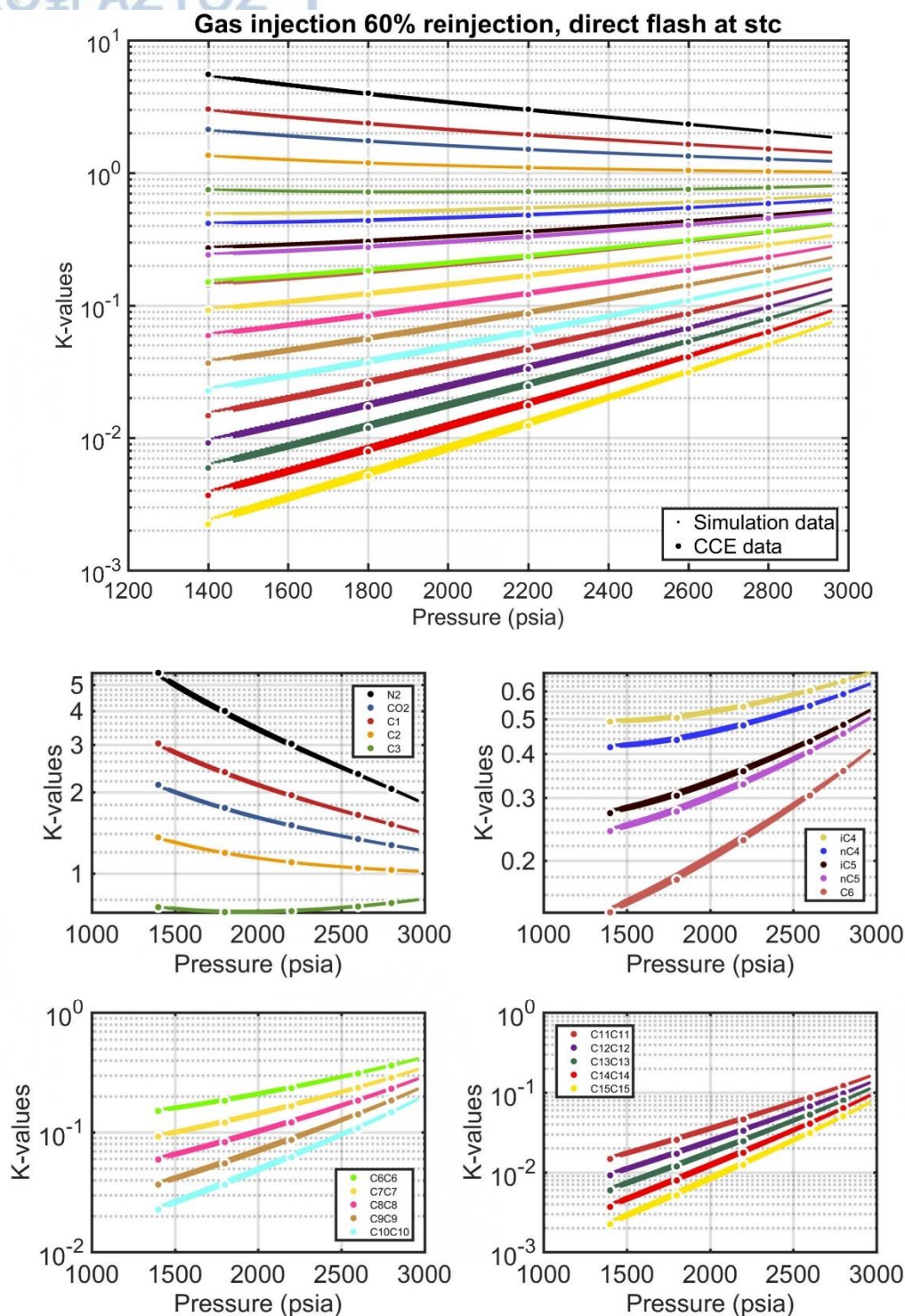
Component	N <sub>2</sub>	CO <sub>2</sub>	C <sub>1</sub>	C <sub>2</sub>	C <sub>3</sub>	iC <sub>4</sub>	nC <sub>4</sub>	iC <sub>5</sub>	nC <sub>5</sub>	C <sub>6</sub>
(%)	3.98778	0.36523	70.99506	11.78553	5.57026	1.16095	2.03428	0.71545	0.9468	0.90164
Component	C <sub>6</sub> C <sub>6</sub>	C <sub>7</sub> C <sub>7</sub>	C <sub>8</sub> C <sub>8</sub>	C <sub>9</sub> C <sub>9</sub>	C <sub>10</sub> C <sub>10</sub>	C <sub>11</sub> C <sub>11</sub>	C <sub>12</sub> C <sub>12</sub>	C <sub>13</sub> C <sub>13</sub>	C <sub>14</sub> C <sub>14</sub>	C <sub>15</sub> C <sub>15</sub>
(%)	0.6729	0.42216	0.2075	0.20194	0.02804	0.00389	0.00048	0.00008	0.00001	0.00000



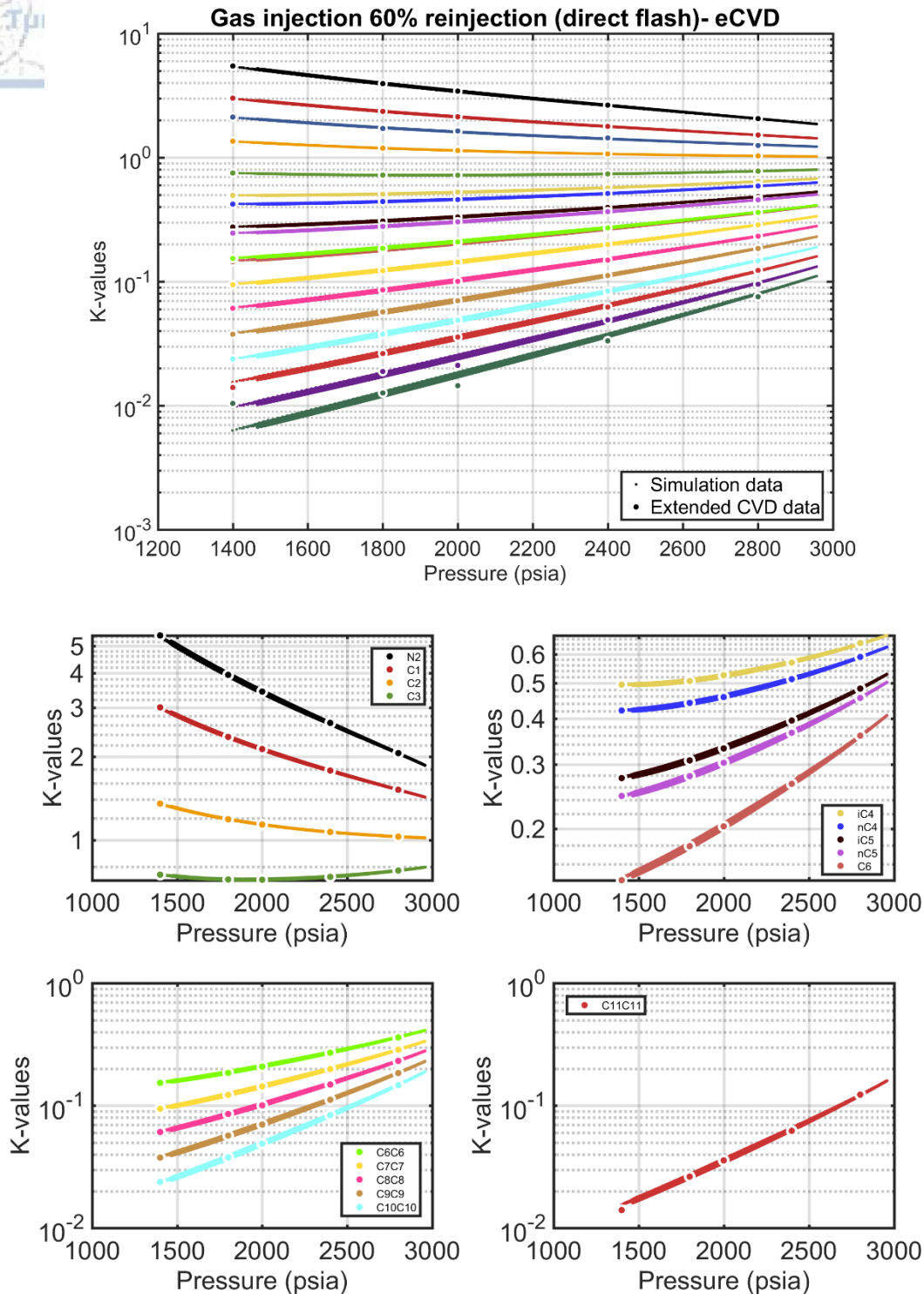
**Figure 5.17:** Average reservoir pressure (psia) for the ten year production period of the gas recycling scenario with reinjection of 60% of the produced gas after its direct flash at surface conditions and its separation from the heavy components. The amount of the re injected gas is not sufficient to provide pressure maintenance and there is a steady decline in reservoir pressure.



**Figure 5.18:** Average liquid condensate saturation (fraction) for the ten year production period of the gas recycling scenario with reinjection of 60% of the produced gas after its direct flash at surface conditions and its separation from the heavy components. The observed revaporisation happens due to a change in the reservoir fluid's composition, as a result of the gas recycling process, in combination with the reduced reservoir pressure.



**Figure 5.19:** Pressure/K-values plots for the gas recycling scenario with reinjection of 60% of the produced gas after its direct flash at surface conditions and its separation from the heavy components, compared with the results of the CCE experiment. The diagrams show a good match between the simulation and the CCE derived data even though the CCE experiment seems to slightly underestimate the K-values for the heavy components. Some scattering is observed at lower pressures but less pronounced than in the previous 80% scenario.

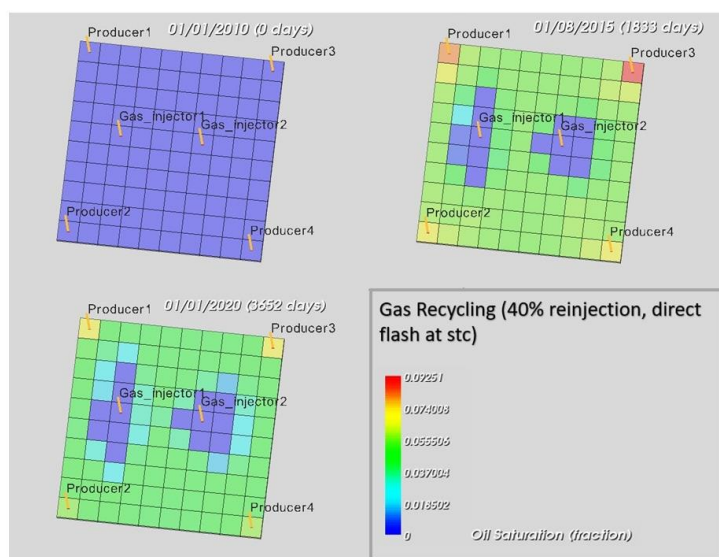


**Figure 5.20:** Pressure/K-values plots for the gas recycling scenario with reinjection of 60% of the produced gas after its direct flash at surface conditions and its separation from the heavy components compared with the results of the eCVD experiment. The simulation data exhibit a perfect match when compared with the results of the extended CVD for components up to C11C11, excluding CO<sub>2</sub>.

### 5.2.3 Gas recycling 40% (direct flash at stc)

In this scenario the dry gas injection rate corresponds to 40% of the amount of the produced gas. The initial reinjection composition is given in Table 5.2. The four production wells were producing at a fixed rate of 7 MMscf/day each for ten years and the two gas injectors were injecting at a fixed rate of 5.6 MMscf/day each for the same time period (Fig. 5.21). The reinjection composition was updated once after 5 years of production based again on the composition of cell (3,2) and is given in Table 5.5. The reservoir pressure was constantly reduced, since the injected amount was not enough to maintain the pressure, and reached 700 psia at the end of the production period (Fig. 5.22). This pressure drop had an impact on the amount of liquid present in the reservoir, as firstly, liquid saturation reached a maximum value of about 0.045 (4.5%) and then it started to decline as a response to this reduced reservoir pressure (Fig. 5.23). This is better understood if one looks at the fluid's phase envelope (Fig. 5.1) where it can be seen that at 700 psia and reservoir temperature of 220 °F, the lower dew point curve is approached, implying that revaporisation of the generated condensate takes place due to the reduced reservoir pressure and not due to the change of reservoir composition as a result of gas recycling. In addition, it can be seen that the reinjection gas is limited in a few blocks around the injection wells (Fig. 5.21) and is not sufficient to cause a reservoir-scale change in composition.

The pressure/K-values plots are similar to the previous scenario of 60% reinjection and present a good match between the examined simulation and CCE derived data with slightly less scattering of the heavy components than the previous scenarios (Fig. 5.24).

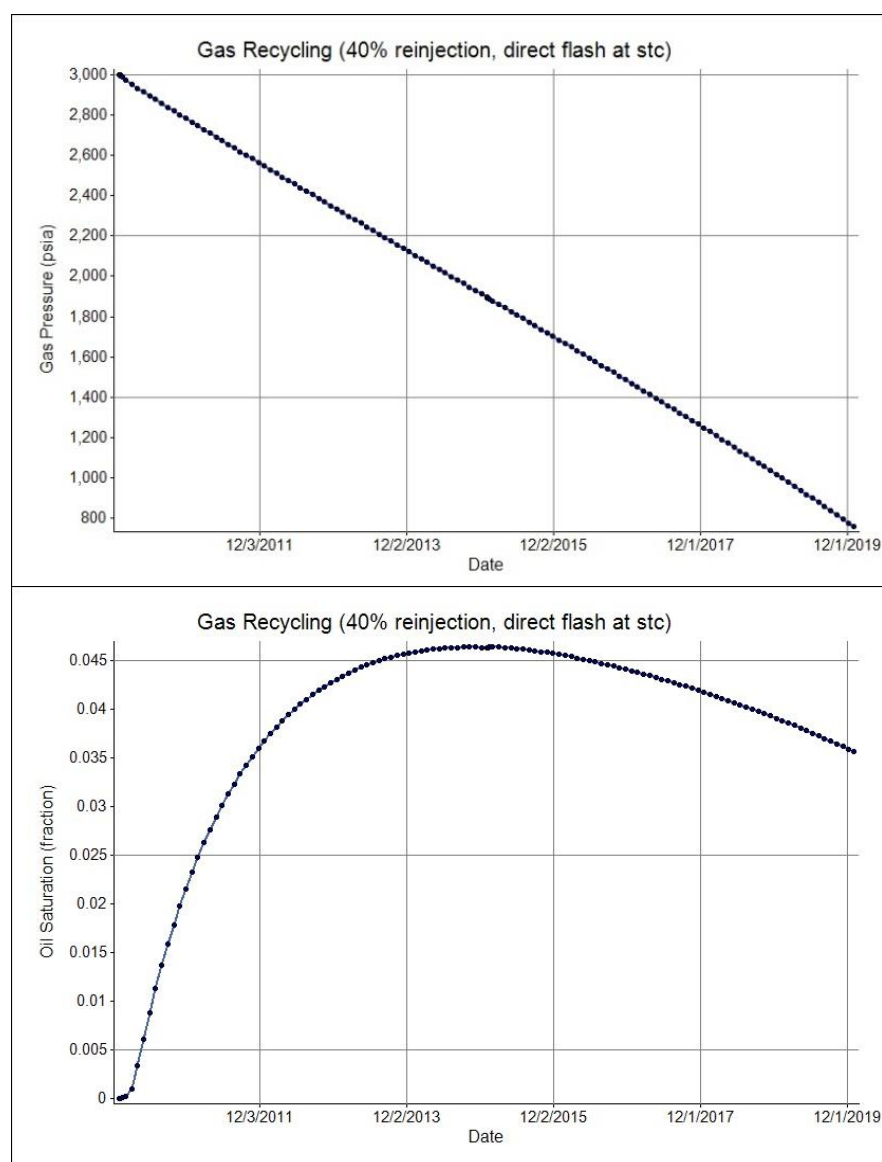


**Figure 5.21:** Gas recycling scenario where 40% of the produced gas is reinjected in the reservoir as dry gas after its direct flash at surface conditions and its separation from the heavy components.



**Table 5.5:** Composition of the injected gas after five years of production calculated based on the composition of cell (3,2) that was regarded as representative of the average reservoir fluid composition after five years of production and the process of dry gas recycling.

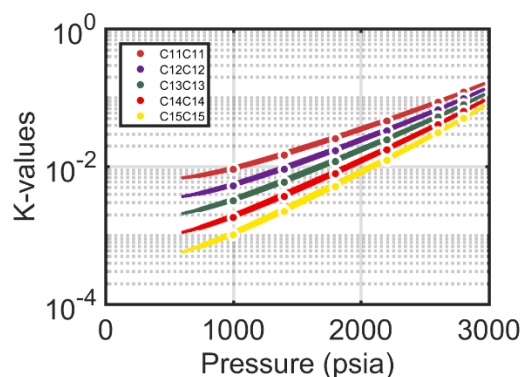
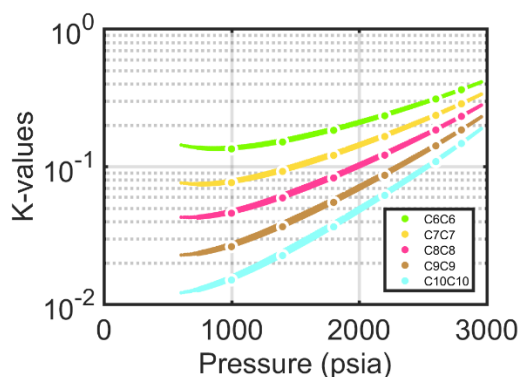
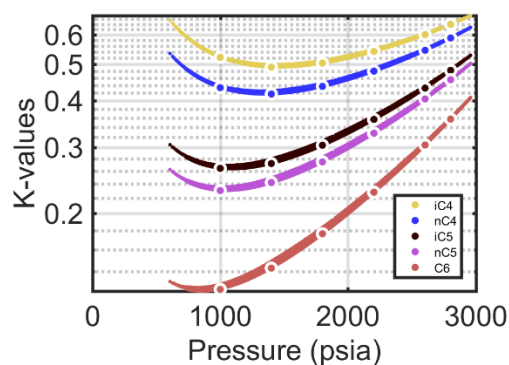
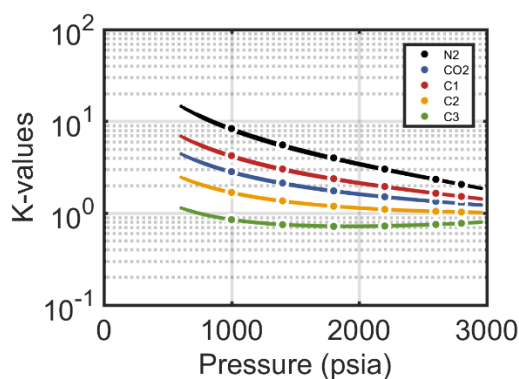
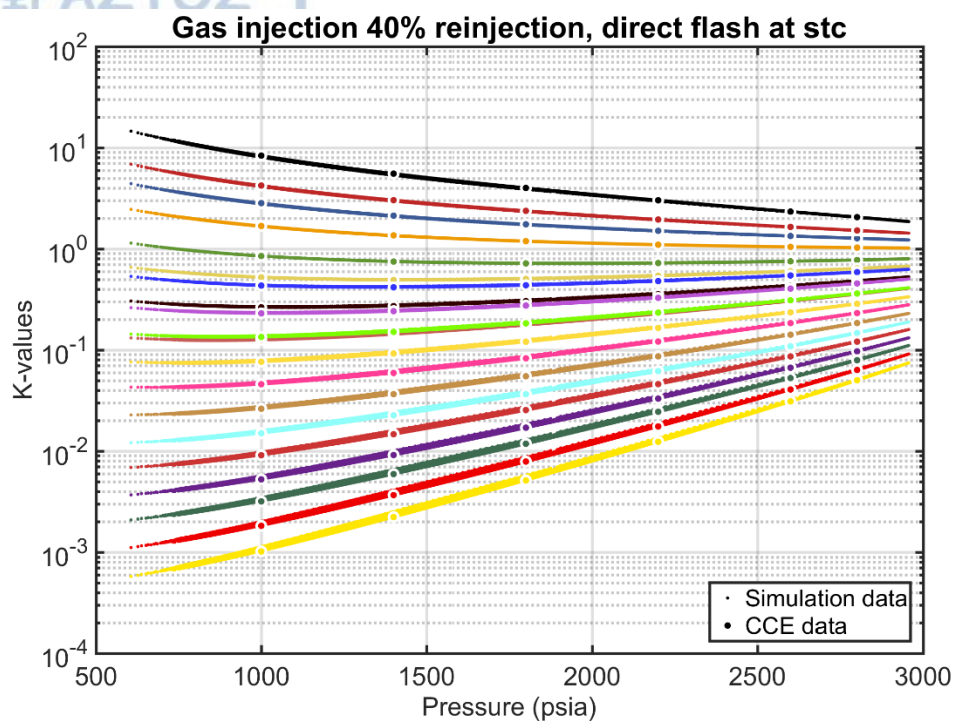
Component	N <sub>2</sub>	CO <sub>2</sub>	C1	C2	C3	iC4	nC4	iC5	nC5	C6
(%)	3.88098	0.36497	70.05562	11.9608	5.83028	1.24341	2.20391	0.80493	1.05708	0.99086
Component	C6C6	C7C7	C8C8	C9C9	C10C10	C11C11	C12C12	C13C13	C14C14	C15C15
(%)	0.75686	0.43746	0.19631	0.18438	0.027	0.00442	0.00063	0.0001	0.00001	0.00000



**Figure 5.22:** Average reservoir pressure (psia) for the ten year production period of the gas recycling scenario with reinjection of 40% of the produced gas after its direct flash at surface conditions and its separation from the heavy components. The amount of the injected gas was not sufficient to provide pressure maintenance and there was a steady decline in reservoir pressure.

**Figure 5.23:** Average liquid condensate saturation (fraction) for the ten year production period of the gas recycling scenario with reinjection of 40% of the produced gas after its direct flash at surface conditions and its separation from the heavy components. Revaporisation happens due the reduced reservoir pressure, since the amount of the injected gas is not sufficient to provide reservoir-scale compositional changes.





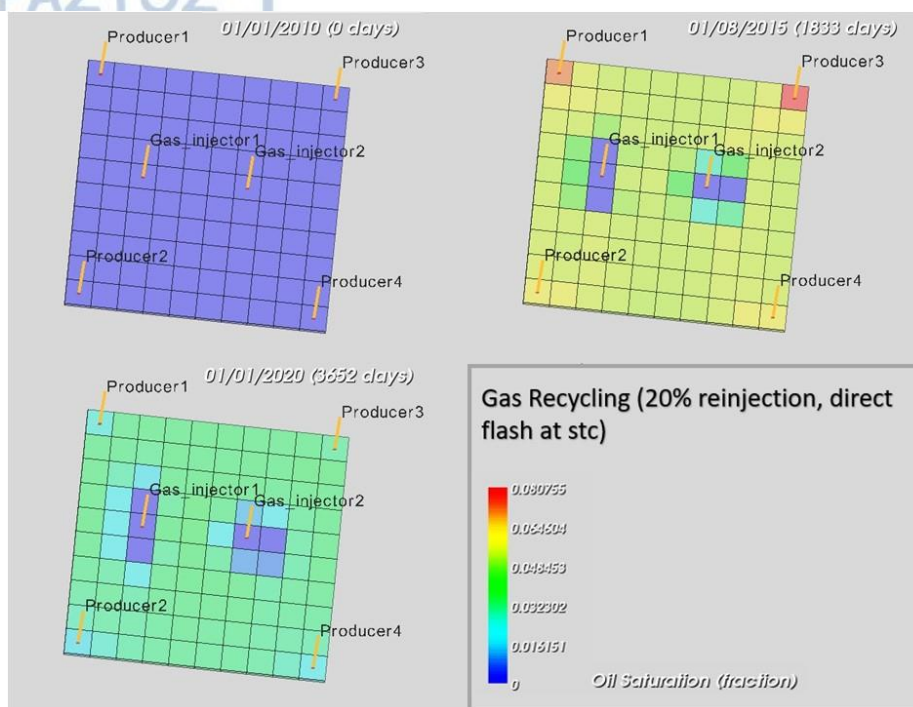
**Figure 5.24:** Pressure/K-values plots for the gas recycling scenario with reinjection of 40% of the produced gas after its direct flash at surface conditions and its separation from the heavy components compared with the results of the CCE experiment. The diagrams show a good match between the simulation and the CCE derived data even though the CCE experiment seems to slightly underestimate the K-values for the heavy components.

#### 5.2.4 Gas Recycling 20% (direct flash at stc)

In this last scenario of direct flash of the produced gas at the surface, the dry gas injection rate corresponds to only 20% of the amount of the produced gas. The four production wells were again producing at a fixed rate of 7 MMscf/day each for a ten year production period, while the two gas injectors were injecting dry gas at a fixed rate of 2.8 MMscf/day each for the same time period (Fig. 5.25). The initial injection composition is given in Table 5.2 and the updated at five years reinjection composition is given in Table 5.6, again based on the composition of cell (3,2). The reservoir pressure at the end of the production period was as low as 260 psia which, clearly, does not correspond to a realistic but only to a research production scenario (Fig. 5.26). This low pressure at the last years of production could not support the appointed production rate and as a result, forced the producing wells to switch from producing with a fixed rate to producing with a fixed bottomhole pressure. However, for consistency reasons among the recycling scenarios, no action was taken in the simulator to provide pressure maintenance for this scenario. The liquid saturation reached a maximum value of 0.05 (5%) before starting to decrease again as a response to the reduction in reservoir pressure (Fig. 5.27). This scenario arrives to a maximum amount of liquid condensation in the reservoir (5%) similar to the depletion scenarios.

It is noteworthy that in the last two scenarios of 40% and 20% reinjection, the gas injection composition after 5 years of gas recycling is heavier than the initial injection composition. This observation, along with the fact that the injected gas in both scenarios cannot provide any pressure maintenance leading to a vast reduction in pressure in the reservoir at the end of the production period, leads to the conclusion that in these scenarios, the dry gas recycling process with such small amounts of injection gas does not benefit the production. Even though it is a fact that some revaporisation is observed in the reservoir, this however is due to the approaching of the lower dew point curve as a result of the large decline in pressure. It is also reminded here, that no operation can continue at such low reservoir pressures, as abandonment of the field takes place much earlier in the process.

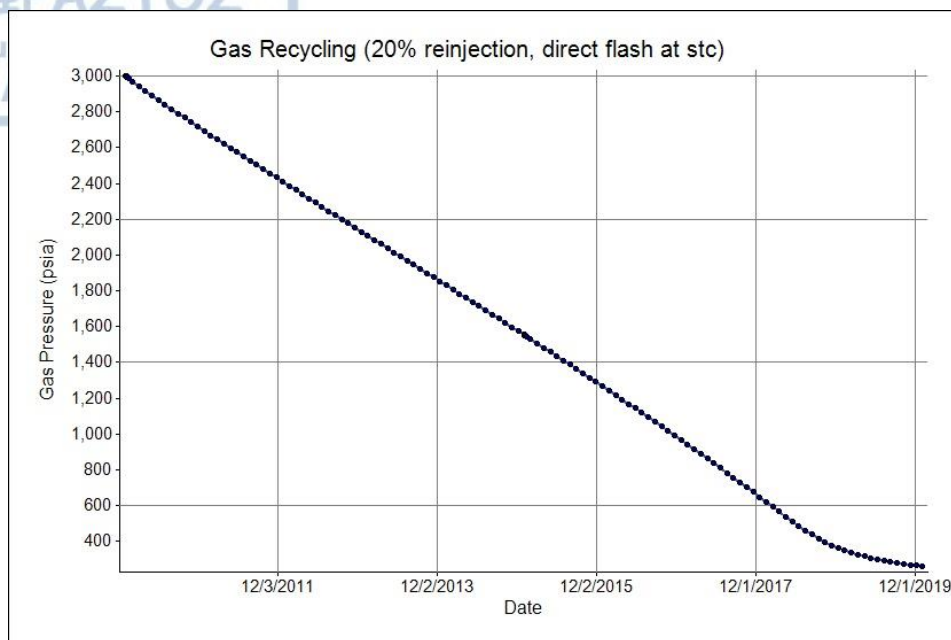
The pressure/K-values plots exhibit a very good match between the simulation derived and CCE derived data as expected, since this scenario is much similar to the depletion scenarios as the amount of injected gas is rather small and does not affect strongly the overall reservoir composition (Fig. 5.28).



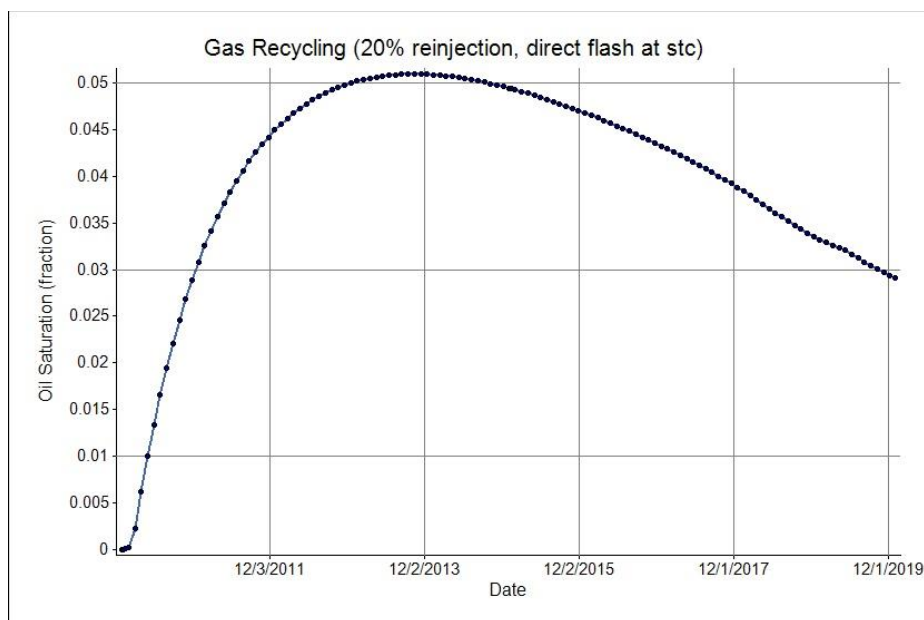
**Figure 5.25:** Gas recycling scenario where 20% of the produced gas is reinjected in the reservoir as dry gas after its direct flash at surface conditions and its separation from the heavy components.

**Table 5.6:** Composition of the injected gas after five years of production calculated based on the composition of cell (3,2) that was regarded as representative of the average reservoir fluid composition after five years of production and the process of dry gas recycling.

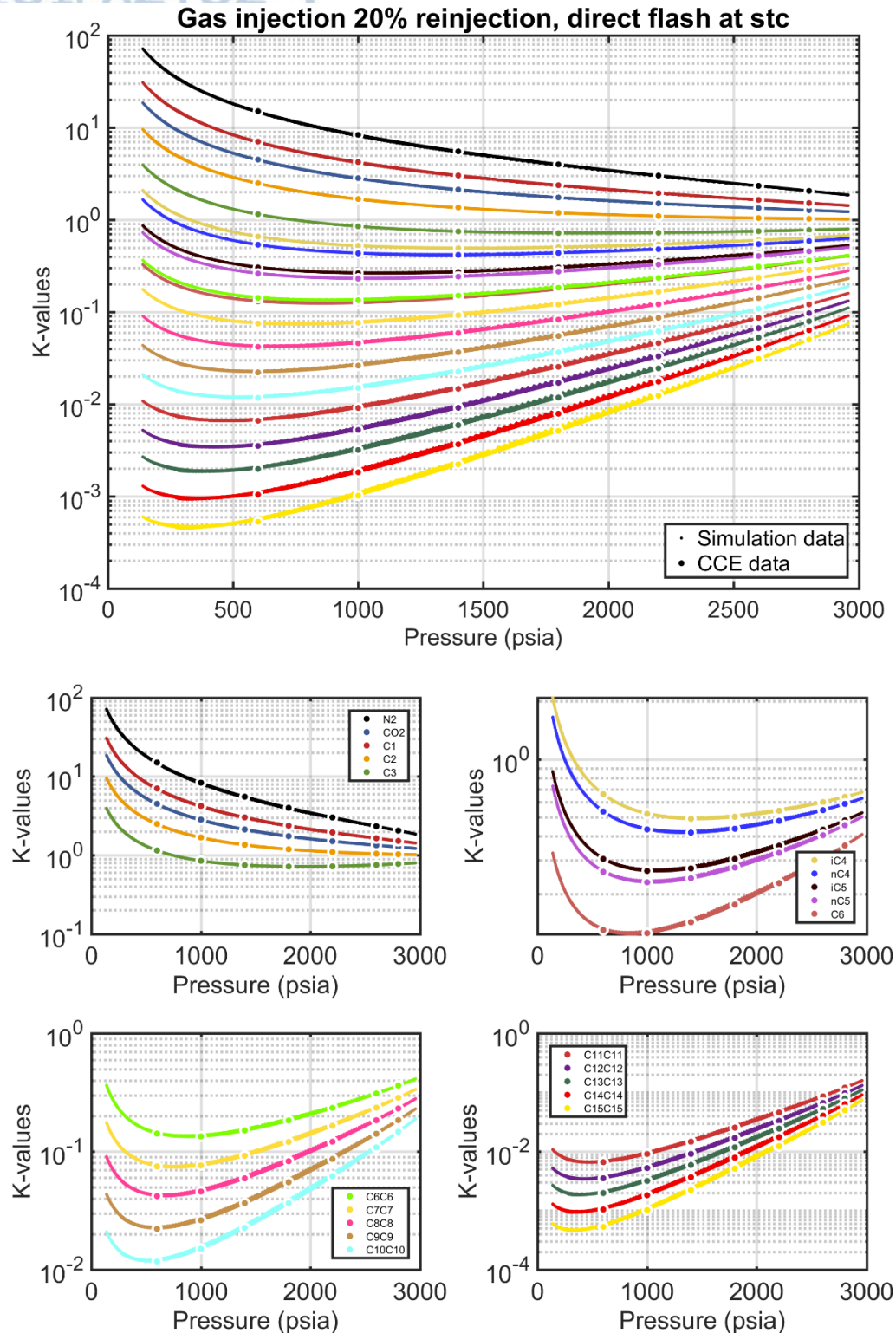
Component	N <sub>2</sub>	CO <sub>2</sub>	C1	C2	C3	iC4	nC4	iC5	nC5	C6
(%)	3.86397	0.3597	69.85465	11.99372	5.88347	1.26551	2.25014	0.81983	1.08192	1.0048
Component	C6C6	C7C7	C8C8	C9C9	C10C10	C11C11	C12C12	C13C13	C14C14	C15C15
(%)	0.76468	0.43964	0.1975	0.18842	0.02702	0.00439	0.00054	0.00009	0.00001	0.00000



**Figure 5.26:** Average reservoir pressure (psia) for the ten year production period of the gas recycling scenario with reinjection of 20% of the produced gas after its direct flash at surface conditions and its separation from the heavy components. In this scenario the reservoir pressure was reduced in such a degree that caused the production wells to switch from producing with a fixed rate to producing with a fixed bottomhole pressure and that explains the change in slope at the end of the diagram.



**Figure 5.27:** Average liquid condensate saturation (fraction) for the ten year production period of the gas recycling scenario with reinjection of 20% of the produced gas after its direct flash at surface conditions and its separation from the heavy components. The liquid saturation curve of this scenario is similar to the liquid saturation curves of the depletion scenarios.



**Figure 5.28:** Pressure/K-values plots for the gas recycling scenario with reinjection of 20% of the produced gas after its direct flash at surface conditions and its separation from the heavy components compared with the results of the CCE experiment. The diagrams indicate a very good match between the simulation and the CCE derived data. This scenario presents less scattering of the K-values since the amount of the reinjection gas is small.



### 5.2.5 Gas Recycling 80% (separators train)

In this recycling scenario the produced gas passed through a train of separators before finally being driven to standard conditions. Four production wells were producing at a fixed rate of 7 MMscf/day each for a period of twenty years. Two injector wells were injecting the first ten years at a fixed rate of 11.2 MMscf/day each and the last ten years at a fixed rate of 12 MMscf/day each (Fig. 5.29).

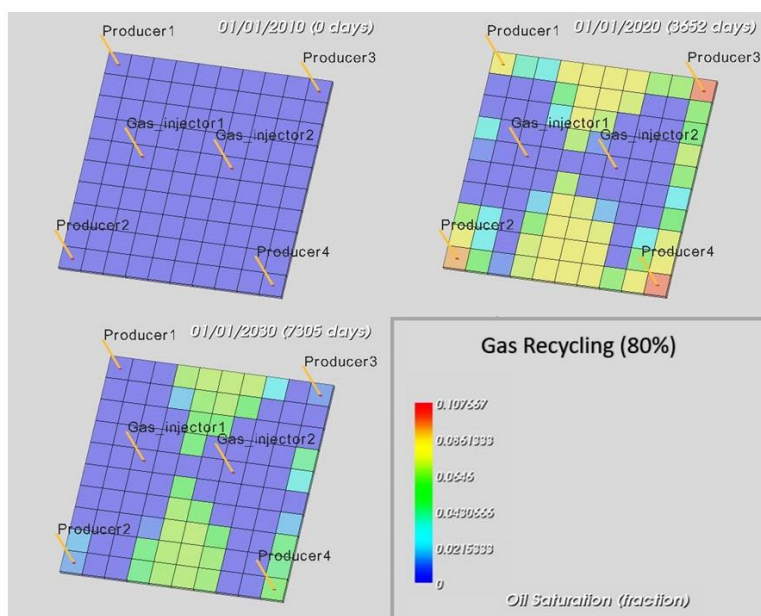
The initial injection composition was calculated by passing the initial overall reservoir fluid composition through a train of separators (Table 5.7). The separator calculations were performed with the assistance of IPM Petroleum Experts' PVTP software. An array of two separators was designed, the first one set at 500 psia and 120 °F and the second at 150 psia and 80 °F. The produced gas was passing first through Separator 1 where it was separated into liquid condensate and dry gas. Then, the generated condensate was passing through Separator 2 where it was further separated into an amount of dry gas and an amount of liquid condensate. The latter was then flashed at standard conditions (14.7 psia and 60 °F) leading again to its final separation into condensate and dry gas (Figs. 5.30 and 5.31). This process ensured the maximum possible condensate yield at surface and consequently, leaner composition of the reinjected gas.

The recycling process provided partial pressure maintenance (Fig. 5.32) and for that reason the production period was extended to twenty years in order to allow for the study of the results of dry gas recycling for a longer time period.

The injection composition was revised three times during the production period, after five, ten and fifteen years of production by gathering each time the composition of cell (3,2) and passing it through the train of separators at the surface. The total amount of dry gas generated throughout the separation process from Separator 1 to the Tank, was recombined by taking into account the gas composition and number of moles at each stage, before being reinjected back into the reservoir. The updated composition of the reinjected gas after five, ten and fifteen years is given in Tables 5.8, 5.9 and 5.10 respectively. These tables show that the reinjected gas at each update becomes leaner in composition, leading to a leaner overall reservoir composition through the recycling process. As a result, condensate revaporisation in the reservoir is observed not because of reduced reservoir pressure, but as a response to this leaner overall reservoir composition. This conclusion is further supported by the liquid saturation curve (Fig. 5.33). This shows a maximum liquid condensation of about 0.038 (3.8%) which later reduces to a great extent after five years of production, reaching a value as low as 0.018 (1.8%) in the reservoir, while the reservoir pressure at this stage at the end of production is about 1,200 psia. During the last 7 years of production a slight change in slope is observed and the curve becomes smoother. This indicates a reduced rate of revaporisation that can be attributed to the fact that at the last years, the overall reservoir composition is no longer getting progressively leaner. Indeed, the reinjection calculation tables (Tables 5.9 and 5.10) exhibit only an

imperceptible change in methane composition, probably due to the fact that the fluid has become as dry as possible through extraction of the maximum possible amount of condensate at the surface. From now on, the gas recycling process could stop and gas production could be continued by depleting the reservoir.

The pressure/K-values diagrams in this scenario do not present a good match between the simulation data and the CCE derived data, especially for the lighter and the heavier components which exhibit a strong scatter of their simulation derived values. Here, since the gas was treated through a series of separators, the most stripping of the intermediate and heavy components has occurred, thus leading to a greater deviation of the k-values (Fig. 5.34). This leads to the conclusion that in a more complicated scenario like the one presented here, which contains a complex process for the treatment of the produced gas at the surface through a train of separators before its reinjection in the reservoir, as well as larger compositional variations due to the increased amount of injected gas, the CCE experiment is not suitable to describe the processes of production and gas recycling in terms of the K-values. On the contrary, the simulation data can be better described in terms of their K-values through the extended CVD experiment for components up to C11C11 and excluding the CO<sub>2</sub>. Even though the simulation-derived and eCVD-derived values do not present a perfect match, the difference is definitely less pronounced than when compared with the classic CCE derived K-values. (Fig. 5.35).



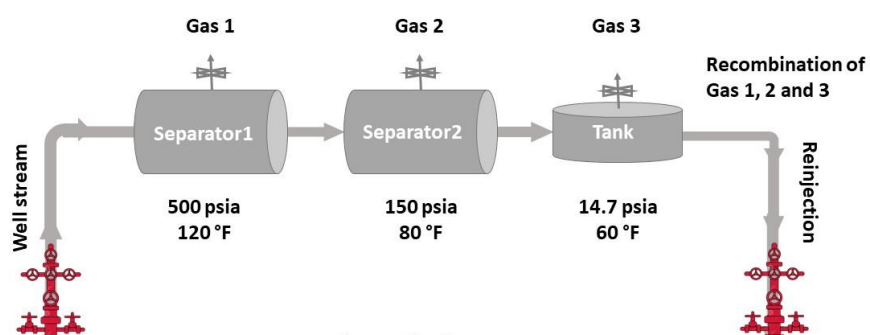
**Figure 5.29:** Gas recycling scenario where 80% of the produced gas is reinjected in the reservoir after passing through a system of two separators before arriving at the tank at surface conditions. Separation of liquid and dry gas is performed at each stage and the total amount of separated dry gas is recombined before being reinjected back in the reservoir.



**Table 5.7:** Calculation of the initial reinjection composition by passing the initial overall reservoir fluid composition through a train of separators.

Components	Initial reservoir fluid composition	Separator 1 (500 psia, 120 °F)	Separator 2 (150 psia, 80 °F)	Tank (14.7 psia, 60 °F)	Recombined/Initial reinjection composition
N <sub>2</sub>	3.79998	0.042188	0.019821	0.002074	4.111141088
CO <sub>2</sub>	0.349998	0.003704	0.005401	0.006094	0.377279793
C <sub>1</sub>	67.9096	0.746504	0.666312	0.189183	<b>73.46354684</b>
C <sub>2</sub>	11.3599	0.118506	0.182975	0.260595	12.21229791
C <sub>3</sub>	5.42997	0.05075	0.078536	0.275564	5.547615037
iC <sub>4</sub>	1.14999	0.009231	0.01292	0.066547	1.039060199
nC <sub>4</sub>	2.02999	0.014868	0.019807	0.11225	1.68197982
iC <sub>5</sub>	0.749996	0.004016	0.004596	0.029003	0.450773047
nC <sub>5</sub>	1.00999	0.004827	0.005259	0.033257	0.538344571
C <sub>6</sub>	1.14999	0.003002	0.002648	0.015897	0.324706667
C <sub>6</sub> ::C <sub>6</sub>	0.830954	0.001397	0.001148	0.006716	0.14969034
C <sub>7</sub> ::C <sub>7</sub>	0.731419	0.000559	0.000374	0.001957	0.058388476
C <sub>8</sub> ::C <sub>8</sub>	0.653924	0.000185	9.64E-05	0.000439	0.018898298
C <sub>9</sub> ::C <sub>9</sub>	1.6269	0.000203	8.61E-05	0.000349	0.020383622
C <sub>10</sub> ::C <sub>10</sub>	0.698846	4.66E-05	1.7E-05	6.32E-05	0.004654354
C <sub>11</sub> ::C <sub>11</sub>	0.300194	1.03E-05	3.19E-06	1.08E-05	0.001017503
C <sub>12</sub> ::C <sub>12</sub>	0.12895	1.88E-06	4.8E-07	1.42E-06	0.000185231

C13::C13	0.0553912	3.2E-07	6E-08	1.7E-07	3.13607E-05
C14::C14	0.0237936	5E-08	1E-08	2E-08	4.88824E-06
C15::C15	0.0102207	1E-08	0	0	9.67218E-07
Mole % Gas	100.00	89.40	1.24	1.79	92.43
Mole % Liquid	0.00	10.6	9.36	7.57	--

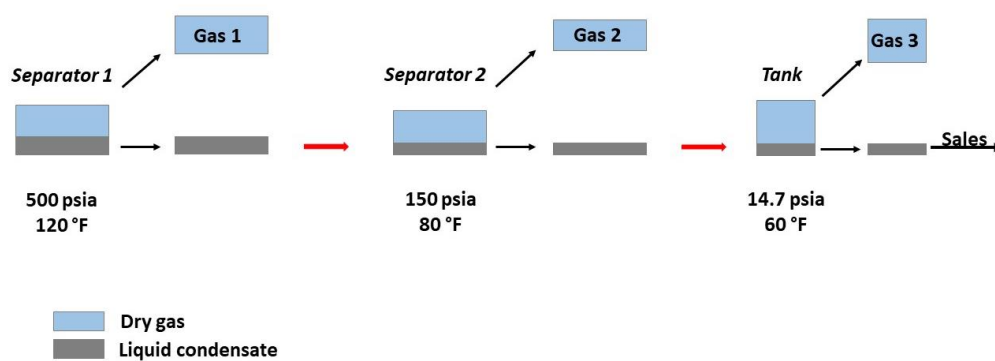


$$y_{recombined} = \frac{y_{Gas1} * NG_1 + y_{Gas2} * NG_2 + y_{Gas3} * NG_3}{NG_1 + NG_2 + NG_3}$$

$y$ : gas composition

$NG$ : number of gas moles

**Figure 5.30:** The produced gas passes through a train of separators before its recombination and reinjection in the reservoir.



**Figure 5.31:** At each separation stage the generated dry gas is collected and the remaining liquid condensate is forwarded to the next separation stage.

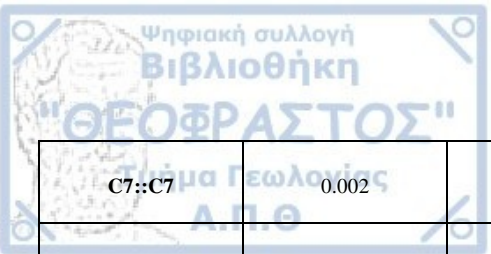
**Table 5.8:** Calculation of the reinjection dry gas composition after five years of production by treating the composition of cell (3,2) through a train of separators for the 80% reinjection scenario.

Components	Composition of cell (3,2) after 5 yrs. of production	Separator 1 (500 psia, 120 °F)	Separator 2 (150 psia, 80 °F)	Tank (14.7 psia, 60 °F)	Recombined/ Reinjection composition at 5 yrs.
N <sub>2</sub>	0.039804	0.041773	0.019546	0.001964	4.126786
CO <sub>2</sub>	0.0036	0.003697	0.005374	0.005825	0.372697
C <sub>1</sub>	0.709371	0.741135	0.658603	0.179478	<b>73.54385</b>
C <sub>2</sub>	0.117912	0.120271	0.185323	0.254194	12.19116
C <sub>3</sub>	0.054705	0.052946	0.081894	0.280351	5.522449
iC <sub>4</sub>	0.010901	0.009763	0.01366	0.069551	1.033873
nC <sub>4</sub>	0.018402	0.015686	0.020888	0.117554	1.665855
iC <sub>5</sub>	0.005901	0.004183	0.004783	0.030247	0.44271
nC <sub>5</sub>	0.007601	0.005011	0.005454	0.034615	0.528729
C <sub>6</sub>	0.007201	0.003081	0.002713	0.016405	0.320212
C <sub>6</sub> ::C <sub>6</sub>	0.0048	0.001441	0.001181	0.006959	0.149065
C <sub>7</sub> ::C <sub>7</sub>	0.0038	0.000569	0.000379	0.001998	0.058093
C <sub>8</sub> ::C <sub>8</sub>	0.0032	0.000187	9.69E-05	0.000444	0.018897
C <sub>9</sub> ::C <sub>9</sub>	0.007601	0.000199	8.42E-05	0.000343	0.019971
C <sub>10</sub> ::C <sub>10</sub>	0.0032	4.53E-05	1.64E-05	6.13E-05	0.004523
C <sub>11</sub> ::C <sub>11</sub>	0.0013	9.47E-06	2.92E-06	9.92E-06	0.000943
C <sub>12</sub> ::C <sub>12</sub>	0.0005	1.56E-06	3.9E-07	1.18E-06	0.000155

<b>C13::C13</b>	0.0002	2.5E-07	5E-08	1.3E-07	2.48E-05
<b>C14::C14</b>	0.0000	0.0000	0.0000	0.0000	0.0000
<b>C15::C15</b>	0.0000	0.0000	0.0000	0.0000	0.0000
<b>Mole % Gas</b>	100.00	94.96	0.6	0.89	96.45
<b>Mole % Liquid</b>	0.00	5.04	4.44	3.55	--

**Table 5.9:** Calculation of the reinjection dry gas composition after ten years of production by treating the composition of cell (3,2) through a train of separators for the 80% reinjection scenario.

<b>Components</b>	<b>Composition of cell (3,2) after 10 yrs. of production</b>	<b>Separator 1 (500 psia, 120 °F)</b>	<b>Separator 2 (150 psia, 80 °F)</b>	<b>Tank (14.7 psia, 60 °F)</b>	<b>Recombined/ Reinjection composition at 10 yrs.</b>
<b>N<sub>2</sub></b>	0.040608	0.041457	0.01936	0.0019	4.123814
<b>CO<sub>2</sub></b>	0.003701	0.003743	0.005432	0.005746	0.375579
<b>C<sub>1</sub></b>	0.724445	0.738183	0.654404	0.174096	<b>73.56705</b>
<b>C<sub>2</sub></b>	0.120024	0.121054	0.186303	0.24985	12.1749
<b>C<sub>3</sub></b>	0.054911	0.054129	0.083698	0.28228	5.513391
<b>iC<sub>4</sub></b>	0.010602	0.010091	0.014117	0.07137	1.035067
<b>nC<sub>4</sub></b>	0.017404	0.016188	0.021549	0.120757	1.662651
<b>iC<sub>5</sub></b>	0.005101	0.00433	0.004948	0.031335	0.444127
<b>nC<sub>5</sub></b>	0.006301	0.005148	0.005599	0.035617	0.527327
<b>C<sub>6</sub></b>	0.005001	0.003168	0.002785	0.01692	0.322248
<b>C6::C6</b>	0.003001	0.001495	0.001223	0.007237	0.151753

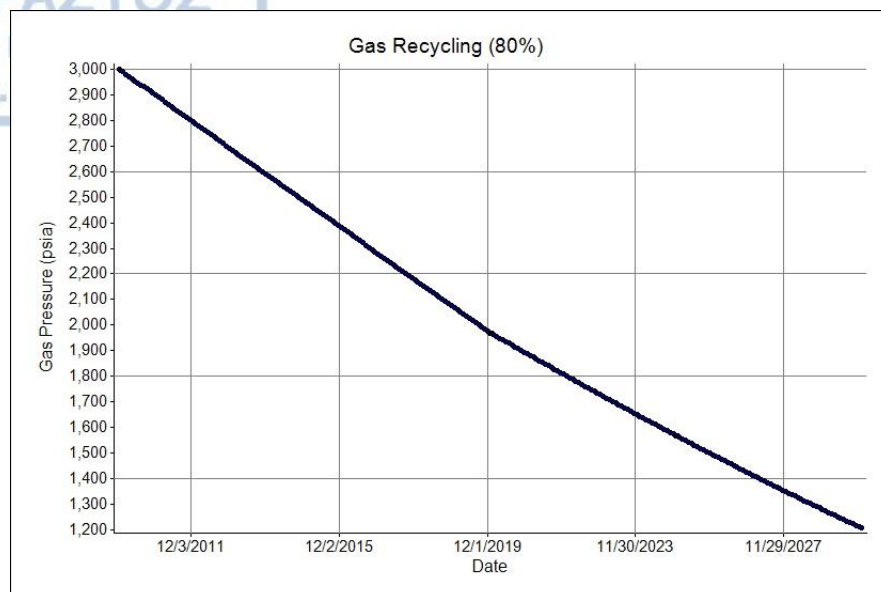


<b>C7::C7</b>	0.002	0.000579	0.000385	0.00204	0.05849
<b>C8::C8</b>	0.0015	0.000189	9.75E-05	0.000449	0.018972
<b>C9::C9</b>	0.003301	0.000194	8.17E-05	0.000334	0.019426
<b>C10::C10</b>	0.0013	4.19E-05	1.52E-05	5.68E-05	0.004192
<b>C11::C11</b>	0.0005	8.39E-06	2.58E-06	8.78E-06	0.000838
<b>C12::C12</b>	0.0002	1.45E-06	3.6E-07	1.09E-06	0.000145
<b>C13::C13</b>	0.0001	2.9E-07	6E-08	1.5E-07	2.89E-05
<b>C14::C14</b>	0.0000	0.0000	0.0000	0.0000	0.0000
<b>C15::C15</b>	0.0000	0.0000	0.0000	0.0000	0.0000
<b>Mole % Gas</b>	100.00	97.81	0.26	0.4	98.47
<b>Mole % Liquid</b>	0.00	2.19	1.93	1.53	--

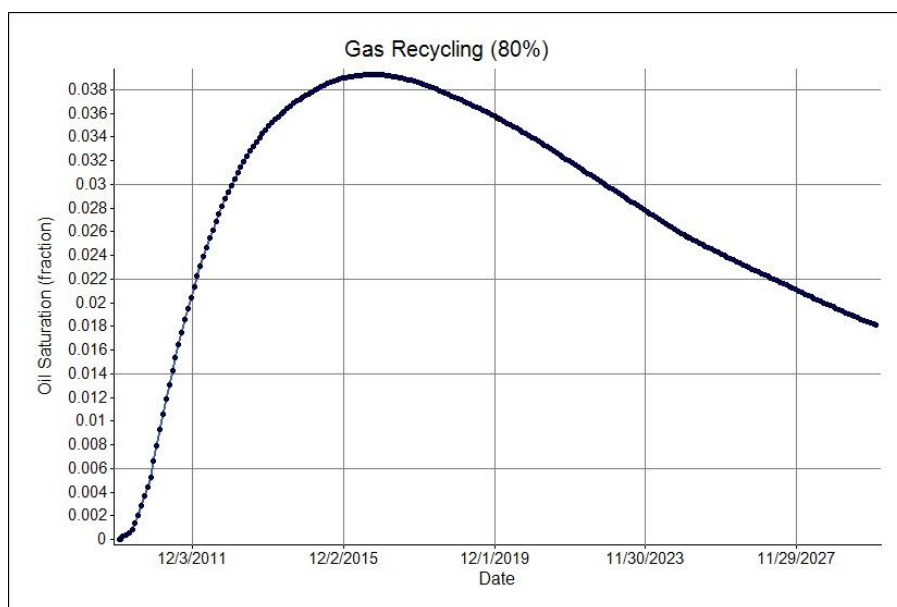
**Table 5.10:** Calculation of the reinjection dry gas composition after fifteen years of production by treating the composition of cell (3,2) through a train of separators for the 80% reinjection scenario.

<b>Components</b>	<b>Composition of cell (3,2) after 15 yrs. of production</b>	<b>Separator 1 (500 psia, 120 °F)</b>	<b>Separator 2 (150 psia, 80 °F)</b>	<b>Tank (14.7 psia, 60 °F)</b>	<b>Recombined/ Reinjection composition at 15 yrs.</b>
<b>N<sub>2</sub></b>	0.0409	0.041353	0.019288	0.001875	4.12379
<b>CO<sub>2</sub></b>	0.0037	0.003723	0.005398	0.00566	0.372903
<b>C1</b>	0.7296	0.736929	0.652543	0.171991	<b>73.56137</b>
<b>C2</b>	0.121	0.121552	0.186983	0.248662	12.19137
<b>C3</b>	0.0551	0.054678	0.084538	0.283524	5.520462

iC4	0.0105	0.010223	0.014302	0.072111	1.036024
nC4	0.017	0.016344	0.021756	0.121722	1.657503
iC5	0.0048	0.004383	0.005008	0.031733	0.444197
nC5	0.0058	0.005181	0.005633	0.035865	0.524616
C6	0.0041	0.003132	0.002753	0.016755	0.316065
C6::C6	0.0023	0.001496	0.001224	0.007251	0.150785
C7::C7	0.0013	0.000563	0.000374	0.001985	0.056603
C8::C8	0.0009	0.000191	9.88E-05	0.000455	0.019188
C9::C9	0.0019	0.000199	8.39E-05	0.000344	0.019939
C10::C10	0.0007	4.12E-05	1.49E-05	5.58E-05	0.004119
C11::C11	0.0003	9.31E-06	2.86E-06	9.75E-06	0.00093
C12::C12	0.0001	1.35E-06	3.4E-07	1.01E-06	0.000135
C13::C13	0.0000	0.0000	0.0000	0.0000	0.0000
C14::C14	0.0000	0.0000	0.0000	0.0000	0.0000
C15::C15	0.0000	0.0000	0.0000	0.0000	0.0000
Mole % Gas	100.00	98.83	0.14	0.21	99.18
Mole % Liquid	0.00	1.17	1.03	0.82	--

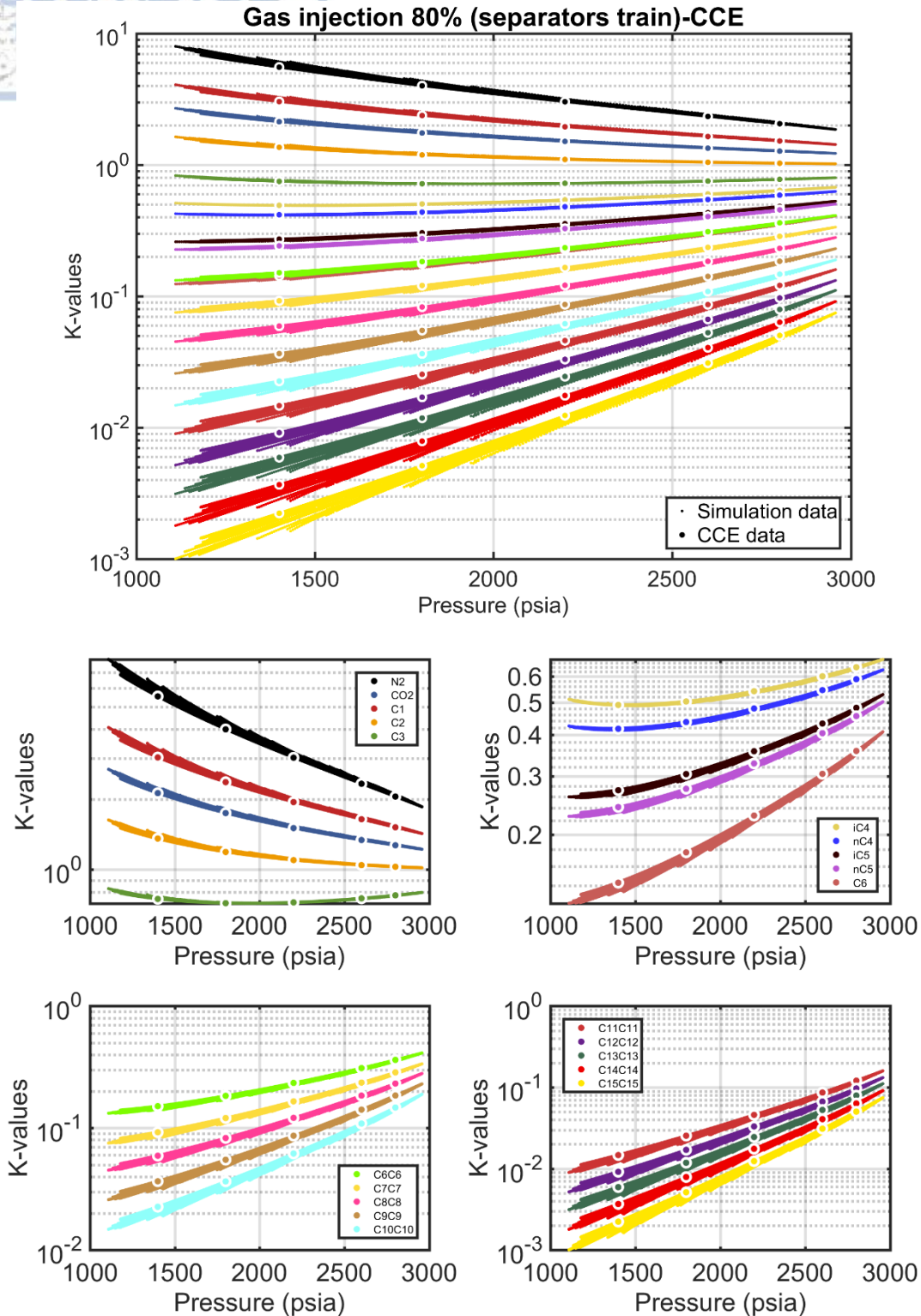


**Figure 5.32:** Average reservoir pressure (psia) for the twenty year production period of the gas recycling scenario with reinjection of 80% of the produced gas, after passing through a system of two separators before reaching the tank surface conditions. Separation of liquid and dry gas is performed at each stage and the total amount of separated dry gas is recombined before being reinjected back in the reservoir. The amount of reinjection gas provides partial pressure maintenance so that the production period can be prolonged to twenty years without major decline in reservoir pressure.

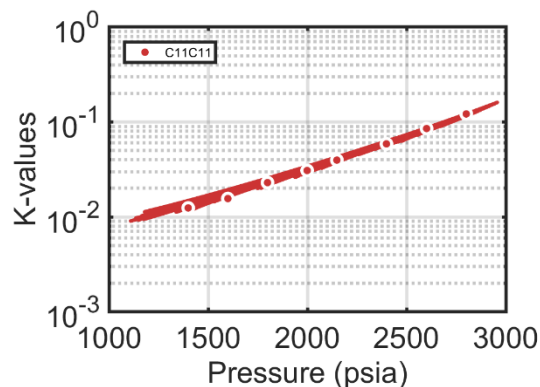
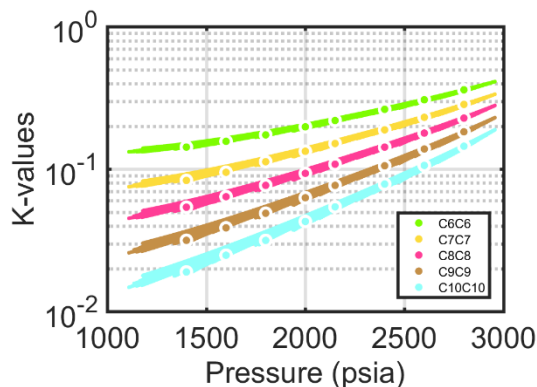
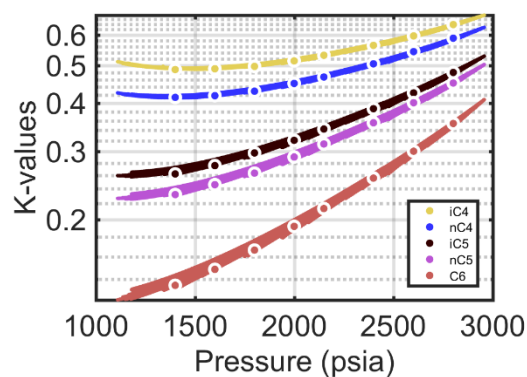
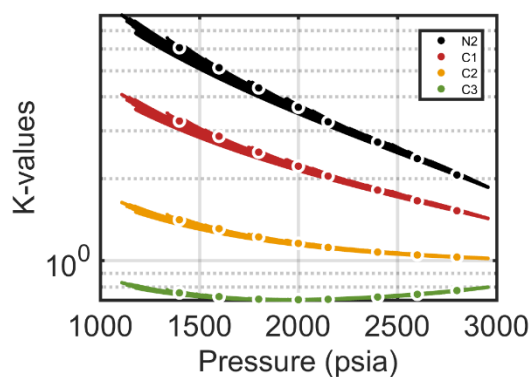
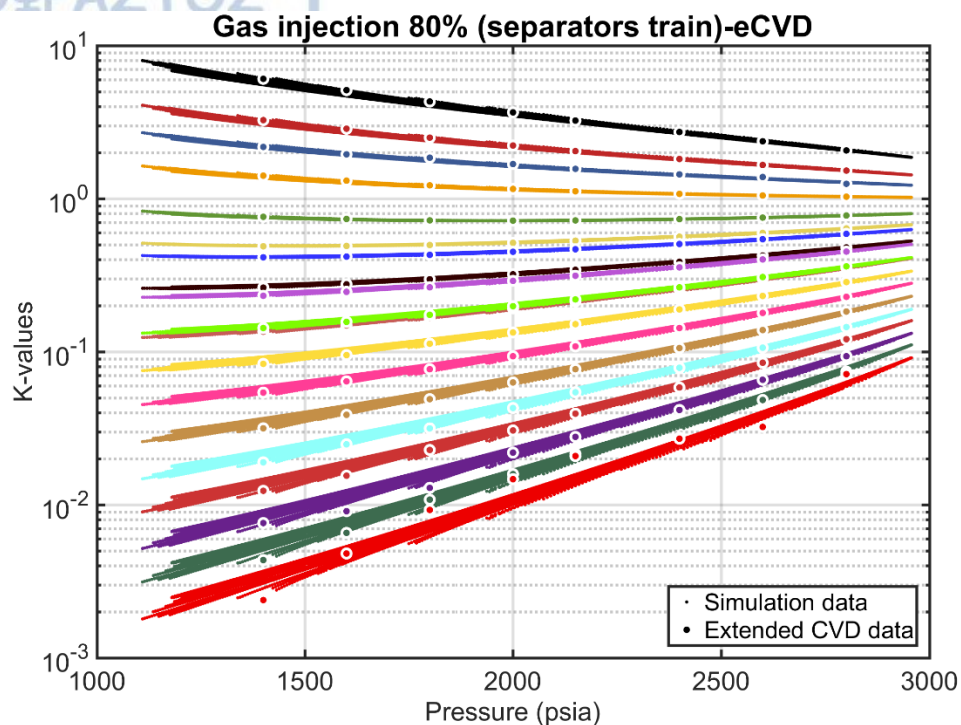
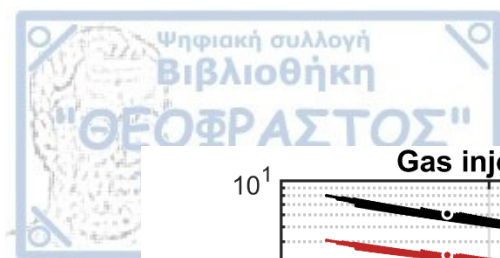


**Figure 5.33:** Average liquid condensate saturation (fraction) for the twenty year production period of the gas recycling scenario with reinjection of 80% of the produced gas after passing through a system of two separators before reaching the tank surface conditions. Condensate revaporisation is happening as a response to the reservoir's overall composition being modified by the gas recycling process rather than reservoir pressure decline.





**Figure 5.34:** Pressure/K-values plots for the gas recycling scenario with reinjection of 80% of the produced gas after passing through a system of two separators before reaching the tank surface conditions. The CCE experiment underestimates the K-values of the light components and overestimates the K-values of the heavy components, therefore it is not suitable to describe the process of production and gas injection of this scenario in terms of the K-values.



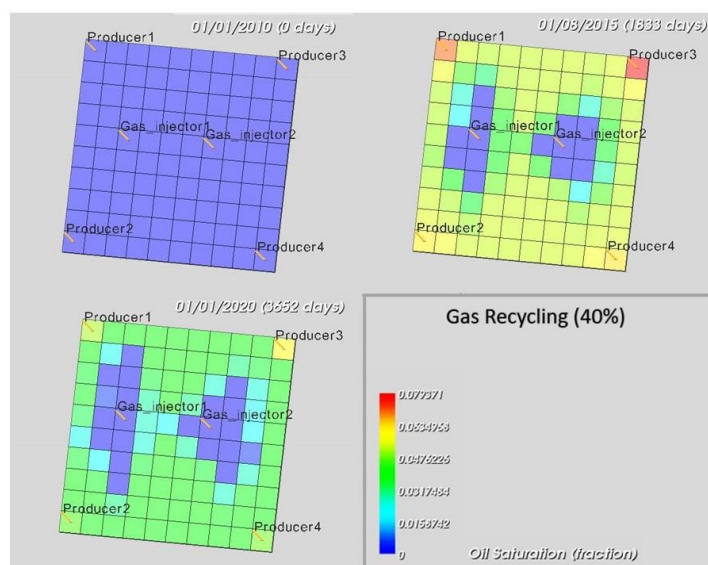
**Figure 5.35:** Pressure/K-values plots for the gas recycling scenario with reinjection of 80% of the produced gas after passing through a system of two separators before reaching the tank surface conditions compared with the results of the eCVD experiment. The extended CVD derived K-values can present a good match with the simulation derived values for components up to C11C11 and excluding the CO<sub>2</sub>, better than the classic CCE experiment.

### 5.2.6 Gas Recycling 40% (separators train)

In this scenario the four production wells were operated at a fixed rate of 7 MMscf/day each for a ten year period and the two gas injectors were injecting surface dry gas at a fixed rate of 5.6 MMscf/day each (Fig. 5.36). The separator arrangement was the same as in the previous scenario, with Separator 1 operating at 500 psia and 120 °F and Separator 2 at 150 psia and 80 °F.

The initial reinjection composition given in Table 5.7, was updated once after 5 years of production (Table 5.11). This updated reinjection composition appears to be heavier than the initial reinjection composition due to the fact that the reinjection amount, as well as the production time, are not sufficient to modify the overall reservoir fluid composition, since the gas production rate is far greater than the dry gas injection rate. This means that most of the lighter components are being produced than being reinjected in the reservoir, leading to a heavier overall reservoir composition. This is typical of all examined gas recycling scenarios with an insufficient amount of reinjection gas.

The reservoir pressure exhibited a constant decline and reached almost 700 psia at the end of the production period (Fig. 5.37). The liquid saturation reached a maximum value of about 0.042 (4.2%) before declining to about 0.03 (3%) at the end of production (Fig. 5.38). This decline is caused by the reservoir reduced pressure and not by the modification of the reservoir overall composition. The pressure/K-values plots show a poor match between the CCE derived and simulation derived K-values since the CCE experiment underestimates the K-values of the light components and overestimates the K-values of the heavy components, although the scattering of the simulation derived K-values is not as intense as in the previous 80% reinjection scenario (Fig. 5.39).

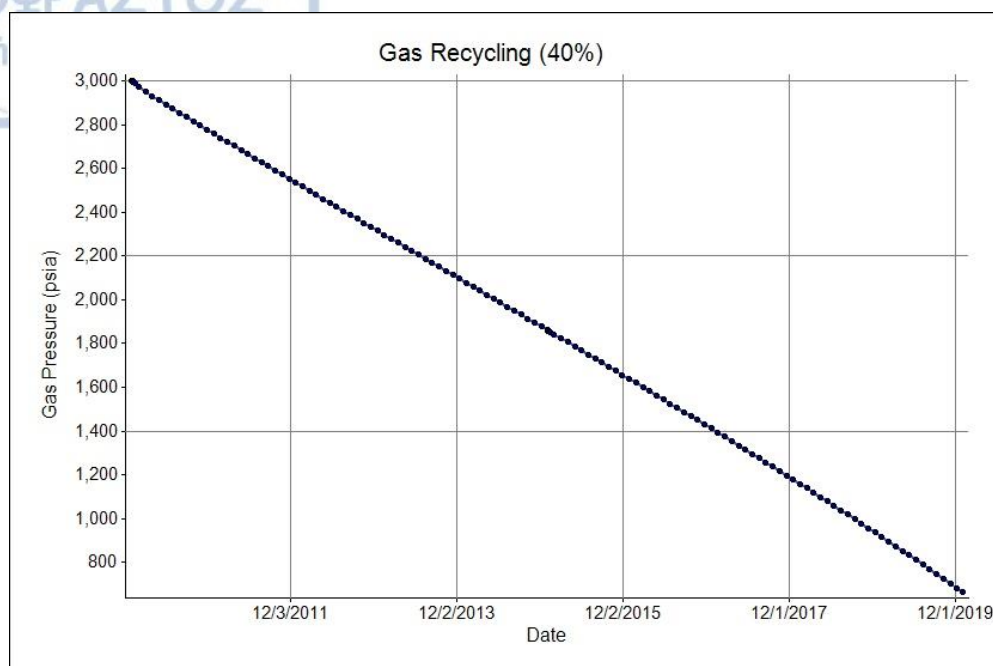


**Figure 5.36:** Gas recycling scenario where 40% of the produced gas is reinjected in the reservoir after passing through a system of two separators before reaching the tank at surface conditions. Separation of liquid and dry gas is performed at each stage and the total amount of separated dry gas is recombined before being reinjected back in the reservoir.

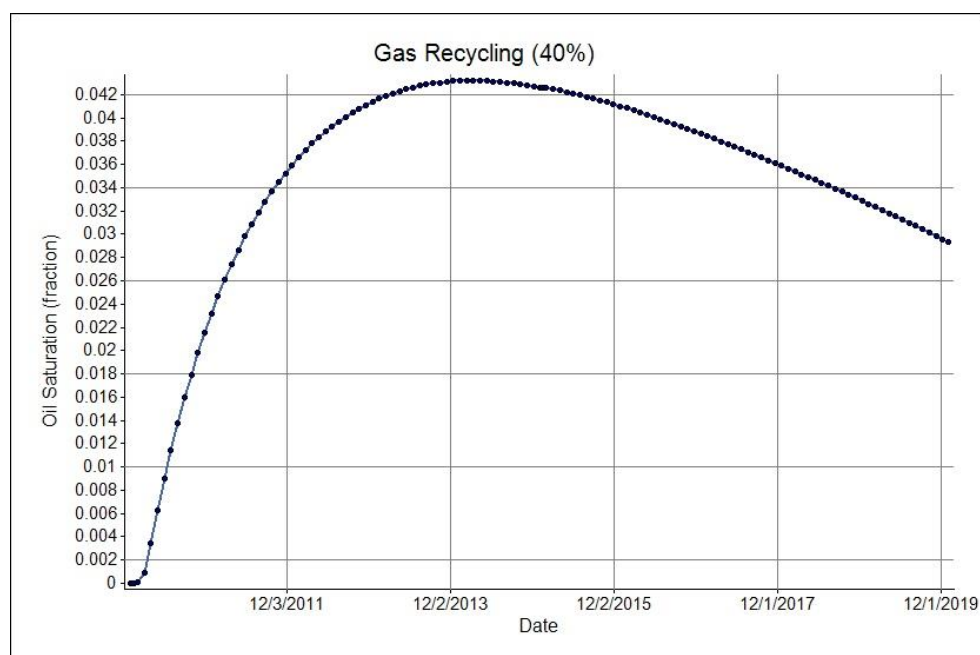
**Table 5.11:** Calculation of the reinjection dry gas composition after 5 years of production by treating the composition of cell (3,2) through a train of separators for the 40% reinjection scenario.

Components	Composition of cell (3,2) after 5 yrs. of production	Separator 1 (500 psia, 120 °F)	Separator 2 (150 psia, 80 °F)	Tank (14.7 psia, 60 °F)	Recombined/ Reinjection composition at 5 yrs.
N <sub>2</sub>	0.0382	0.04165	0.019479	0.002001	4.076316
CO <sub>2</sub>	0.0036	0.003773	0.005494	0.006103	0.383003
C <sub>1</sub>	0.6874	0.743421	0.661139	0.184286	<b>73.34477</b>
C <sub>2</sub>	0.1164	0.120575	0.185864	0.260666	12.35651
C <sub>3</sub>	0.0555	0.052453	0.081093	0.281644	5.648489
iC <sub>4</sub>	0.0114	0.009465	0.013237	0.067818	1.045334
nC <sub>4</sub>	0.0197	0.015107	0.020114	0.113618	1.675981
iC <sub>5</sub>	0.0068	0.003949	0.004516	0.028507	0.435396
nC <sub>5</sub>	0.0089	0.004662	0.005076	0.03213	0.511207
C <sub>6</sub>	0.0093	0.002772	0.002443	0.0147	0.296152
C <sub>6</sub> ::C <sub>6</sub>	0.0063	0.00123	0.001011	0.005931	0.130418
C <sub>7</sub> ::C <sub>7</sub>	0.0055	0.000497	0.000332	0.001746	0.051581
C <sub>8</sub> ::C <sub>8</sub>	0.0051	0.000173	8.98E-05	0.00041	0.017549
C <sub>9</sub> ::C <sub>9</sub>	0.0137	0.000204	8.69E-05	0.000353	0.020551
C <sub>10</sub> ::C <sub>10</sub>	0.0065	5.2E-05	1.9E-05	7.06E-05	0.005197
C <sub>11</sub> ::C <sub>11</sub>	0.003	1.23E-05	3.83E-06	1.3E-05	0.001224
C <sub>12</sub> ::C <sub>12</sub>	0.0015	2.63E-06	6.6E-07	1.99E-06	0.00026

<b>C13::C13</b>	0.0007	4.9E-07	1E-07	2.6E-07	4.82E-05
<b>C14::C14</b>	0.0003	8E-08	1E-08	3E-08	7.84E-06
<b>C15::C15</b>	0.0002	2E-08	0.0000	1E-08	1.96E-06
<b>Mole % Gas</b>	100.00	91.16	1.03	1.52	93.71
<b>Mole % Liquid</b>	0.00	8.84	7.81	6.29	--

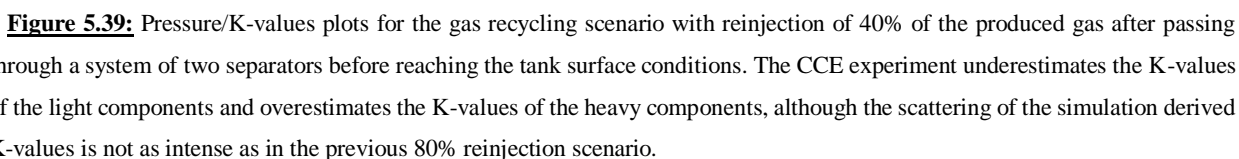


**Figure 5.37:** Average reservoir pressure (psia) for the ten year production period of the gas recycling scenario with reinjection of 40% of the produced gas, after passing through a system of two separators before reaching the tank surface conditions. The amount of reinjection gas does not provide much pressure maintenance and the reservoir pressure reaches almost 700 psia at the end of the production period.



**Figure 5.38:** Average liquid condensate saturation (fraction) for the ten year production period of the gas recycling scenario with reinjection of 40% of the produced gas after passing through a system of two separators before reaching the tank surface conditions. Condensate revaporisation is happening as a response to the reservoir's decline in pressure and not the reservoir overall composition being modified by the gas recycling process.



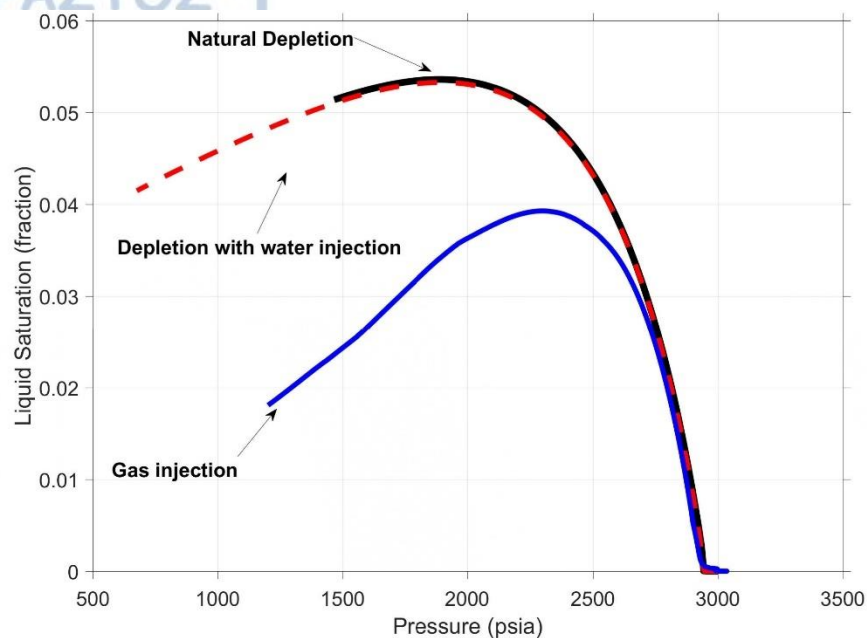




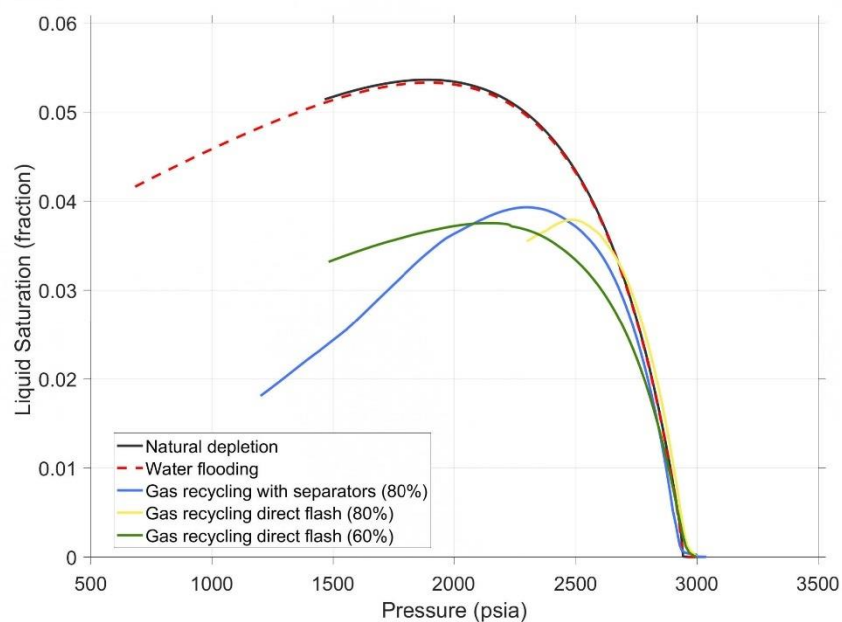
### 5.3 Conclusions

In this thesis a total of eight reservoir simulation scenarios were set up, two production by pressure depletion scenarios and six production with dry gas recycling scenarios. The corresponding equilibrium coefficient values of each scenario were retrieved and compared against the equilibrium coefficient values of a Constant Composition Expansion (CCE) experiment performed each time at the same conditions and with the same parameters as the simulation scenario it was compared against. Furthermore, the equilibrium coefficients of three of the gas recycling scenarios, namely, two scenarios were 80% of the produced gas was reinjected in the reservoir as dry gas and one scenario were 60% of the produced gas was reinjected in the reservoir as dry gas, were compared against the results of an extended CVD experiment that was designed and performed for the purposes of this thesis. This extended CVD experiment was constructed as a tool that could provide representative sets of K-values in a short amount of time, corresponding to the simulation scenarios which were complex enough to be represented by the K-values of the classic CCE experiment.

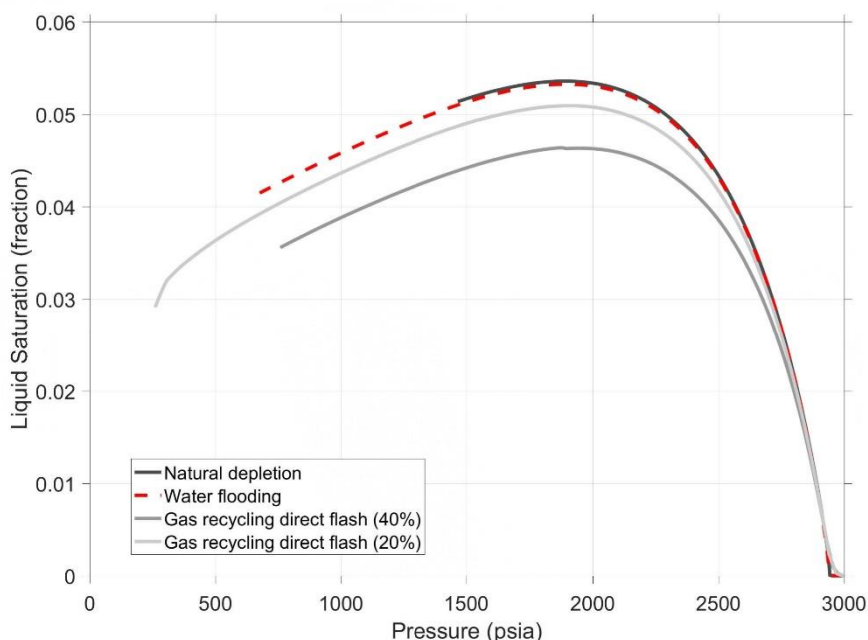
From all the above considered gas recycling scenarios, the ones which actually appeared to assist production by providing pressure maintenance, as well as liquid condensate revaporisation in the reservoir by altering the overall reservoir fluid composition, are the 80% reinjection scenarios with and without the use of separators at the surface, and the 60% reinjection scenario without the use of separators at the surface (Figs. 5.40 and 5.41). All three of the above scenarios, efficiently promote liquid condensate revaporisation in the reservoir and consequently, the smallest percentages of remaining condensate in the reservoir at the end of production, i.e., 1.8% for the reinjection scenario of 80% of the produced gas with the use of a system of separators at the surface. The rest of the gas recycling scenarios that were examined could not provide a sufficient amount of injection gas to the reservoir so as to at least partially maintain pressure or change the overall reservoir fluid composition. Therefore, any revaporisation that was observed in these scenarios was attributed to the low reservoir pressure at the last years of production and the approaching of the lower dew point curve at the phase envelope of the reservoir fluid (Fig. 5.42).



**Figure 5.40:** Pressure/Liquid saturation plot demonstrating the change in average liquid saturation in the reservoir for the scenarios of natural depletion, water flooding and gas injection. The reduced amount of liquid condensate in the reservoir throughout the production is evident for the scenario of gas injection.



**Figure 5.41:** Pressure/Liquid saturation plot for the comparison of the depletion scenarios and the gas injection scenarios where the gas recycling process benefits the production.



**Figure 5.42:** Pressure/Liquid saturation plot for the comparison of the depletion scenarios with the gas injection scenarios with an insufficient amount of injection gas. The liquid saturation curves of the 20% and 40% reinjection scenarios are very similar to the saturation curves of the depletion scenarios.

Examination of the pressure/K-values diagrams constructed for each of the above mentioned scenarios indicated that the classic Constant Mass experiment can describe very well the simulation results of the natural depletion and water flooding scenarios, as well as the reinjection scenarios with 40% reinjection of the produced gas, either when it is directly flashed at standard conditions or when it passes through a series of separators, and the reinjection scenario with 20% reinjection of the produced gas that was directly flashed at standard conditions. These last scenarios are equivalent to the depletion scenarios since the amount of reinjected gas is not sufficient to cause reservoir-scale changes during the production time of ten years and for that reason their K-values can be represented by the K-values of a classic CCE experiment as in the case of regular depletion.

As the simulation scenarios become more complex concerning the amount of reinjection gas or the use of a separator train at surface, as opposed to the direct flash at standard conditions, the classic CCE experiment cannot fully describe these processes since it is either underestimating the K-values of the heavy components, as is the case of the 80% and 60% reinjection scenarios with direct flash at standard conditions, or it is overestimating the K-values of the heavy components as in the case of the 80% and 40% reinjection scenarios where a train of separators is used at the surface. In other words, the more the produced gas is stripped from its heavy components at the surface and consequently, the more dry it becomes before being

reinjecting in the reservoir, the more the K-values diverge from the classic CCE experiment ones. The plotted data exhibit a scattering of their values at the lighter and heavier components, especially for low pressures.

In this case, the principle of composition independency starts to get violated and the corresponding K-values are not only pressure dependent, as in the depletion and small reinjection amount scenarios, but become also composition dependent. In these scenarios therefore, the extended CVD experiment appears to provide more suitable average values of the equilibrium coefficients, especially for pressures of 2,000 psia and greater, since their comparison with the simulation derived K-values give a perfect match at these conditions. However, this method only works for components up to C11C11, while it also appears inappropriate to describe the behaviour of CO<sub>2</sub> as well. Even though the extended CVD experiment cannot provide representative K-values for all the components present in the reservoir fluid, it is still a simple and quick way to generate representative K-values for the more complex gas recycling scenarios.

All the above conclusions point to the fact that a classic CCE experiment is a suitable means to generate vast amounts of K-values with minimum error for a natural depletion or a water flooding scenario to be used for the education of a machine learning system that could predict the required during reservoir simulation K-values, thus eliminating the need for their calculation through complex time-consuming flash calculations and therefore leading to the acceleration of the reservoir simulation process.

In the case of more complex gas recycling scenarios as the ones where 80% of the amount of the produced gas is reinjected in the reservoir, either by passing through a series of separators at the surface, or being directly flashed at standard conditions, as well as the scenario with reinjection of 60% of the produced gas after being directly flashed at standard conditions, a small modification to the classic CCE should be made to account for the extraction of the liquid condensate at the surface at each step of the recycling procedure. Accordingly, the extended CVD experiment is suggested for the generation of the K-values to be used for the education of the machine learning tool when gas recycling scenarios are concerned.

Consequently, if a fine-tuned Equation of State is available for the gas condensate reservoir fluid, the classic CCE experiment could be used as a means to provide representative K-values for the natural depletion scenario and the water flooding scenario and the scenarios equivalent to these. On the other hand, if dry gas recycling is performed in the reservoir in a sufficient amount to make the overall reservoir fluid composition leaner and provide partial pressure maintenance, the extended CVD experiment should be used where applicable, to provide representative K-values. The extended CVD experiment is simple enough to perform, slightly different from the classic CCE and CVD experiments and it can predict the simulation results more accurately than the classic CCE, for most pressures and especially above 2,000 psia.

Using one of the above suggested experiments, classic CCE or extended CVD, an automatic procedure for the prediction of K-values can be developed based on machine learning techniques. The machine learning system will be educated using numerous pressure/K-value sets derived from either the classic CCE or the extended CVD experiment regarding depletion scenarios or gas recycling scenarios respectively, to automatically predict the K-values at any pressure. Since the machine learning system is suggested as a replacement of the extremely time-consuming determination of the K-values through complex flash calculations, and subsequently the main concern is the speed of the computations, an appropriate machine learning tool must be chosen that is primarily characterised for its speed when performing calculations and secondly for its accuracy. For that reason, time-consuming approaches like the decision tree method, are not appropriate machine learning tools for the generation of K-values. On the other hand, neural networks might be demanding as far as their training is concerned, although upon completion of their development they are extremely fast in performing calculations. For that reason they are suitable to be used as K-value generators as they can provide rapid calculations during reservoir simulation since our main goal is the acceleration of phase behaviour calculations.



## REFERENCES

**Abou-Kassem, J. H., Farouq-Ali, S. M., & Islam, M. R.** (2013). Petroleum Reservoir Simulations. Elsevier.

**Afidick, D., N. Kaczorowski, and S. Bette.** (1994). "Production performance of a retrograde gas reservoir: a case study of the Arun Field." SPE Asia Pacific Oil and Gas Conference. Society of Petroleum Engineers SPE-28749-MS.

**Ahmed, T.** (2013). Equations of state and PVT analysis. Elsevier.

**Ahmed, T.** (2007, 2016). Equations of State and PVT analysis Applications for Improved Reservoir Modelling. Elsevier Inc.

**Ahmed, T.** (2010). Reservoir Engineering Handbook. Elsevier.

**Baker, L. E., Pierce, A. C., & Luks, K. D.** (1982). Gibbs energy analysis of phase equilibria. Society of Petroleum Engineers Journal, 22(05), 731-742.

**Barnum, R., F. Brinkman, T.W. Richardson, and A.G. Spillette.** (1995). "Gas condensate reservoir behaviour: productivity and recovery reduction due to condensation." SPE Annual Technical Conference and Exhibition. Society of Petroleum Engineers. SPE-30767-MS.

**Campbell, J. M.** (1976), Gas Conditioning and Processing, Vol. 1. Norman, OK: Campbell Petroleum Series.

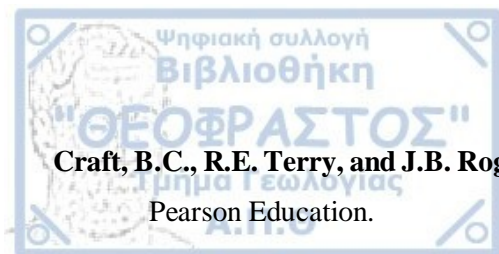
**Cao, H.** (2002). Development of techniques for general purpose simulators (Doctoral dissertation, Stanford University).

**Coats, K. H.** (1980). An equation of state compositional model. Society of Petroleum Engineers Journal, 20(05), 363-376.

**Coats, K. H.** (2000). A note on IMPES and some IMPES-based simulation models. SPE Journal, 5(03), 245-251.

**Coats, K.H.** (1985). "Simulation of gas condensate reservoir performance." Journal of Petroleum Technology 37 (10). SPE-10512-PA.

"Core Laboratories Good Oil Company Oil Well No. 4 PVT Study," Core Laboratories, Houston.



**Craft, B.C., R.E. Terry, and J.B. Rogers.** (2015). Applied Petroleum Reservoir Engineering (3rd Edition). Pearson Education.

**Dake, L.P.** (2001). The practice of reservoir engineering (Revised Edition). Elsevier.

**Danesh, A.** (1998). PVT and phase behavior of reservoir fluids. Developments in Petroleum Science.

**Ezekwe, N.** (2010). Petroleum reservoir engineering practice. Pearson Education.

**Fanchi, J. R.** (2005). Principles of applied reservoir simulation. Elsevier.

**Gaganis, V.** (2020). Perturbation Theory and Phase Behavior Calculations Using Equation of State Models. In Perturbation Theory. IntechOpen.

Gas Processors Suppliers Association (1978), Engineering Data Book, 10th Ed.

**Glasø, O. and Whitson, C.H.:** “The Accuracy of PVT Parameters Calculated From Computer Flash Separation at Pressures Less Than 1,000 psia,” JPT (August 1980) 1811.

**Hadden, J. T.,** “Convergence Pressure in Hydrocarbon Vapor-Liquid Equilibria,” Chem. Eng. Progr. Symposium Ser., (1953), Vol. 49, No. 7, p. 53.

**Hameed, M.M.** (2015). “Studying the effect of condensate saturation bank development around a production well in Siba Field/Yamama Formation.” Master's Thesis, University of Baghdad.

**Hinchman, S.B., and R.D. Barree.** (1985). “Productivity loss in gas condensate reservoirs.” SPE Annual Technical Conference and Exhibition. Las Vegas, Nevada. 22-26.

**Hoffmann, A.E., Crump, J.S., Hocott, R.C.,** (1953). Equilibrium constants for a gas condensate system. Trans. AIME 198, 1–10

**Ikoku, C. U.** (1984,1992). Natural Gas Reservoir Engineering. Krieger Publishing Company.

**Jhaveri, B. S., & Youngren, G. K.** (1988). Three-parameter modification of the Peng-Robinson equation of state to improve volumetric predictions. SPE reservoir engineering, 3(03), 1033-1040.

**Jianyi L., Ping G., Shilun L., et al.** (2001). “Experimental Evaluation of Condensate Blockage on Condensate Gas Well.” Nat. Gas Ind. 20 (5) 67-69.

**Katz, D., et al.,** (1959). Handbook of Natural Gas Engineering. McGraw-Hill, New York.

**Katz, D.L., Hachmuth, K.H.,** (1937). Vaporization equilibrium constants in a crude oil/natural gas system. Ind. Eng. Chem. 29, 1072.



**Kay, W. B.** (1938). “The Ethane-Heptane System”. Ind. & Eng. Chem. 30,459.

**Lohrenze, J., Clark, G., Francis, R.,** (1963). A compositional material balance for combination drive reservoirs. J. Pet. Technol

**Michelsen, M. L.** (1982). The isothermal flash problem. Part I. Stability. Fluid phase equilibria, 9(1), 1-19.

**Michelsen, M. L.** (1993). Phase equilibrium calculations. What is easy and what is difficult?. Computers & chemical engineering, 17(5-6), 431-439.

**Muskat, M.** (1945). “Some theoretical aspects of cycling, Part 2. Retrograde condensate about wellbores.” Oil Gas J. 45 (5) 53-60.

**Nagy, Z. and Shirkovskiy, A.I:** “Mathematical Simulation of Natural Gas Condensation Processes Using the Peng-Robinson Equation of State,” paper SPE 10982 presented at the 1982 SPE Annual Technical Conference and Exhibition, New Orleans, 26–29 September

**Noor M.M., Groeneweg E., Gunarso I.** (2005). “A condensate blockage study in north Belut Field.” Indonesian Petroleum Association .

**Pedersen, K. S., Christensen, P. L., & Shaikh, J. A.** (2014). Phase behavior of petroleum reservoir fluids. CRC press.

**Peneloux, A., Rauzy, E., Freze, R.,** (1982). A consistent correlation for Redlich-Kwong-Soave volumes. Fluid Phase Equilib. 8, 7–23.

**Peng, D., Robinson, D.,** (1976a). A new two constant equation of state. Ind. Eng. Chem. Fundam. 15 (1), 59–64.

**Peng, D., Robinson, D.,** (1978). The Characterization of the Heptanes and Their Fractions: Research Report 28. Gas Producers Association, Tulsa, OK.

**Rahimzadeh A., Bazargan M., Darvishi R. Mohammadi A. H.** (2016). “Condensate blockage study in gas condensate reservoir.” J. Nat. Gas Sci. Eng. 33 634-643.

**Redlich, O., Kwong, J.,** (1949). On the thermodynamics of solutions. An equation of state. Fugacities of gaseous solutions. Chem. Rev. 44, 233–247.

**Reid, R.C., Prausnitz, J.M., and Polling, B.E.:** The Properties of Gases and Liquids, fourth edition, McGraw-Hill Book Co. Inc., New York City (1987)

**Robinson, D.B., Peng, D.Y., and Ng, H.Y.:** “Capabilities of the Peng Robinson Programs, Part 2: Three-Phase and Hydrate Calculations,” *Hydrocarbon Proc.* (1979) 58, 269

**Rzasa, M. J., Glass, E. D., and Opfell, J. B.,** “Prediction of Critical Properties and Equilibrium Vaporization Constants for Complex Hydrocarbon Systems,” *Chem. Eng. Progr. Symposium Ser.*, 1952, Vol. 48, No. 2, p. 28.

**Sheng J.J., Mody F., Griffith P.J. et al.** (2013). “Potential to increase condensate oil production by huff-n-puff gas injection in a shale condensate reservoir.” *J. Nat. Gas Sci. Eng.* 2 (8) 46-51.

**Silpngarmlers N., Ayyalasomayajula P.S., Kamath J.** (2005). “Gas condensate well deliverability: Integrated laboratory-simulation-field study.” *International Petroleum Technology Conference.*

**Soave, G.,** (1972). Equilibrium constants from a modified Redlich-Kwong equation of state. *Chem. Eng. Sci.* 27, 1197–1203.

**Standing, M. B.** (1977). *Volumetric and Phase Behavior of Oil Field Hydrocarbon Systems.* Texas: SPE, Richardson.

**Standing, M.B.,** (1979). A set of equations for computing equilibrium ratios of a crude oil/natural gas system at pressures below 1,000 psia. *J. Pet. Technol.* 31 (9), 1193–1195.

**Van der Waals, J.D.,** (1873). *On the Continuity of the Liquid and Gaseous State.* Sijthoff, Leiden, The Netherlands (Ph.D. dissertation).

**Wang Z., Zhu S., Zhou W. et al.** (2018). “Experimental research of condensate blockage and mitigating effect of gas injection.” *Petroleum* 4 292-299.

**Whitson, C. H., & Brulé, M. R.** (2000). *Phase behavior* (Vol. 20, p. 233). Richardson, TX: Henry L. Doherty Memorial Fund of AIME, Society of Petroleum Engineers.

**Whitson, C. H., and Torp, S. B.,** “Evaluating Constant Volume Depletion Data,” SPE Paper 10067 presented at the SPE 56th Annual Fall Technical Conference, San Antonio, TX, Oct. 5-7, 1981.

**Whitson, C.H., O. Fevang, and T. Yang.** (1999). “Gas Condensate PVT-What's really important and why.” IBC Conference "Optimisation of Gas Condensate Fields". London.

**Wilson, G.,** (1968). A modified Redlich-Kwong EOS, application to general physical data calculations. In: Paper 15C, presented at the Annual AIChE National Meeting, Cleveland, May 4–7, 1968.

**Winn, F. W.,** “Simplified Nomographic Presentation, Hydrocarbon Vapor–Liquid Equilibria,” *Chem. Eng. Progr. Symposium Ser.*, 1954, Vol. 33, No. 6, pp. 131–135.

**Yong T., Zhimin D., Lei S. et al.** (2007). “Research status and progress of removing condensate blockage around well in low-permeability gas condensate reservoir.” Nat. Gas Ind. 27 (6) 88-89.

**Young, L. C., & Stephenson, R. E.** (1983). A generalized compositional approach for reservoir simulation. Society of Petroleum Engineers Journal, 23(05), 727-742.